Order Number 9510741

Properties of fractional quantum Hall systems and non-equilibrium Green's function method of transport in nanostructures

Zang, Jun, Ph.D.

City University of New York, 1994

U·M·I
300 N. Zeeb Rd.
Ann Arbor, MI 48106

Properties of Fractional Quantum Hall Systems

and

Non-Equilibrium Green's Function Method of Transport in Nanostructures

by

Jun Zang

A dissertation submitted to the Graduate Faculty in Physics
in partial fulfillment of the requirements for the degree of
Doctor of Philosophy, The City University of New York.

1994

This manuscript has been read and accepted for the Graduate Faculty in Physics in satisfaction of the dissertation requirement for the degree of Doctor of Philosophy

27 Sept 1994
Date

Joseph L. Birman
Chairman of Examining Committee

September 23, 1994
Date

Edward Tryon
Acting Executive Officer

Supervisory Committee:

_____ Prof. G. Gumbs, Hunter College of CUNY

_____ Prof. Melvin Lax, City College of CUNY

_____ Dr. Peter Littlewood, AT&T Bell Laboratory

_____ Prof. Bunji Sakita, City College of CUNY

_____ Prof. David Schmeltzer, City College of CUNY

THE CITY UNIVERSITY OF NEW YORK

Abstract

Properties of Fractional Quantum Hall Systems

and

Non-Equilibrium Green's Function Method of

Transport in Nanostructures

by

Jun Zang

Adviser: **Joseph L. Birman**

This dissertation contains two parts.

In part I the properties of the fractional quantum Hall effect (FQHE) systems are presented. I have numerically studied the Laughlin wave function in disk geometry. The hierarchy structure of FQHE is studied and a global phase diagram is proposed. The magnetoexciton in the FQHE system is studied and photoluminescence as well as resonance Raman scattering is calculated. I also calculated the Fermi edge singularities in the double layer FQHE systems.

In part II, the resonant tunneling through nanostructures was studied using the non-equilibrium Green's function approach. The intrinsic bistability

due to many-body electron-electron interaction effects in the double barrier structure is studied. I also derived an exact Breit-Wigner formula for the resonant tunneling in the multiple-barrier structures, and showed that it is useful in the study of conductance fluctuations of electron transport through a strongly disordered quantum wire.

Dedication

To My Parents

and My Wife

Acknowledgements

I am deeply indebted to my mentor, Prof. Joseph L. Birman, for his scientific and academic guidance, encouragement, advice and endless discussions in my dissertation research as well as other topics. With his guidance in these four years, I grew up to be an independent researcher from a fresh graduate student without any research experience. I am sure I will be benefitted, grateful, and influenced in all aspects for the years to come.

I thank all the Faculty in this department of CCNY for their education and discussions. I thank especially the following professors from whom I benefitted directly in my dissertation research: Prof. David Schmeltzer for his constant discussions, advice and cooperation; Prof. Melvin Lax for his education in condensed matter theory and numerical methods; Prof. Bunji Sakita for his education and discussion, and Prof. Joel Koplik for his introduction to Mathematica and IMSL libraries.

I must thank many visiting scientists from whom I got such a wonderful experience. They include: Prof. Bing-Shen Wang, Prof. Segei Tikhodeev, Prof. Zhao-Bin Su, Prof. Shumel Goshen, Prof. Jovo Jaric, Prof. Lu Yu, Dr. A Kuklov, Prof. Nguyen Ai Viet, Prof. Alan Solomon. Among them, I was indebted to Prof. Bing-shen Wang, Prof. Sergei Tikhodeev, and Prof. Zhao-Bin Su, for their numerous discussions and advice, I especially benefited from Prof. Sergei Tikhodeev for his discussions about the non-equilibrium Green's function method, computations and LaTeX!

I would like to thank all the members of our groups, friends, and fellow

students in this department, for their help, discussions, and cooperation. My thanks to: Dr. Maurizio Artoni, Mr. Alexi Bulatov, Mr. Lenny Tevlin, Mr. Andrey Krakovsky, Dr. Wei Cai, Dr. Joseph Malinsky, Mr. Weimin Du, Mr. Ming Zhang, Mr. Zhongmo Ju, Dr. Gen Li, Dr. Peihua Dai, Dr. Yuzhu Zhang and many others.

Contents

List of Figures

List of Tables

Part I

FQHE And Optical Properties

Chapter 1

Introduction to FQHE

1.1 Integer Quantum Hall Effect

Recent advances in semiconductor fabrication technologies makes the construction of novel low dimensional electron systems possible. The early examples of 2D electron systems proved to have extremely fascinating physical properties. The integer and fractional quantum Hall effects [1, 2, 3] are among the most interesting ones exhibited by them. In this section, I give a very brief introduction to the IQHE.

Consider a 2D electron gas confined to the (x-y) plane with uniform magnetic field $B = B\hat{z}$. By using the classical (Drude) theory, we easily derive the resistivity tensor [ρ]. Assume the electrons have isotropic effective mass m^*, in the steady state, the equation of motion of the electron is:

$$\vec{v} = \frac{e\tau_0}{m^*}\left(\vec{E} + \frac{1}{c}\vec{v} \times \vec{B}\right) \tag{1.1}$$

where τ_0 is the relaxation time of the electrons. Using $\vec{j} = ne\vec{v}$, then

$$E_x = \frac{m^*}{ne^2\tau_0} j_x - \frac{B}{nec} j_y$$

$$E_y = \frac{m^*}{ne^2\tau_0} j_y + \frac{B}{nec} j_x \tag{1.2}$$

The resistivity tensor is defined by $E_\lambda = \sum_\nu [\rho]_{\lambda\nu} j_\nu$. So the resistivity tensor is given by

$$[\rho] \equiv \begin{pmatrix} \rho_{xx} & \rho_{xy} \\ \rho_{yx} & \rho_{yy} \end{pmatrix} = \begin{pmatrix} \rho_0 & -B/(nec) \\ B/(nec) & \rho_0 \end{pmatrix} \tag{1.3}$$

with $\rho_0 = 1/\sigma_0$ and σ_0 is the conductivity given by the Drude formula $\sigma_0 = ne^2\tau_0/m^*$. The conductivity tensor $[\sigma]$ is given by the inverse of the resistivity tensor $[\sigma] = [\rho]^{-1}$. Define the cyclotron frequency ω_c by $\omega_c \equiv eB/m^*c$, the conductivity tensor can be written as:

$$\begin{aligned} \sigma_{xx} &= \sigma_{yy} = \frac{\sigma_0}{1+\omega_c^2\tau_0^2} \\ \sigma_{xy} &= \frac{nec}{B} + \frac{1}{\omega_c\tau_0}\sigma_{xx} \end{aligned} \tag{1.4}$$

Remarkably, it was discovered in 1980 by Von Klitzing *et al.* [1] that, the conductivity tensor $[\sigma]$ takes a step-like form with the plateau value

$$[\sigma] = \begin{pmatrix} 0 & i_I e^2/h \\ -i_I e^2/h & 0 \end{pmatrix} \tag{1.5}$$

or $\rho_{xx} = \rho_{yy} = 0$; $\rho_{xy} = (1/i_I)(h/e^2)$. Here $i_I = 0, 1, 2, \cdots$. The quantization of σ_{xy} (ρ_{xy}) with extremely high accuracy, and the vanishing of σ_{xx} and σ_{yy} can not be explained by the semiclassical transport theory. A full quantum theory is needed to understand this phenomena. A brief resumé of it will nw be given.

In the Landau gauge, the 2D vector potential is $\vec{A} = \vec{B} \times \vec{r} = (-yB, 0)$. The Schrodinger equation for the wave function ψ is

$$\frac{\hbar^2}{2m}[(\frac{1}{i}\frac{\partial}{\partial x} - \frac{eB}{\hbar c}y)^2 - \frac{\partial^2}{\partial y^2}]\psi = H_0\psi = E\psi \tag{1.6}$$

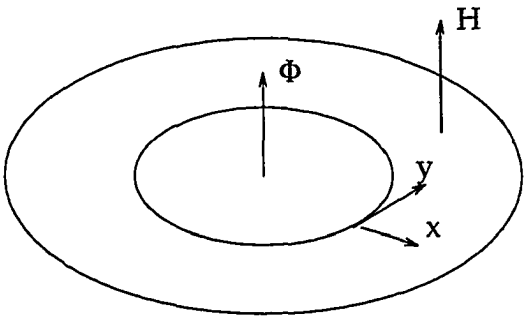

Figure 1.1: Corbino disk in Laughlin's gauge principle argument of IQHE.

The eigenfunctions are

$$\psi_{nk} = e^{ikx} H_n(\frac{y - y_0(k)}{l_0}) e^{-[y-y_0(k)]^2/2l^2} \tag{1.7}$$

Here $y_0(k) = l^2 k$ and $l_0 = \sqrt{\hbar c/eB}$ is the magnetic length. The eigenenergy of the single electron state ψ_{nk} is: $E_{nk} = \hbar\omega_c(n + 1/2)$. For the Landau level n, the degeneracy per unit area is $n_B = 1/(2\pi l^2) = eB/(hc)$

This degeneracy is lifted by effects of impurities. It is believed [4, 5] that the Landau level is broadened so that only the states closest to the center of the Landau levels are extended, others are localized states. So in the plateau region, the Fermi level is in the localized region (mobility gap), there is no longitudinal current, *i.e.* $\sigma_{xx} = 0$. The quantization of transverse conductivity $\sigma_{xy} = i\frac{e^2}{h}$ at integer i can be understood from Laughlin's gauge principle argument [6, 7]. Since QHE is a bulk effect, it is independent of the geometry we choose. In this argument, we will use a Corbino disk as shown in Fig.1.1. If we adiabatically increase one flux unit $\Delta\Phi = hc/e$, in the disk each filled Landau level has one electron move from the outer edge to the inner edge of the system. There will be a change of energy $\Delta\varepsilon = eE_xL$ for

each electron, where L is the distance between the outer edge and inner edge of the disk. The current density due to each electron is obtained from its energy change [6, 7]

$$j_y = \frac{c}{L}\frac{\partial \varepsilon}{\partial \Phi} = \frac{e^2}{h}E_x \tag{1.8}$$

So if i is the number of Landau levels under the Fermi surface, the Hall conductance is $\sigma_{xy} = i\frac{e^2}{h}$, and thus σ_{xy} changes in a step-wise fashion as i changes from one integer to the next.

1.2 Fractional Quantum Hall Effect

The discovery of the FQHE in 1982 by Tsui *et al.* [2] reveals more surprising phenomena in that σ_{xy} is quantized at special *odd*-denominator rational fractions. The transport properties of a system showing FQHE are very similar to the IQHE, except that the quantization takes places at fractional values: p/q (q is an odd integer).

At the root of the quantization in the IQHE is a set of special electron densities, $\nu = i(eB)/(hc)$, where i Landau levels are exactly filled and there is a finite gap of the excitation spectra *i.e.* the fluid is *incompressible* [8]. This suggests that if there is some mechanism that selects special filling fractions at which the excitations inquire a finite gap, then the FQHE can be understood similarly as IQHE. We expect that this *incompressibility* at special filling fractions is due to electron-electron interaction.

The incompressible states of FQHE at *fundamental* filling fractions $\nu = 1/m$ (m is odd integer) were first described by Laughlin using his celebrated

variational Laughlin wavefunction [8]

$$\Psi_m(z_1, z_2, \cdots, z_N) = \mathcal{N} \prod_{i<j}^{N} (z_i - z_j)^m e^{-(\sum_i |z_i|^2)/4l_0} \tag{1.9}$$

Here $(z_1, \cdots, x_N)$ are the 2D coordinates of the electrons confined to the x-y plane expressed as complex variables: $z_j = x_j + iy_j$. This wavefunction has proven very successful in describing the properties of electronic ground states of FQHE, such as the ground state energies, the quasiparticles, and the strong electron-electron correlations.

Various theories for FQHE at other filling fractions were developed based on Laughlin's theory for $\nu = 1/m$. One is the hierarchy theory developed by Haldane [9], Laughlin [10], and Halperin [11] more or less independently. In this theory, the incompressible states of FQHE at other filling fractions result from condensation of quasipaticles into Laughlin states for $\nu = 1/3$. The shortcoming of this theory is that it is difficult to compare stabilities of the FQHE at different filling fractions. A more recent theory was given by Jain [12, 13, 14], in which he suggests that the stability of FQHE at different filling fractions can be understood using condensation of "composite Fermions" (an object consisting of an electron bound with one or more flux). Although this binding of electrons and fluxes into composite Fermions has never been justified theoretically, it is under investigation experimentally and it is supported by very recent experiments [15], which measured the effective mass of the composite Fermions.

In the theoretical studies of FQHE, the effective field theory with a Chern-Simons [16] term (topological mass term [17]) or the Chern-Simons field theory (CSFT) [18, 19] plays a very important role. Like the Ginzburg-

Landau theory in superconductivity, many of the results obtained by "microscopic" theory or numerical studies can be rederived very efficiently by CSFT [20, 21, 22]. CSFT has been used to obtain many useful insights and predictions that can not be obtained easily from other approaches [23, 24, 25, 26, 27, 28, 29, 30].

Recently, optical properties of FQHE systems were studied experimentally [31, 32, 33, 34]. Correlated with these activities is the extensive effort on theoretical studies on the excitation spectra [35, 36] and linear response functions of the FQHE using the CSFT [23, 26, 37] as well as numerical approaches such as single-mode-approximations (SMA) by Girvin *et al* [38, 39, 36]. Some theoretical studies of optical properties of FQHE systems have also been carried out by Wang *et al* [40], MacDonald *et al*, [41], Alpalkov and Rashba [42], Chen and Quinn [43]. However, because of the intrinsic difficulties of this problem, both the theoretical study of the linear response theory and optical properties are far behind the experimental studies.

Another dimension of this interesting problem appears in *double layer* FQHE systems [44, 45, 46, 47, 48, 49, 50]. Because of the interplay of inter-layer electron-electron interaction, intra-layer electron-electron interaction, and inter-layer tunneling of the electrons, various kinds of novel electronic strongly correlated states were discovered [47, 48, 49, 50], such as the FQHE at *even*-denominator fractions [47, 48]. Theoretical studies [51, 52, 53, 54] of these systems are mostly based on the techniques as well as concepts developed in the study of single layer FQHE.

1.3 Organization of the Thesis (Part I)

In Chapter 2, I will present results of my studies of the Laughlin wavefunctions. The Laughlin wavefuction was first proposed as a *variational* wavefunction using the disk geometry. It was later shown numerically that the Laughlin wavefunctions are extremely good approximations for coulomb interactions in spherical geometry. In the first part of this chapter, I will present numerical proof that the Laughlin wave function is a good approximation in the case of Coulomb interaction in the disk geometry. A naive argument will be given for this. In the second part of this chapter, I will study the ground states for different interactions, and in order to understand the approximate interaction, based on pseudo-potentials for which the Laughlin wavefunction is a good approximation to the ground state.

In Chapter 3, I will give a hierarchy structure of FQHE constructed using the Farey series. The physical basis of this hierarchy structure is the composite Fermion theory. Using this hierarchy structure, a phase diagram of the FQHE is proposed, which differs in certain aspects from other proposed phase diagrams. The use of Farey series is original.

In Chapter 4, the photoluminescence and inelastic resonance Raman scattering of FQHE is studied using spherical geometry. In the first section of this chapter, I study the many-body magneto-exciton system. The two "phases" found for these magneto-excitons depend on the distance d between conduction electrons and valence holes. In the second section of this chapter, the photoluminescence is studied for different values of d. In the third section of this chapter, inelastic Raman scattering is studied.

In Chapter 5, I present a theory of the Fermi-edge-singularities (FES) for double layer FQHE systems. I propose that the FES can be used to detect the gapless neutral mode in these systems.

In Chapter 6 I will conclude the results presented in this part of the thesis and discuss open questions.

Chapter 2

Laughlin's Wave function and the Ground State of FQHE

2.0 Introduction

The Laughlin-*Jastrow* wave function [8] for the ground states at $\nu = 1/m$ (m odd integer) forms the basis of most of the theoretical understanding of the FQHE. However, the validity of these *Jastrow-type* trial wave functions are not well established. Fano *et al.* [55] found that for up to 9 electrons in spherical geometry, the overlap of the Laughlin wave function with the *exact* ground state is exceptionally good. Haldane [3] also showed that for special short range interactions (pseudo-potentials), the Laughlin wave function is the exact ground state. Some support from microscopic Chern-Simon-field-theory (CSFT) can also be obtained provided the associated mean-field solutions are stable [56, 57, 58]. However, the CSFT argument is in the spirit of the *composite fermion* approach [12] namely, that the validity of the Laughlin wave function can be *proved* only if the stability of the mean-field-solution (MFS) (Laughlin wave function) can be justified. In Section 2.3

I will show explicitly how to construct specific models with long or short range interactions for which the Laughlin wave function has *small* overlap with the ground state wave functions. For these specific models, the mean-field-solution is *unstable*, and the Laughlin wave function fails to be a good approximation.

2.1 Formalism and Symmetry Properties in the Disk Geometry

Three geometries [3, 59] have been used in finite-size numerical studies of FQHE: (i) rectangular; (ii) disk geometry; (iii) spherical geometry. The translationally invariant symmetry can be easily conserved in the rectangular geometry, so it was widely used in early studies of the ground state properties. After its introduction by Haldane [9], spherical geometry became more popular because it can keep both translationally and rotational invariance, and the finite-size effects can be minimized.

In this chapter, we will use the disk geometry to study the Laughlin wave function, which we think is a more natural geometry to work with in some cases. And we will show that this geometry has some elegant properties which are analogues to those in the spherical geometry.

Let us first introduce the Hilbert space of wave functions in the lowest Landau level in the disk geometry.

We consider electrons confined to the x-y plane and subject to a magnetic field $B\hat{z}$. In the symmetrical gauge with vector potential $\vec{A} = (B/2)(x\hat{y} - y\hat{x})$, it is convenient to regard the $x - y$ plane as a complex plane, $z = x + iy$,

$\bar{z} = x - iy$, then

$$\partial_z = \tfrac{1}{2}(\partial_x - i\partial_y) \quad \partial_{\bar{z}} = \tfrac{1}{2}(\partial_x + i\partial_y) \tag{2.1}$$

The single-particle normalized eigenfunction in the lowest Landau level can be written as:

$$\varphi_m(z) \equiv |m\rangle = (2\pi 2^m m!)^{-1/2} z^m e^{-|z|^2/4} \tag{2.2}$$

Here m is a non-negative integer. Since $\hat{l}_3 = \hbar\partial_z$, it is easy to see that $\hat{l}_3|m\rangle = m\hbar|m\rangle$. The average area covered by the state $|m\rangle$ can be estimated using $\langle m|r^2|m\rangle = 2(m+1)$.

Here we take the magnetic length $l_0 = \sqrt{\hbar c/eB} = 1$ the Coulomb interaction energy scale is taken as $E_c = e^2/(\epsilon l_0) = 1$ [1] respectively, and we assume no mixing of Landau levels, and ϵ is the dielectric coefficient.

In the disk geometry, different kinds of boundary conditions can be used. One of the frequently used boundary conditions is the open boundary. Using this boundary condition no confining potential is applied except that the total angular momentum L_z is fixed: $\sum_i m_i = S$. An alternative boundary condition is to use a "hard edge" confining potential: $m_i \leq m(N-1)$ for filling fraction $\nu = 1/m$. Also as in the study of quantum dots, a natural confining potential can be used such as harmonic potential. As we will see below the results in this paper are insensitive to the boundary conditions. Since the open boundary conditions are most frequently used and generate the most controversies, we will concentrate on the open boundary condition

[1] Throughout this part of the thesis, the energy and length will be scaled to 1 by E_c and l_0

in this study. However, we will also calculate the overlap of the LWF with the ground state in the closed boundary condition for comparison.

Define an inner product on the N-particle function space $\mathcal{F}_N$ via $(f,g) = \int d\mu[z]\bar{f}[z]g[z]$ with measure $d\mu[z] = \frac{1}{2\pi}\prod_{i=1}^{N} e^{-|z_i|^2/2}dx_i dy_i$. The one-particle eigenfunction can be written as $\phi_m(z) = (2^m m!)^{-1/2} z^m$, *i.e.* absorbing the Gaussian factor into the measure. In this Hilbert space denoted $\mathcal{F}_N$, the two operators $z/2$ and ∂_z are adjoint [60, 61]. The Hilbert space $\mathcal{AF}_N$ is based on the set of homogeneous polynomials $f(z) = \sum_{[k]} a_{[k]} z^{[k]}$, where $[k] = [k_1, k_2, \cdots, k_N]$, $z^{[k]} = \prod_{i=1}^{N} z_i^{k_i}$.

For the FQHE system, the total angular momentum $\hat{L}_z$ is a good quantum number. So the subspace with different total angular momentum S is an invariant of the Hamiltonian. If we restrict the wave function to be translationally invariant, the center of mass carries no angular momentum (see later discussion), and the relation between the magnetic flux N_Φ of the system and the total angular momentum S is $S \sim N_\Phi N/2$, so the filling fractions are given by $\nu = N(N-1)/2S$ [62]. If we relax this constraint of translational invariance, the center of mass will carry angular momentum. The area of the system will increase for a finite disk in comparison to the system with no angular momentum carried by the center of the mass and with the relative coordinate part of electron wave function being the same. Therefor we think this definition of the filling factor is still valid [63]. For later convenience, we will call the total angular momentum S the *total* flux in this paper, and the quanta of angular momentum called flux in the above sense.

In FQHE systems, since the Zeeman energy is relatively large, we can

assume the ground states are fully spin polarized. The spin polarization will be discussed in Section 2.2. In this case, the Hilbert space $\mathcal{AF}_N$ is based on antisymmetric homogeneous polynomials $f(z) = \mathcal{A}\sum_{[k]} a_{[k]} z^{[k]}$ with $\mathcal{A}$ as the anti-symmetrizer. Laughlin proposed a *Jastrow-type* wave function for $\nu = 1/m$ ground states [2]:

$$\Psi_m[z] = \mathcal{N}\prod_{i<j}^{N}(z_i - z_j)^m \tag{2.3}$$

with m being an odd integer to satisfy the antisymmetric condition.

Ψ_m is an eigenstate of $\hat{L}_z$ with eigenvalue of $M = mN(N-1)/2$. For z_i, the highest power is $m(N-1)$, which should be equal to $N_S - 1$ where N_S is the flux number. So for large N, we can obtain the filling fraction for the Laughlin states: $\nu \approx N/N_S \sim 1/m$.

Halperin [64] has shown that the m-fold vanishing of the wave function when two electrons come close helps minimize the Coulomb repulsion. So the Laughlin wave function ties together: the Pauli principle, analyticity, and Coulomb repulsion to select the $\nu = 1/m$ filling fractions.

2.2 Properties of Laughlin Wave Functions in Disk Geometry

Despite the success of the Laughlin wave function in spherical geometry, a criticism of the Laughlin wave function in disk geometry has been given by Tao [65], who argued that the Laughlin wave functions are not good approximations to the ground states for large N in the disk geometry. I will

[2]The gaussian factor is absorbed in the measure, see also Eq. 1.9

first briefly review his argument here, and at the same time introduce the definitions which will be used in this chapter.

The Hilbert space $\mathcal{AF}_N$ has an orthonormal basis set of functions $|[k_i]\rangle$ which can be written in Slater-Determinant (SD) form as:

$$|[k_i]\rangle = \frac{1}{\sqrt{N!}} \prod_{i=1}^{N} \frac{1}{\sqrt{2^{k_i} k_i!}} \begin{vmatrix} z_1^{k_1} & z_1^{k_2} & \dots & z_1^{k_N} \\ z_2^{k_1} & z_2^{k_2} & \dots & z_2^{k_N} \\ \vdots & \vdots & \ddots & \vdots \\ z_N^{k_1} & z_N^{k_2} & \dots & z_N^{k_N} \end{vmatrix} \tag{2.4}$$

where

$$\sum_i k_i \equiv N_S; \quad k_1 > k_2 > \cdots > k_N \tag{2.5}$$

The dimension $\mathcal{D}_N$ of the Hilbert space $\mathcal{AF}_N$ is given by the number of partitions $\{k_i\}$ of N_S with constraint Eq.[2.5]. If we expand the Laughlin wave function in the basis $\{|[k_i]\rangle\}$ of Eq.[2.5], the dimension d_N of Laughlin wave function Ψ_m is defined as the number of nonzero expansion coefficients. It is easy to check: $d_N \ll \mathcal{D}_N$ for $N \gg 5$. For Ψ_m, the largest k_1 is $m(N-1)$, while generally in $|[k_i]\rangle$, the largest k_1 is $mN(N-1)/2 - (N-1)(N-2)/2$. Because of this effect, Tao argued that the distribution of Ψ_m in $\mathcal{AF}_N$ is unphysical [65]. And hence Ψ_m are not good approximations at large N. Since the Coulomb interaction is long range, he claimed that the ground state should be randomly distributed in the basis $\{|[k_i]\rangle\}$.

But, the above arguments might not be correct since the scattering of electrons is coherent, so the ground state wave functions do not necessarily have *random* distribution in the basis $\{|[k_i]\rangle\}$. Furthermore, based on the results we will discuss in the following subsection, we suggest the Laughlin wave

functions is a good approximation because of its unique distributions in the Hilbert space $\mathcal{AF}_N$ and its particular symmetry property. In other words, the Laughlin wave function Ψ_m picks out just those components $\{|[k_i]\rangle\}$ needed to get a coherent superposition of the SD states which yields the minimum energy.

2.2.1 Symmetries in the Disk Geometry

Since the kinetic energy in the lowest Landau level is constant, the Hamiltonian contains only Coulomb interaction:

$$\hat{H} = \sum_{k_1}\sum_{k_2}\sum_{k_3}\sum_{k_4}\langle k_1 k_2|\frac{1}{r}|k_3 k_4\rangle \hat{a}^\dagger_{k_1}\hat{a}^\dagger_{k_2}\hat{a}_{k_4}\hat{a}_{k_3} \tag{2.6}$$

The Hamiltonian matrix element can be written as:

$$\begin{aligned}\langle k_1 k_2|\frac{1}{r}|k_3 k_4\rangle = \delta_{k_1+k_2,k_3+k_4}\sum_{j=0}^{k_1+k_2}\langle k_1 k_2|k_1+k_2,j\rangle \\ \times\langle k_3 k_4|k_1+k_2,j\rangle\frac{\pi^{1/2}}{2^{2j+1}}\frac{(k_1+k_2-j)!(2j)!}{j!}\end{aligned} \tag{2.7}$$

where

$$\langle k_1 k_2|k_1+k_2,j\rangle = \frac{1}{\sqrt{2^{k_1+k_2}k_1!k_2!}}\sum_{\alpha=0}^{j}(-1)^\alpha\binom{k_1}{\alpha}\binom{k_2}{j-\alpha} \tag{2.8}$$

Eqn.(2.7) is similar to the matrix element in spherical geometry [55], when $\langle k_1 k_2|k_1+k_2,j\rangle$ corresponds to the Clebsch-Gordan coefficients. It was previously believed there exists only rotational symmetry in disk geometry (N_S is fixed). Now we will recall that there is an additional symmetry in the disk geometry for any two-body interaction $V(|\vec{r}_1-\vec{r}_2|)$, provided no confining

potential other than the magnetic flux is used (open boundary condition). This symmetry characterizes the motion the *center of mass*. The relevant operator in the stereographic mapping of this symmetry to the spherical geometry is just the total angular momentum L^2.

Define the operators: $\hat{L}^+ = \sum_i \hat{l}_i^+ = \sum_i z_i/2$; $\hat{L}^- = \sum_i \hat{l}_i^- = \sum_i d/dz_i$; and $\hat{C}_2 = \hat{L}^+\hat{L}^-$. Since $(\hat{L}^+)^\dagger = \hat{L}^-$, $\hat{C}_2$ is hermitian and positive definite. The eigenfunctions $f_0[z]$ of $\hat{C}_2$ with eigenvalue 0 have the property $(d/dz_1 + d/dz_2 + \cdots + d/dz_N) f_0[z] = 0$ and thus are translationally invariant N-particle wave functions. The operator $\hat{C}_2$ is just $\vec{P}_{CM}^2$ of the *center of mass*, and corresponds to the total angular momentum in the spherical geometry after stereographic mapping. Since in the open boundary condition, the center of mass can be separated from relative coordinates for any two body interaction $V(|\vec{r}_1 - \vec{R}_2|)$, it is physically easy to see that $\hat{C}_2$ is a good quantum number.

Because of this, we can show that in the spin polarized case, the wave function of the center of mass in the eigenstate has a simple form.

Transform $[z]$ to the normalized Jacobi coordinate $[\zeta]$, *i.e.* $\zeta_1 = \frac{z_1+z_2+\cdots+z_N}{N}$, $\zeta_i = \left[\frac{i-1}{i}\right]^{1/2} [z_i - \frac{1}{i-1}\sum_{j=1}^{i-1} z_j]$ $(i = 2, 3, \cdots, N)$. Since this is a linear transformation, any homogeneous polynomial in $[z]$ of degree S $f[z] = \sum_{[k_i]} a_{[k_i]} z^{[k_i]}$ will be transformed to a homogeneous polynomial in $[\zeta]$ of degree S $f[\zeta] = \sum_{[k_i']} b_{[k_i']} \zeta_1^{k_1'} \zeta_2^{k_2'} \cdots \zeta_N^{k_N'}$. From the definition of $\hat{C}_2$, we see that $\hat{C}_2 f[\zeta] = \sum_{[k_i']} N k_1' b_{[k_i']} \zeta_1^{k_1'} \zeta_2^{k_2'} \cdots \zeta_N^{k_N'}$. So the eigenfunction of $\hat{C}_2$ must be in the form: $f[z] = (z_1 + z_2 + \cdots + z_N)^k g^{S-k}[z]$ where $g^{S-k}[z]$ is an antisymmetric homogeneous polynomial of degree $S - k$ and is translational invariant since $\hat{C}_2 g^{S-k}[z] = 0$. This result gives nothing but the separation of the center of

mass and relative coordinates, which is physically transparent.

2.2.2 Properties of Laughlin States

The decomposition coefficients of LWF at $\nu = 1/m$ defined by $\Psi_m[z] = \sum_{[k]} a_{[k]}|[k_i]\rangle$ can be calculated using the following equations [65]:

$$\begin{aligned} a_{[k]} &= \mathcal{N}[k_1 \cdots k_N]^{1/2}(-)^{mN(N-1)/2} \\ &\sum_{m_i(j)}{}' \prod_{\substack{m_i(j) \\ 1\le i<j\le N}} \left[\frac{(-)^{m_i(j)}m!}{(m-m_i(j))!m_i(j)!}\right] \end{aligned} \tag{2.9}$$

where $\mathcal{N}$ is the normalization factor and the prime on the summation denotes the following conditions on $m_i(j)$:

$$\sum_{j=i+1}^{N} m_i(j) + \sum_{j=1}^{i-1}(m - m_i(j)) = k_i \tag{2.10}$$

The coefficients were calculated for N up to 9 using a recursive procedure. Using these coefficients, we have calculated the density distributions, the distribution of angular momentum, and the renormalized density-density correlation function

$$g(r) = \frac{\langle\rho(r)\rho(0)\rangle}{\langle\rho(r)\rangle\langle\rho(0)\rangle} \tag{2.11}$$

for the LWF for different number of particles [see Fig.2.1]. From our calculations [see Fig.2.1 for some of the results], it can be seen that our calculated properties of the LWF for small number of electrons at $\nu = 1/3$ are very similar to that of the Monte Carlo results [66, 67] for large N, where the finite size effect of LWF at $\nu = 1/5, 1/7$ are more severe.

We have also calculated the exact numerical wave function using the configuration interaction (CI) method [55]. Our results for $\nu = 1/3$ are

Table 2.1: Comparison of LWF with the numerical exact ground state at $\nu = 1/3$.
E_0 is the energy of the LWF, E_{exact} is the energy of the exact ground state, $\langle\psi_0|\psi_{exact}\rangle$ is the overlap of the LWF and exact ground state wave function. (a) disk geometry with open boundary condition; (b) spherical geometry; (c) disk geometry with closed boundary condition.

(a) disk geometry with open boundary condition

N	Dimension of $\mathcal{AF}_N$	Dimension of LWF	E_0	E_{exact}	$\langle\psi_0\|\psi_{exact}\rangle$
3	7	5	0.23977	0.23884	0.9910
4	34	16	0.32765	0.32643	0.9788
5	192	59	0.40614	0.40545	0.9850
6	1206	247	0.47740	0.47669	0.9827
7	8033	1111	0.54318	0.54214	0.9616

(b) spherical geometry*

N	Dimension of $\mathcal{AF}_N$	E_0	E_{exact}	$\langle\psi_0\|\psi_{exact}\rangle$
3	5	-0.50378	-0.50378	1
4	18	-0.47482	-0.47502	0.9980
5	73	-0.45940	-0.45951	0.9991
6	338	-0.44995	-0.45017	0.9964
7	1656	-0.44352	-0.44374	0.9964
8	8512	-0.43887	-0.43909	0.9954
9	45207	-0.43534	-0.43559	0.9941

* Our results agree with that in Fano *et. al* [55].

(c) disk geometry with closed boundary condition†

N	Dimension of $\mathcal{AF}_N$	E_0	E_{exact}	$\langle\psi_0\|\psi_{exact}\rangle$
3	5	0.23977	0.23909	0.9936
4	18	0.32765	0.32666	0.9831
5	73	0.40614	0.40560	0.9882
6	338	0.47740	0.47684	0.9861
7	1656	0.54318	0.54232	0.9683
8	8512	0.60466	0.60388	0.9721

† Our results agree with that in [68].

Table 2.2: Comparison of LWF with the numerical exact ground state at $\nu = 1/5$ and $\nu = 1/7$ on open boundary disk geometry

ν	N	Dimension of $\mathcal{AF}_N$	Dimension of LWF	E_0	E_{exact}	$\langle\psi_0\|\psi_{exact}\rangle$
$\frac{1}{5}$	3	19	13	0.18492	0.18416	0.9854
	4	169	76	0.25230	0.25085	0.9475
	5	1747	521	0.31332	0.31232	0.9397
$\frac{1}{7}$	3	37	25	0.15564	0.15526	0.9895
	4	478	213	0.21205	0.21111	0.9566

listed in Table 2.1. For other $1/m$ such as $1/5$ and $1/7$ all the results are similar, so we only list in Table 2.2 some results in the open boundary disk geometry. The ground state energies for $N \leq 5$ in the disk geometry with open boundary condition were calculated in Ref. [69] and agree with our results in Table 2.1(a). Table 2.1(b) agrees with that in Fano *et al* [55]. The overlap of the ground states with the LWF in disk geometry with closed boundary were calculated by Dev and Jain [68] for $N = 6, 7, 8$, but their results agree with that in our Table 2.1(c).

2.2.3 A Naive argument for the Laughlin Wave Function

From Table 2.1, we can see that our results are quite different from that of Tao [65], whose result for the overlap at $\nu = 1/3$ is: 0.99, 0.979, 0.955, 0.938 respectively for $N = 3, 4, 5, 6$; and the overlap he estimated for $N = 7, 8$ is 0.90 and 0.88. In our result the overlap of LWF with the exact ground states is 0.962 for $N = 7$, still very good for $N = 7$. And there is no sign of exponential decaying of the overlap with increasing N. However, one question which was

Table 2.3: Comparisons of Tao's results and our calculation results. $\langle\psi_0|\psi_{exact}\rangle_1$ is the overlap of LWF with the exact ground state wave function calculated by Tao; $\langle\psi_0|\psi_{exact}\rangle_2$ is that calculated by us.

N	$\langle\psi_0\|\psi_{exact}\rangle_1$	$\langle\psi_0\|\psi_{exact}\rangle_2$
3	0.99	0.991
4	0.979	0.9788
5	0.955	0.9850
6	0.938	0.9827
7	0.90*	0.9616

* This is an extimated value.

raised in Ref.[65] needs to be answered in the open boundary disk geometry. First, we recall that the space of LWF is much smaller than $\mathcal{AF}_N$. Then, comparing the diagonal Hamiltonian matrix element for different SD states, we note that many missing components (*i.e.* missing SD states) in LWF have comparable or low expectation value of energy to those SD states included in the LWF. Hence, why is the LWF a good approximation to ground states?

Although the LWF occupies only a small part of the Hilbert space $\mathcal{AF}_N$, it occupies a large portion of the SD states with $k_1 \leq m(N-1)$; these are globally energetically more favorable. There are some SD states in the LWF which have small diagonal Hamiltonian matrix elements, which are distributed in the region of $k_1 > m(N-1)$. Translational invariance is a strong constraint for the eigenfunctions, as it requires: $(\sum_i d/dz_i)\sum_{[k_i]} a_{[k_i]} z_1^{k_1}\cdots z_N^{k_N} = 0$. So the coefficients of the neighboring SD are strongly correlated. For the translationally invariant eigenstates, the most inexpensive way (lowest energy) is if all the electrons are grouped into the part of $k_1 \leq m(N-1)$ consistent with all constraints. For $\nu = 1/m$, the electrons can easily adapt to this kind of

ground state. So the ground state wave functions are translationally invariant ($C_2 = 0$). For the excited translationally invariant eigenstates, because of the constraint, the wave functions can not clump together in the same way as for the LWF, so they must have small overlap with the LWF. Moreover, all the other eigenstates with a different value C_2 of $\hat{C}_2$ are orthogonal to the LWF. Since the eigenstates of the Hamiltonian are a complete orthonormal basis, and all the excited states either are orthogonal to, or have small overlap with the LWF, the ground state must have large overlap with LWF. To demonstrate this in a example, we show in Fig.2.2 the components of the 4 lowest translationally invariant wave functions for system of $N = 4$ at $\nu = 1/3$. They are calculated using direct diagonalization of the Hamiltonian matrix. Apparently the figures confirm our above statement.

From this argument, we can speculate that if we add one more flux to the system, then the most energetically inexpensive way for electrons to adapt to each other in the presence of this extra flux, is to let the center of mass have one flux, *i.e.* $C_2 = 1$, and the translationally invariant part of the wave functions enjoy the rest of it. And actually this is the case.

In Fig. 2.3 we show the diagonal matrix elements of SD states together with the coefficients of the LWF and exact ground state wave functions for $N = 5$. The "index" $I_{[k_i]}$ of the SD is defined as $I_{[k_i]} = \sum_i 2^{k_i}$. The values on the x-axis are the (reverse) ordinal number of index (not the index itself). For example, for $N = 3$, the index of $|6, 3, 0\rangle$ is $2^6 + 2^3 + 2^0 = 73$ while the (reverse) order is 3. In table 2.4, the index and (reverse) ordinal number of all the SD states for $N = 3$ is listed. So in space $\mathcal{AF}_N$ for $\nu = 1/3$

Table 2.4: Index and (reverse) ordinal number of the SD states for $N = 3$.

SD State $\|\{k_i\}\rangle$	$I_{[k_i]}$	ordinal number
$\|8,1,0\rangle$	259	1
$\|7,2,0\rangle$	133	2
$\|6,3,0\rangle$	73	3
$\|6,2,1\rangle$	70	4
$\|5,4,0\rangle$	49	5
$\|5,3,1\rangle$	42	6
$\|4,3,2\rangle$	28	7

the SD state with the largest (reverse) order is $|2N-2, 2N-3, \cdots, N-1\rangle$ since it has the smallest index; the SD state with (reverse) order 1 is $|S-(N-1)(N-2)/2, N-2, N-3, \cdots, 0\rangle$ since it has the largest index. In the Fig. 2.3, we subtract the average of the diagonal energy matrix elements from the diagonal energy matrix elements. From Fig.2.3 we can see that the LWF has only components in the "valley" region of the energy "potential". For the exact ground states, the dominant parts are also located in the "valley" region. The coefficients are very small for $k_1 > m(N-1)$ and can be thought of as the "tail" of the dominant states. Another fact to support this argument is that the overlap of the LWF with the exact ground state wave function using the closed boundary condition [see Table 2.1(c)] (within a much smaller space) is approximately the same as that with an open boundary condition [see Table 2.1(a)].

2.2.4 Discussion of Large N Systems

With increase of N, the portion of occupied SD components in the subspace of $k_1 \leq m(N-1)$ will decrease. However, most missing states have the property that $k_N + k_{N-1} < m$ or the index of the SD states is larger than that of state $|3N-3, 3N-6, \cdots, 0\rangle$, *i.e.* the boundary region between the "valley" and "hill" [see Fig. 2.3], and thus have larger energy. Since the ground states and LWF will occupy the same area and all excited states with translationally invariant property have a different dominant region in the Hilbert space $\mathcal{AF}_N$, therefore they have small overlap with LWF. We can conclude that the overlap of ground states with the LWF will decrease very slowly. This can be seen from Table 2.1.

From the above arguments, we suggest that the two properties such as: **translational invariance** and $\mathbf{k_1 \leq m(N-1)}$ make the LWF a good approximation to the ground state even at large N. From Fig.2.1 we can see that the density-density correlation function $g(r)$ for small N is quite similar to large N Monte Carlo results [66, 67]. Since the the density-density correlation function $g(r)$ is relevant to the total energy of the state, we think this similarity supports our suggestion. To check this in a different fashion, we use some analytic relations discovered by Dunne [70] for the LWF decomposition on SD states. In Laughlin states, there are simple formulae for some physically significant states. For example:

(LN1) the uniformly distributed states $|3N-3, 3N-6, \cdots, 0\rangle$ have coefficient 1;

(LN2) the most bounded states $|2N-2, 2N-3, \cdots, N-1\rangle$ have coefficient

$(2N-1)!!$;

(LN3) the states which are made from "squeezing" the innermost and outermost electrons in LN1 by 1 $|3N-4, 3N-6, \cdots, 3, 1)$, has coefficient $3 \cdot 2^{N-2}$;

(LN4) the state which is the most bounded states of $N-1$ electrons, has coefficient $(2N-3)!!$.

It is easy to see that for small N the most compact state which is LN2 has the largest weight in LWF, and the uniform state has the smallest weight. This is reasonable since the small droplet has the lowest energy because of the strong exchange "interaction". In Fig.2.4, we draw the Hamiltonian matrix elements for two particles, and from it we can see that a two particle pair has lowest energy when the electrons are near each other. When their separation is larger than 5 or 6 orbits (magnetic length), the electrons then repel each other, but the magnitude of the potential decreases very slowly (since the interaction is Coulombic). So, it is energetically unfavorable to form a large droplet. *With the number of electrons N increasing from the small to the large limit, we expect the ground states will transform from small droplet (small N) to separated small droplets (medium N), then to uniform distribution in the thermodynamic limit.* To check the changing of the weights of the above mentioned components in LWF, we calculated the coefficients for different N [see Fig.2.5] and the expectation value of energy in each of these states. The turnover of these coefficients with the energies is clearly shown in Fig.2.5.

2.2.5 Energy Cusps in Disk Geometry

Several groups studied the cusps in the dependence upon filling factors in the disk geometry, and some controversy still exists. Our calculation for the spin polarized systems agrees with that of Girvin and Jach [71] and also is similar to results in rectangular geometry [72]. There are global downward cusps at $\nu = 1/3, 3/7, 3/11$ [see Fig.2.6], and the ground state energies for the filling factors with one more flux than that at "magic" numbers are equal to the ground state energy at the "magic" fillings. This is easy to understand: since at each magic filling, the electrons can find a significant way to lower the energy, when one more flux is added to this system, this flux can be "carried" by the center of mass of this finite system. Hence the residual part will be the same, and so is the ground state energy. We calculated the full spectrum at some magic filling fractions and their neighbors, the results confirm our statement. In Govari *et al*'s calculations [69], they removed the center of mass degree of freedom. The ground states at the magic fillings are translationally invariant, but for neighboring states with one more flux, the ground states are not translationally invariant. What they calculated are translationally invariant excited states. So they obtained much deeper downward cusps in their "ground state" energy, because they were comparing ground state energy at magic filling and excited state energy of its neighboring filling fraction with one more flux, rather than comparing to *ground* state energy with one more flux.

Various theories use the concept of "binding" of an electron with the fluxes to explain the incompressibility of the system at magic filling numbers.

We offer this view of the "binding" for the incompressible states. "Binding" means that at stable energy (*i.e.* locally minimum) energy a simple algebraic relation can be found between the number of electrons and the number of fluxes. When such an algebraic relation is possible, the electrons can find a significant way to adapt themselves to a low energy ground state. Increasing (or decreasing) one flux in the system makes it energetically expensive for electrons to adapt to another *translationally invariant* state. Since in the thermodynamic limit, the changing of flux is equivalent to exciting one quasiparticle, there is a gap for the excitations in these incompressible states, *i.e.* a finite energy cost.

As found in the literature [71, 73, 69], the magnitude of the step of the downward cusps in the figure [Fig. 2.6] of ground state energy vs flux is 4 flux for $N = 4$. More generally [71, 73], the step of the downward cusps for N-electron system is N, *i.e.* the location of the downward cusp can be written as:

$$\nu = \frac{N-1}{N-1+2k} \tag{2.12}$$

where k is a positive integer. Note here the magic numbers for systems with different number of electrons are different. We think this is a finite system effect. For all the finite systems, there are downward cusps located at $\nu = 1/m$ with m an odd integer, which suggests the $\nu = 1/m$ is a significant stable incompressible state. For N-electrons the states with flux deviating by kN from the flux of $\nu = 1/m$ states are also located at downward cusps. A naive explanation is that the addition or removal of kN flux quanta can be easily distributed to N electrons, so the system has a relatively stable

translationally invariant ground state, and its neighbor with one more flux has *non-translationally invariant* ground state, and so forms a downward cusp.

The ground states at "magic" filling of different origin (hierarchy level [74]) have quite different stability [for example, see below the discussions about the spin polarization of the ground states]. For finite N, many states at these downward cusp filling fractions are not incompressible states when passing to the thermodynamic limit (for example downward cusps can take place at *even-denominator* filling fractions for finite N). However we suggested [74] that all states at odd-denominator filling fractions are incompressible states in the thermodynamic limit without disorder. We think the gaps of the excitations for states at some magic fillings such as $\nu = 1/m$ are stable against disorder while gaps at other filling fractions are unstable against disorder. The hierarchy structure can be constructed using the algebraic mappings between different filling fractions [75] and Farey series [74] as shown below in Chapter 3.

2.2.6 Spin polarization

In our discussions so far, we have assumed the Zeeman energy is large enough so that the spin is fully polarized. If we restore the spin degree of freedom (assume the Zeeman energy is zero), the electrons will have more freedom to arrange themselves. Chang and Chakraborty [76] studied the ground state for $N = 4$ using rectangular geometry at some magic filling factors. They found that the spectrum is independent of S_z, but depends on the total spin

operator S_{tot}. The ground states for $\{1/3\}$, $\{2/7, 2/5\}$, $\{4/13, 4/11, 4/9\}$ are respectively states with $S_{tot} = 2$, 0, 1.

Our results in the disk geometry show the same properties. The spectrum for $N = 4, S_z = 0$ at $\nu = 1/3$ are shown in Fig.2.7. The spectrum for $S_z = 1$ can be easily obtained from Fig.2.7 by extracting the $S_{tot} = 2, 1$ part, for $S_z = 2$ by extracting the $S_{tot} = 2$ part. The degeneracy in S_z can not be split by the electron-electron interaction, which is consistent with Kohn's theorem [77] which states that: in a translationally invariant electron gas subject to a magnetic field, the collective density mode has a zero-momentum gap ω_c (cyclotron frequency) which is independent of the electron-electron interaction. According to Kohn's theorem (generalized to the spin-density mode [78]), the gap $\Delta(\omega = 0)$ for the lowest Landau level spin density wave must equal the Zeeman energy. If there is non-degeneracy in S_z, then $\Delta(\omega = 0)$ can not equal the Zeeman energy. It is also natural, that for $\nu = 1/m$, the ground states are spin polarized. But for other filling fractions the spectrum can find a more energetically favorable configuration by adjusting the spin degree of freedom. Fig.2.6 shows that the ground state energy has no downward cusps for systems with $S_z = 0$. In real systems, the magnetic field will make the electron systems polarized and incompressible at the magic filling.

2.3 Pseudopotentials and the Laughlin Wave Function

In this section, I will formulate this many-electron problem in relative electron coordinates to give a better understanding of the Laughlin wave func-

tion. Define $\hat{X}_m(l,j)$ as the annihilation operator of an electron pair (i,j) in the state $|k_i + k_j, m\rangle$ with wave function $\mathcal{N}(z_i + z_j)^{k_i+k_j-m}(z_i - z_j)^m$. The Hamiltonian [2.6] can be rewritten as

$$\hat{H} = \sum_{i,j}\sum_{m} V_m \hat{X}_m^{\dagger}(i,j)\hat{X}_m(i,j) \tag{2.13}$$

Where $V_m = \langle k_i + k_j, m|V(|r_i - r_j|)|k_i + k_j, m\rangle$ is the *pseudopotential* first introduced by Haldane [9]. The pseudopotential for Coulomb interaction and for logarithmic interaction are shown in Fig.[2.8].

In this section, we will only study the spin polarized system. Only the V_m with m odd are relevant. Since for any electron pairs, the wave function must be anti-symmetric, only states $|k_i + k_j, m\rangle$ with odd m are nonzero. Haldane showed [79] that the Laughlin wave function Ψ_n is the exact ground state for the following interactions

$$V_m > 0 \ (m \leq m_0) \text{ and } V_m = 0 \ (m > m_0)$$

with condition $m > m_0$. Although this potential represents ultra-short range interactions, it is encouraging that the Laughlin wave function is the exact ground state for any number N of electrons. Since we showed in the last section that the Laughlin wave functions are good approximations for long-range interactions like the Coulomb interaction, it is reasonable to speculate that they will be good approximations for some other general interactions. It has been claimed [57] the Laughlin wave function is a *universal* ground state at least for short range interaction.

However, counter examples which demonstrate that Laughlin wave functions are not good approximations can be easily given. For example, in the harmonic interaction model [71] with $V(|\vec{r}_1 - \vec{r}_2|) = a^2|\vec{r}_1 - \vec{r}_2|^2$, the Laughlin

wave functions are eigenstates having *largest* eigenvalue of the Hamiltonian. Numerous examples can be artificially constructed by making $V_m > 0$ ($m > m_0$) sufficiently strong. Fig.[2.9] shows the overlap of Laughlin wave function at $\nu = 1/3$ with exact ground states when we turn on longer range interactions than V_1. The interactions are chosen as follows: suppose the Coulomb potential is decomposed to pseudopotentials $V_{coulomb} \equiv \{c_0V_0, c_1V_1, \cdots\}$, and the interaction $V^{(k)}(x) \equiv \{c_1V_1, xc_3V_3, \cdots, xc_kV_k\}$ is defined using parameter x to control the strength of the perturbation added to c_1V_1. My result from Fig.[2.9] is that the Laughlin wave function has very small overlap with the ground state wave function for interaction $V^{(3)}(1)$. In this case, the interaction is still short range and c_1V_1 is still stronger than c_3V_3. Another interesting result is that after we turn on a longer range interaction than V_3, the overlap of the LWF with the exact ground state will be improved. A natural question is then: for what kind of interaction is the Laughlin wave function favored? This question will be answered below in Section 2.3

2.3.1 A New Basis

Here we will introduce a new (over)complete basis for the translationally invariant functions in Hilbert space $\mathcal{A}\mathcal{H}_N$. The basis functions are written as [3]

$$f_{\{m_{ij}\}}[z] = \mathcal{A}\prod_{i<j}(z_i - z_j)^{m_{ij}} \tag{2.14}$$

where $\mathcal{A}$ is the anti-symmetrizer and $\sum_{i<j} m_{ij} = N_s \equiv mN(N-1)/2$, with m_{ij} a positive integer.

[3] See footnote 1 in page 14

Using the Jocobi coordinate representation of $f_{\{m_{ij}\}}[z]$, it is easy to see that the basis $f_{\{m_{ij}\}}[z]$ is overcomplete, and then, the following properties can be used to reduce the number of $\{m_{ij}\}$.

i) The basis $f_{\{m_{ij}\}}[z]$ with $m_{ij} \geq 1$ is (over)complete.

Proof: Any translationally invariant anti-symmetric polynomial can be written as

$$\begin{aligned} f[z] &= \prod_{i<j}(z_i - z_j) \times \{symmetric\text{-}function\} \\ &= \prod_{i<j}(z_i - z_j)\mathcal{S}\sum_{\{p_{ij}\}}(z_i - z_j)^{p_{ij}} \\ &= \sum_{\{p_{ij}\}}\prod_{ij}(z_i - z_j)^{p_{ij}+1} \end{aligned}$$

Here $\mathcal{S}$ is the symmetrizer and p_{ij} is some positive integer.

ii) if $\sum_{i<j} m_{ij} = N_s \equiv mN(N-1)/2$, and $m_{ij} \geq m-1$, then $f_{\{m_{ij}\}}[z]$ can be written as $C\prod_{i<j}(z_i - z_j)^m$.

Proof: Since $m_{ij} \geq m-1$ and m is odd, define $p_{ij} \equiv m_{ij} - (m-1)$. Then

$$\mathcal{A}\prod_{i<j}(z_i - z_j)^{m_{ij}} = \prod_{i<j}(z_i - z_j)^{m-1}\mathcal{A}\prod_{i<j}(z_i - z_j)^{p_{ij}}$$

However as in the last proof:

$$\mathcal{A}\prod_{i<j}(z_i - z_j)^{p_{ij}} = \prod_{i<j}(z_i - z_j)\sum_{\{\Delta_{ij}\}}(z_i - z_j)^{\Delta_{ij}}$$

since $\sum_{i<j} p_{ij} = N(N-1)$,

so $\sum_{i<j}\Delta_{ij} = \sum_{i<j} p_{ij} - N(N-1) = 0$,

result $\Delta_{ij} \equiv 0$ (since $\Delta_{ij} \geq 0$),

i.e. $\mathcal{A}\prod_{i<j}(z_i - z_j)^{m_{ij}} = C\prod_{i<j}(z_i - z_j)^m$.

From (ii), we can easily obtain that for such electron-electron interaction that $V_p > 0$ $(p < m)$ and $V_p = 0$ $(p \geq m)$, the Laughlin wave function Ψ_m is the unique *non-degenerate* ground state wave function.

iii) The following *Anzatz* is very useful for later discussions but I can not prove it at the present time for general N [4].

Ansatz: for translationally invariant anti-symmetric polynomials of degree $mN(N-1)$ *(m odd integer), the basis* $f_{\{m_{ij}\}}[z] = \mathcal{A}\prod_{i<j}(z_i - z_j)^{m_{ij}}$ *with* m_{ij} *is odd integer, is overcomplete.*

2.3.2 A Non-Variational Argument for the Laughlin Wave Function

Since for an interaction $\tilde{V}$: with pseudopotential $V_p > 0$ $(p < m)$ and $V_p = 0$ $(p \geq m)$, the Laughlin wave function is the *non-degenerate* ground state wave function, Haldane suggested [79] one might treat the residual part of the *real* interaction as a perturbation to $\tilde{V}$. The nice point is that V_p with $(p < m)$ are always the largest for the natural repulsive interactions. It is natural to think that additional longer range interactions will perturb the ground state further and make the overlap of LWF with ground state smaller. However, from Fig.[2.9], we observe that the longer range pseudopotentials can make the Laughlin wave function converge *better* to the ground state, contrary to an expectation that these V_p for $p \geq m$ would worsen the convergence. Below I will give some explanation of this phenomenon,

Let's first expand $f_{\{m_{ij}\}}[z]$ according to $(z_1 - z_2)$, for two fixed electrons

[4] Verification of this Ansatz for $N = 3, 4, 5$ can be given numerically.

1 and 2.

$$(z_1 - z_2)^{m_{12}} \prod_{i \neq 1,2} (z_1 - z_i)^{m_{1i}} (z_1 - z_i)^{m_{1i}} - (z_1 \longleftrightarrow z_2)$$
$$= g_0(\frac{z_1 + z_2}{2}, [z'])(z_1 - z_2)^{m_{12}} + g_2(\frac{z_1 + z_2}{2}, [z'])(z_1 - z_2)^{m_{12}+2}$$
$$+ \cdots + g_{2l}(\frac{z_1 + z_2}{2}, [z'])(z_1 - z_2)^{m_{12}+2l} \quad (2.15)$$

where m_{12} is odd, $l = [\sum_{i>2}(m_{1i} + m_{2i})/2]$, and $g_i(\frac{z_1+z_2}{2}, [z'])$ are translationally invariant polynomials with $[z'] \equiv \{z_3, \cdots, z_N\}$. The coefficients g_i contain the information on the distribution function of the relative angular momentum of electron pairs. Then the interaction $V(1,2)$ operating on Eq. [2.15] gives:

$$V_{m_{12}} g_0(\frac{z_1 + z_2}{2}, [z'])(z_1 - z_2)^{m_{12}} + V_{m_{12}+2} g_2(\frac{z_1 + z_2}{2}, [z'])(z_1 - z_2)^{m_{12}+2}$$
$$+ \cdots + V_{m_{12}+2l} g_{2l}(\frac{z_1 + z_2}{2}, [z'])(z_1 - z_2)^{m_{12}+2l} \quad (2.16)$$

Now let us discuss $\nu = 1/3$ at $N = 5$ as an example. For $\nu = 1/3$, the *average* m_{ij} is 3. If only $V_1 > 0$, and $V_p = 0$ (for $p > 1$), then we know the Laughlin wave function Ψ_3 is a non-degenerate ground state with eigenenergy $E = 0$. Fig.[2.10] shows the distribution functions of the relative angular momentum of the electron pairs. If we turn on V_3 gradually, then $|\langle \Psi_3 | \Psi_{exac} \rangle|$ will decrease gradually (see Fig.[2.9]), since lower energy states than Laughlin wave function $|\Psi_3\rangle$ can be found by decreasing $P(3)$ while at the same time increasing $P(1)$, $P(5)$ (see Fig.[2.11]). If we turn on V_5 ($V_5 < V_3$) at the same time, the effects of V_5 is to make the increase of $P(5)$ energetically more expensive, so the combined effect of V_3 and V_5 is to make the ground state wave function converge better to the Laughlin

N	Potential $V(r)$	$\lvert\langle\Psi_3\lvert\Psi_{exact}\rangle\rvert$
5	$1/r$	0.9850
	$-logr$	0.9425
	$\exp(-1.5r^2)$	0.9898
	$\exp(-2.0r^2)$	0.9966

Table 2.5: Overlaps of Laughlin wave function with the ground state for different interactions.

wave function. A naive way to think is that the pseudopotential V_m mostly influences the probability $P(m-1)$, $P(m)$ and $P(m+1)$ in the ground state (see Fig.[2.11]). The effect of V_3 is to make the ground state Ψ_{exac} deviate from the Laughlin wave function by decreasing $P(3)$ and increasing $P(1)$ and $P(5)$ of the ground state, while the V_5 will make the increase of $P(3)$ and $P(7)$ and simultaneous decrease of $P(5)$ energetically more favorable. So a considerable V_5 will make the ground state converge better to the Laughlin wave function. Using the same logic, the V_7 will compensate the deviation due to V_5, etc. This is the reason for the results demonstrated in Fig.[2.9].

A conjecture is that the Laughlin wave function is a good approximation for electron-electron interactions such that V_p are in decreasing order which is fast enough especially at the turning point $p = m$ for $\nu = 1/m$, *i.e.* $V_{m-2} \gg V_m$. Table [2.5] shows the overlaps for different interactions for $N = 5$ at $\nu = 1/3$. From Table [2.5], we can see that the Laughlin wave function is a better approximation for the Coulomb potential than for the logarithmic potential. The Laughlin wave function is also a good approximation to the ground state for the Gaussian potential with short enough decay length.

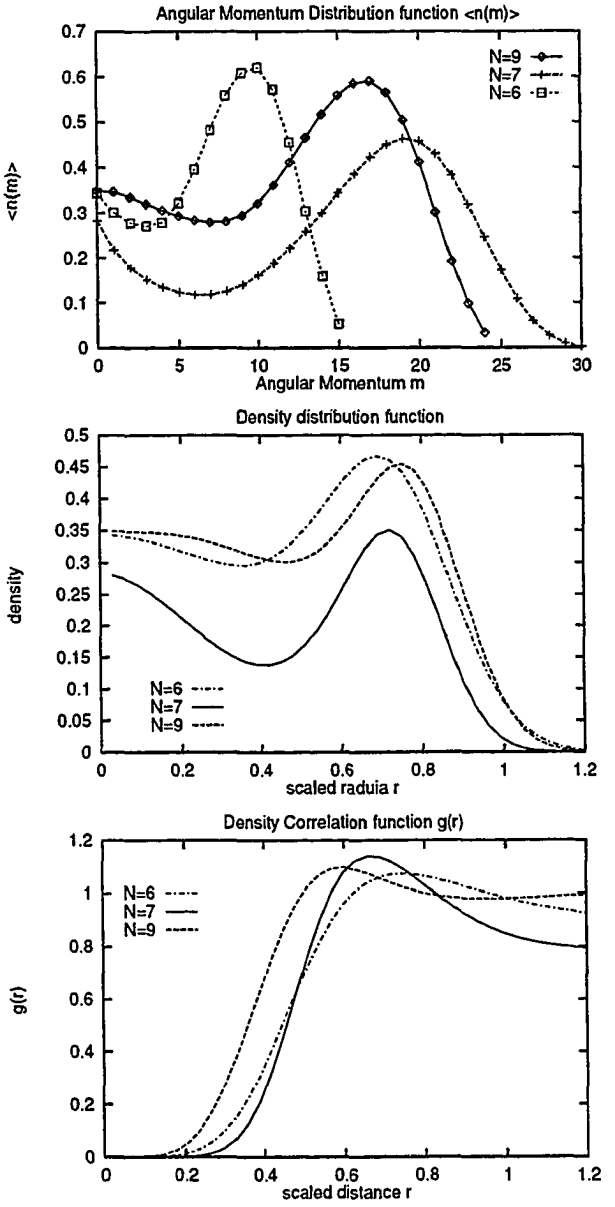

Figure 2.1: The properties of Laughlin States of $N = 6, 7, 9$.
Angular momentum distribution function $\langle n(m) \rangle$ (upper), density profile (middle), density correlation function $g(r)$ (lower) vs scaled radius $r/(mN)^{1/2}$. States of $N = 6, 9$ are at $\nu = 1/3$; States of $N = 7$ are at $\nu = 1/5$.

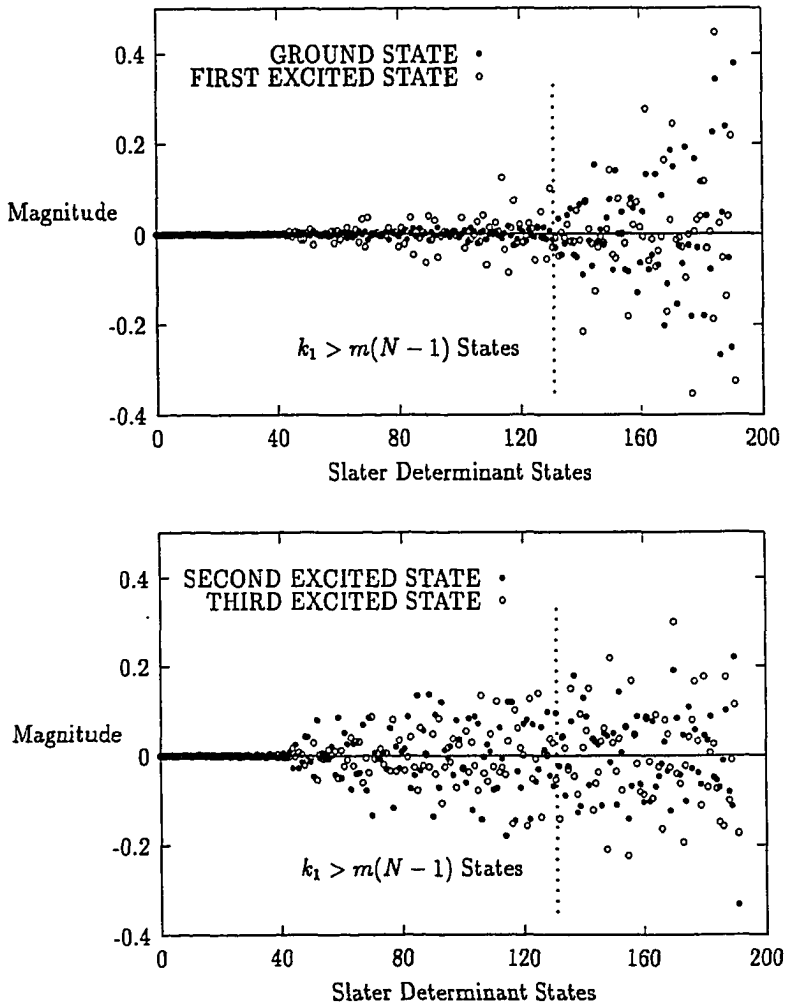

Figure 2.2: The distribution of 4 lowest translationally invariant eigenstates.

The coefficients of the SD components vs (reverse) ordinal number of the index of SD states (see text for definition of ordinal number index page 23).

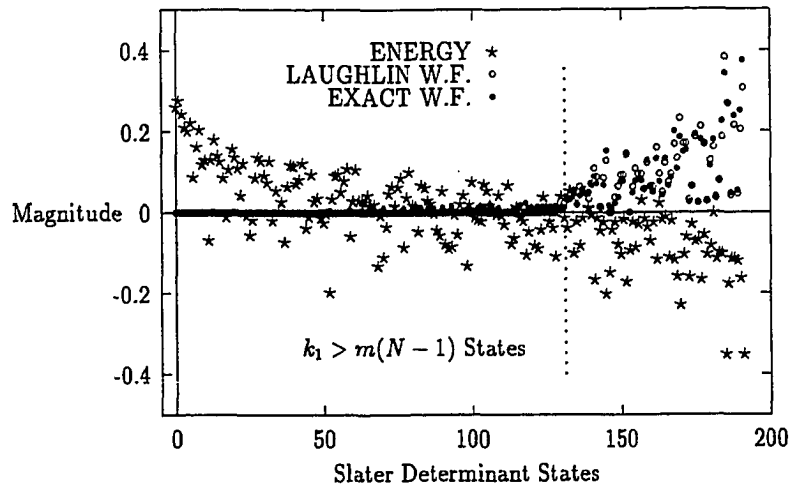

Figure 2.3: The distribution of components and expectation value in the Hilbert space with SD basis.
The x axis is the (reverse) ordinal number of the index of SD states (see text for definition of ordinal number index page 23).

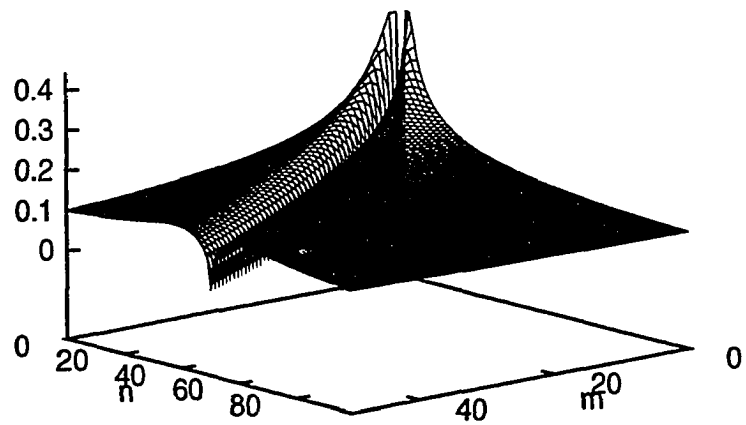

Figure 2.4: Matrix elements $\langle mn|\frac{1}{r}|mn\rangle - \langle mn|\frac{1}{r}|nm\rangle$

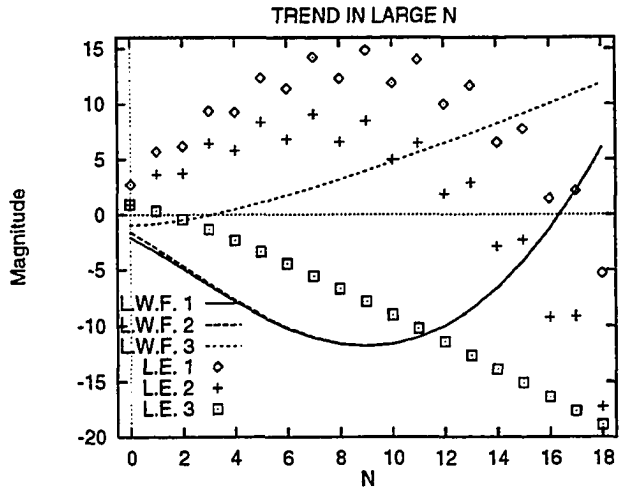

Figure 2.5: The relative coefficients and energies of SD states in LWF for different number of particle at $\nu = 1/3$.
L.W.F.i – log(coefficient of LN$(i+1)$/coefficient of LN1); L.E.i – energy of LN$(i+1)$– energy of LN1.

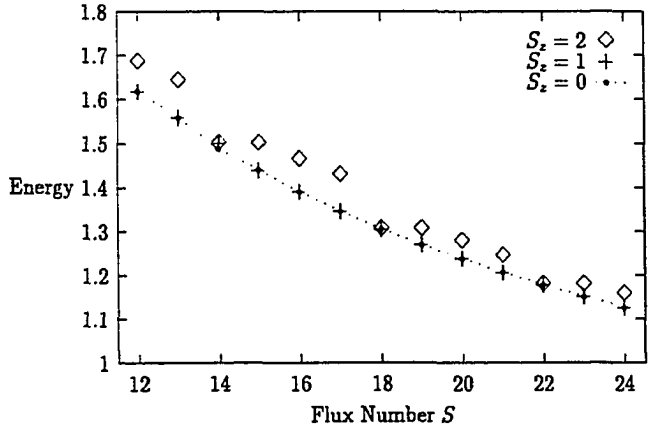

Figure 2.6: Ground state energy vs flux number for $N = 4$.

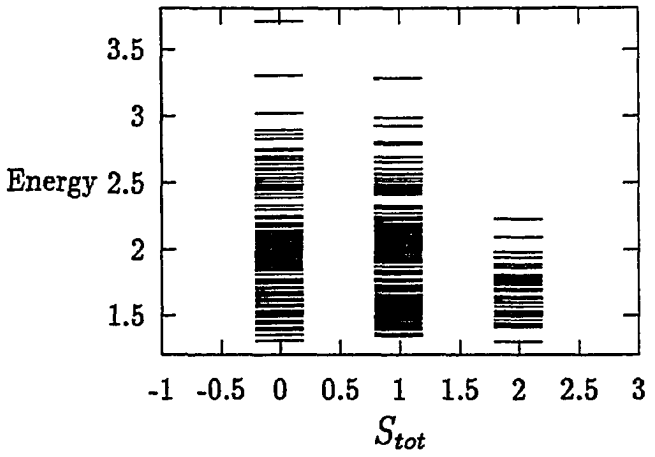

Figure 2.7: Eigenenergy vs S_{tot} for electron system at $N = 4, S_z = 0$

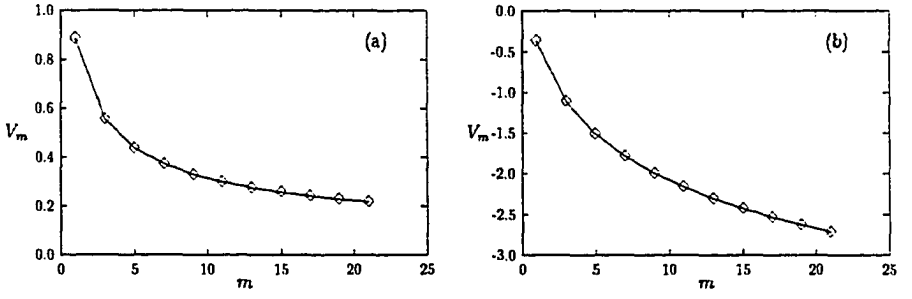

Figure 2.8: The pseudopotentials (a) for Coulomb interaction; (b) for logarithmic interaction.

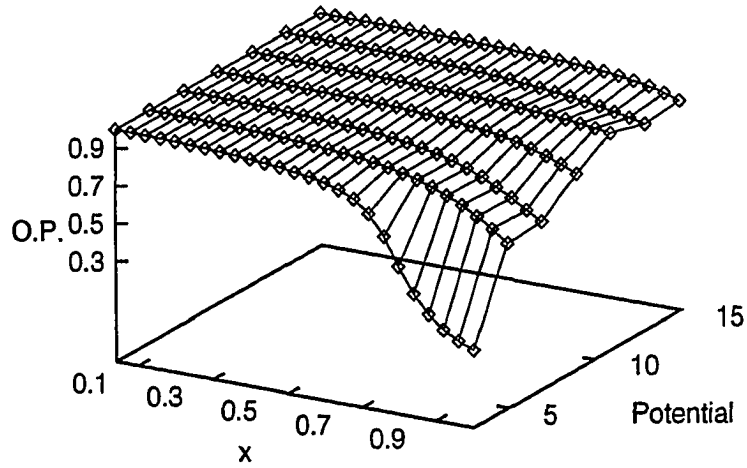

Figure 2.9: Overlaps of Laughlin wave functions with exact ground states for different interaction.

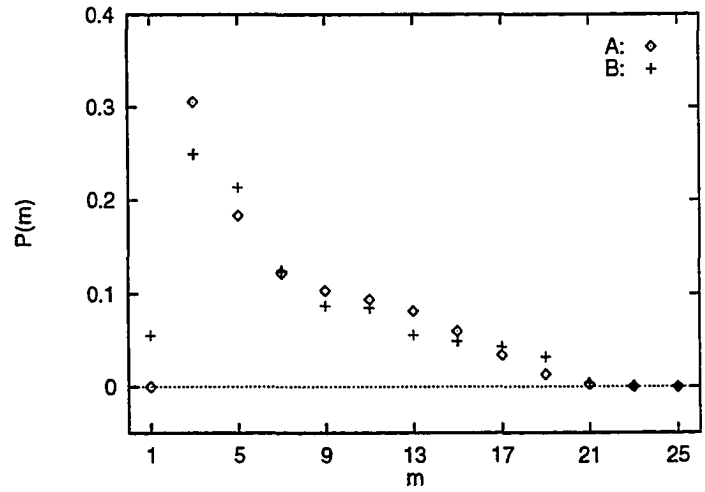

Figure 2.10: The distribution functions $P(m)$ of the relative angular momentum m of the electron pairs.
A: Laughlin wave function Ψ_3; B: wave function $\mathcal{NA}(z_1 - z_2)^5(z_1 - z_3)\prod'_{i<j}(z_i - z_j)^3$ after orthogonalization to Ψ_3.

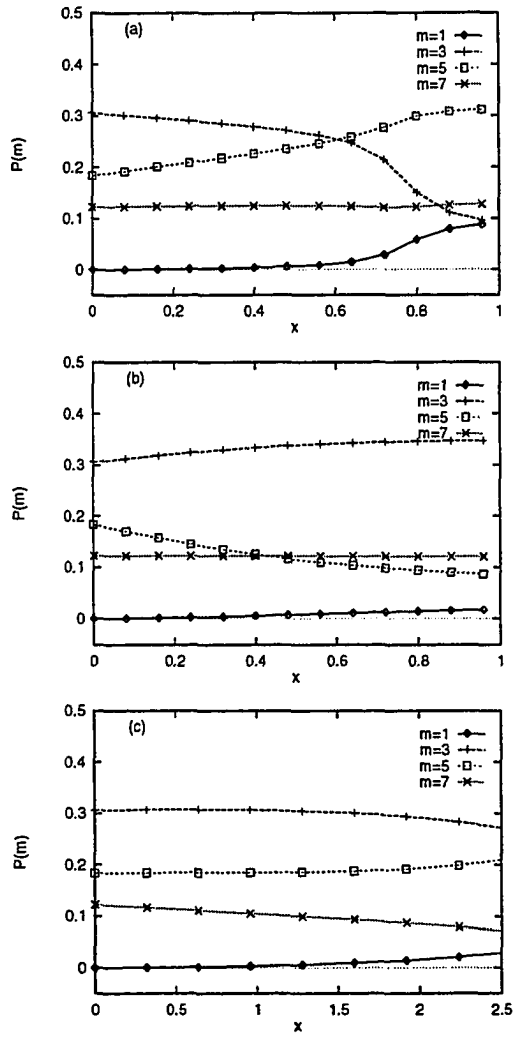

Figure 2.11: The distribution functions $P(m)$ of the relative angular momentum m of the electron pairs in the ground state wave functions for different potentials.
Potentials (a) $c_1V_1 + xc_3V_3$; (b) $c_1V_1 + xc_5V_5$; (c) $c_1V_1 + xc_7V_7$. Where c_i is the coefficients in the Coulomb potential.

Chapter 3

Farey Series, Hierarchy Structure, and Phase Diagram of FQHE

3.0 Introduction

In the last chapter, I studied the FQHE at $\nu = 1/3$. As discussed in Chapter 1, various theories for FQHE at other filling factors have been suggested, such as the Laughlin-Haldane-Halperin hierarchy theory [3] and the more recent composite Fermion theory proposed by Jain [12, 13, 80]. In this chapter I will propose a approach to the unique construction of the hierarchy structure of FQHE [74] based on Jain's composite Fermion approach. Using this hierarchy structure, I will propose a global phase diagram of the FQHE and its stability at various filling fractions.

3.1 Microscopic Models of FQHE

3.1.1 Previous Approaches

We begin with the Laughlin wave function Ψ_m for the state with $\nu = 1/m$, in the following suggestive form due to Jain [12]:

$$\Psi_m[z] = \prod_{i<j}^{N}(z_i - z_j)^{m-1}\Psi_1[z] \tag{3.1}$$

where $\Psi_1[z]$ is the incompressible IQH state at filling factor $\nu = 1$, *i.e.*

$$\Psi_1[z] = \prod_{i<j}^{N}(z_i - z_j) \tag{3.2}$$

Here I have moved the Gaussian factor to the measure [see Section 2.1 footnote in page 14].

This factorization has been interpreted as presenting the Laughlin state as the result of a dynamical generation of a local gauge field which produces the solenoids, which in turn partially screens the external magnetic flux [12, 25]. The amount of screening is sufficient to turn the fractional filling of a Landau level of the bare external field into the complete filling of a Landau level of the residual part of the field. Another way to say this is that in the Laughlin state, the electrons nucleate enough flux so that the bound states (composite particles) exactly fill up an integer number of Landau levels of the residual part of the field (screened field). This particle-flux-nucleation has been clearly described by the Chern-Simons term (topological mass term, for example, see the last term in Eq.(5.10)) in a Ginzburg-Landau field theoretic formulation of FQHE [18, 19]. In Eq.[3.1], the phase associated with the factor multiplying $\Psi_1[z]$ represents an even number $(m-1)$ of flux quanta

which are attached to each coordinate z_i where an electron is present. In this way, the composite particle is still fermionic, and the filling factor of the physical electrons state is $f = (m - 1 + 1/n)^{-1}$, where n is the number of Landau levels filled by the composite particles [1]. Here we chose the flux attached to the particles to have the same direction as the physical flux: this is physically reasonable and necessary for the unique construction of the QHS in our approach, as we will discuss below.

As first proposed by Jain [13], the QHS can be generalized from the Laughlin state at $1/m$, to the filling fraction $n/(n(m-1)+1)$. We should notice that only n *fictitious* Landau levels are needed, so that in this sense the IQHS of the composite particles are not the usual IQHS. When constructing the wave function of this IQHS, we can use the lowest Landau level wave function for all "levels".

Other odd-denominator fractions QHS can be obtained by the observation that: the complete filling of an integer number of fictitious Landau levels by the composite particles is not necessary for the formation of the incompressible QHS. What is essential is the incompressibility of the IQHS of composite particles, *i.e.* the existence of an energy gap for the excitations of the composite particle state. It has been shown [81, 58] that in the Chern-Simons gauge field theory of QHE this is true at the level of the semi-classical solution. It is presently believed [3] that if there is a incompressible state at ν, then there will also be one at $\nu + n$, and by electron-hole symmetry, at $1 - \nu$ and $n + 1 - \nu$. So if f is the filling fraction of some incompress-

[1] The number of Landau levels filled by the composite particles is defined as ν = (# of composite particles)/(degeneracy of Landau level).

ible state, then the corresponding composite fermion state at filling factor $\nu = \{f, 1-f, n+f, n+1-f\}$ of the unscreened part of field is also an incompressible state, which is an incompressible state of the true bare electrons at filling factor $\nu^* = (2m + 1/\nu)$.

The above construction can give all the odd-denominator fractions [12, 13, 14], but the construction is non-unique for most filling factors. To be specific, ν^* can be given using any construction by the fact that $\nu^* = [2m_1 + (2m_2 + 1/\nu)^{-1}]^{-1}$ gives the same filling factor provided $m = m_1 + m_2$ and $m_1, m_2 \in [0, 1, 2, \cdots]$. Although there are some minor differences in the physical arguments, the construction of a quantum Hall state (QHS) up to this point is well described in Jain's theory.

3.1.2 Present Approach

First we will give our physical arguments to obtain a unique construction for the QHS. Physically it is easy to understand the above non-uniqueness: if we don't use filling fractions $1-f$, $n+f$, $n+1-f$, then to go down to the $(i+1)$th level from ith level only means that we put $2m_i$ more flux on the composite particles. But if the total number of flux attached to an electron (composite particle) in two different ways are equal, *i.e.* $\sum_i m_i = \sum_j m_j'$, we have the same filling factor of the incompressible state, as well as the same physical state. The equivalence of these incompressible states can be proved in CSGL gauge field theory [81, 58]. So we can construct the QHS uniquely by attaching only 2 flux to each electron (composite particles) each time we construct a QHS from an incompressible state of composite fermions.

Following the arguments given above, we obtain the construction rules (**R1**) for the hierarchy structures of FQHS at filling fractions $\nu < 1$ summarized below:

R1-i) The first level QHS have filling fractions $\nu = (2+1/n)^{-1}$, $1-(2+1/n)^{-1}$, which are IQHS of composite particles. These are two symmetrical first level families of FQHS;

R1-ii) The infinite images $\nu^* = (2 + 1/\nu)$, (with $\nu = \{f, n + f\}$) of the last two symmetrical families $\{f, 1 - f\}$ and their electron-hole symmetrical reflections [3] $1 - \nu^*$ give the second level of the hierarchy structure of FQHE;

R1-iii) Repeating ii) will give all the odd-denominator fractions and the self-similar hierarchy structure of FQHE Fig.[3.1].

3.2 Farey Numbers and Hierarchy Structure

Following the construction rules discussed in Section 3.1.2, the hierarchy structure comes out as shown in Fig.[3.1]. I now demonstrate the relation of this hierarchy to the Farey series discussed in standard works on number theory [82]. The main feature of the hierarchy structure is as following:

1) The structure is quasi-self-similar. This property can be easily obtained using another construction rule (**R2**) of the hierarchy structure of FQHE, described as following:

R2-i) The first level [see Appendix A] generated by $(0/1, 1/1)$ is the two Farey series between $(0/1, 1/2)$ and $(1/2, 1/1)$.

$$1/3, 2/5, 3/7, \cdots, i/(2i+1), \cdots$$

$$2/3, 3/5, 4/7, \cdots, (i+1)/(2i+1), \cdots$$

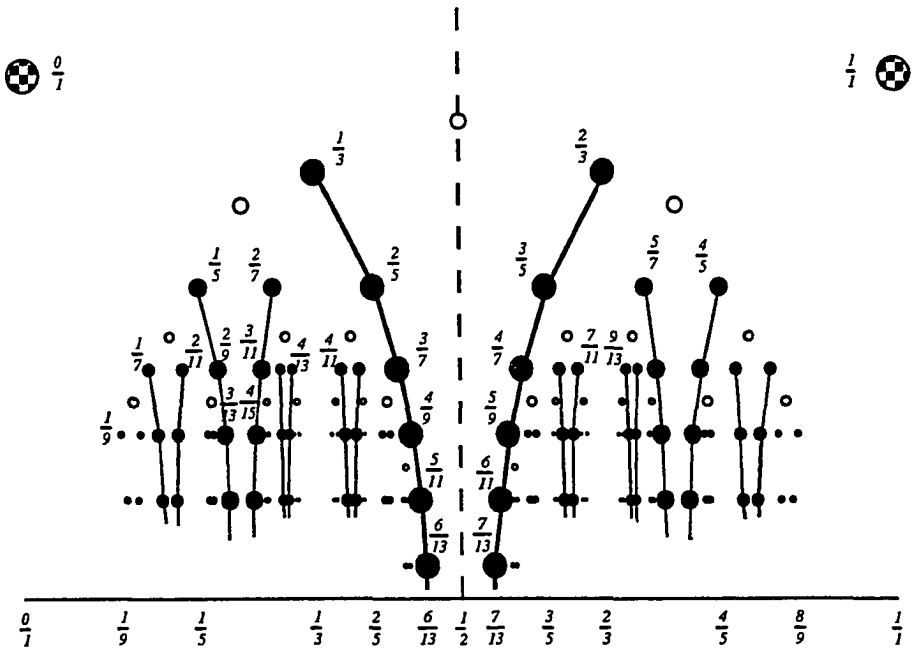

Figure 3.1: Hierarchy structure of the FQHE constructed by a rule illustrated in Fig.3.2.
Closed circles correspond to the even-denominator *critical fractions.* The Farey series in the same level are connected by a line for illustration. The QHE's observed in experiments are labeled explicitly.

Here our Farey series [82] between $(n/m, p/q)$ (where $m+p$ is odd and $n/m < p/q$) are defined as (after reduction to irreducible fractions)

$$\frac{n+q}{m+p}, \frac{n+2q}{m+2p}, \frac{n+3q}{m+3p}, \cdots, \frac{n+iq}{m+ip}, \cdots \qquad \text{if } p \text{ is even}$$

$$\frac{n+q}{m+p}, \frac{2n+q}{2m+p}, \frac{3n+q}{3m+p}, \cdots, \frac{in+q}{im+p}, \cdots \qquad \text{if } m \text{ is even}$$

It is easy to see that they are Farey series of order infinity, *i.e.* the series length is infinite.

R2-ii) The next level can be generated by rule (**R1**) at the end of Section 3.1.2. An equivalent but more appealing way is by using the Farey sum rule to construct the second level hierarchy: generating two Farey series by any two adjacent Farey numbers $(n/m, q/p)$. [see Appendix A] The method of generating is: (a) first construct the critical fraction of the generators using the Farey sum rule $c = n/m \oplus q/p \equiv (n+q)/(m+p)$; (b) the Farey series generated are just the infinite order Farey series between $(n/m, c)$ and $(c, q/p)$ as defined above (notice that $m+p$ is even and $n+q$ is odd). Repeatedly using this alternative to construct the hierarchy structure shown in Fig.[3.1], we see that our hierarchy structure exhibits self-similarity. This alternative construction (R2) has been illustrated in Fig.[3.2].

2) The infinite tree structure uniquely gives all the odd-denominator fractions [82]. Since the structure in Fig.[3.1] can also be constructed by our rule in Section 3.1.2, our construction is unique.

3) Any two Farey series generated by (ν, μ) converge to the even-denominator

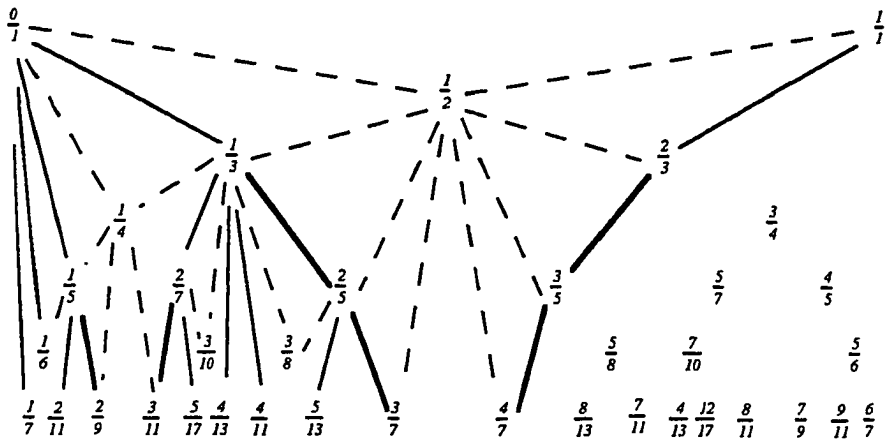

Figure 3.2: Constructing the hierarchy structure using Farey series. Each even-denominator fraction (critical fraction) θ is connected (dashed line) with two adjacent Farey numbers (generators of next level Farey number) (ν,μ) by $\theta = \nu \oplus \mu$. The Farey number for the two Farey series (connected by thick lines) generated by (ν,μ) are connected (thin line) with ν (or μ) and θ by $\nu \oplus \theta$ (or $\mu \oplus \theta$).

critical fraction $\nu \oplus \mu$.

The hierarchy structure described here is similar to the $SL(2,Z)$ tree structure in the Self-Dual model of QHE [75]. In the Self-Dual model the filling fractions (location of Hall plateaus) can also be constructed by the Farey sum rule. But in that picture, including even fractions is essential for the self-duality and for the $SL(2,Z)$ symmetry. The nodes in the $SL(2,Z)$ tree are repulsive fixed points ($E3$) and saddle points ($E2$) in the RG flow diagram projected on the $\sigma_{xx} - \sigma_{xy}$ plane [75].

The second rule and our self-similar hierarchy structure are our principal new results in this section and is the starting point of our scaling theory of FQHE.

3.3 Stability and Scaling Theory of FQHE

Let us start by describing the suggested relationship of our hierarchy structure to the energy gap Δ of the excitations of QHS. Our hierarchy structure suggests a devil's staircase structure of the energy gap Δ: the energy gap will decrease rapidly with increase of the level of the hierarchy structure, *i.e.* the energy gap for excitations in the incompressible state of the composite particles is much smaller than the gap of excitations in the same incompressible state of electrons. At the same level, the energy gap will decrease relatively slowly (in comparison to the previous case) with an increase of the denominator. One possible way to understand the decrease of the gap with the increase of the denominator is: with the increase of the number (not necessary integer) of the Landau levels filled by composite particles, the (residual

percentage of the) gap will decrease after projection to the lowest Landau level of electrons. A justification of this or a more rigorous reason should be given by CSGL theory [27]. Such a result has been suggested [11, 64, 83] numerically where a rough relation $\Delta \propto$ (fraction denominator)$^{-2.5}$ was empirically found.

As in the IQHE, the incompressibility of the FQHS is caused by the existence of an energy gap Δ for the excitations. When the disorder is sufficient to destroy the energy gap, the FQHE will be destroyed. This occurs when the collision time τ in the sample in the absence of a magnetic field becomes smaller than the inverse gap: $\tau < \hbar/\Delta$. The stability of the FQHE will decrease, along with the smaller energy gap Δ. Hence the stability of FQHS at filling factor ν ($\nu < 1$) can be described by our hierarchy structure as shown in Fig.[3.1]: in a sample with disorder, the phase diagram of FQHE is nested, so the stability will decrease rapidly with increase of the level of hierarchy, and decrease relatively slowly with increase of the denominator in the same level.

We have compared our results as given above to the experiments in the literature [59], and this gives us confidence in our hierarchy structure: the predicted appearance and order of stability of QHS at various filling fractions are in agreement with experiments. We show the experimentally observed fractions in Fig.[3.1]. We see that our hierarchy structure gives a reasonable variation of the stability of a QH state with various fractions $\nu < 1/2$. In our approach we have use the symmetry between ν and $1 - \nu$, *i.e.* particle-hole symmetry. Since there are not enough experimental results, this symmetry

can not be seen in Fig.[3.1].

In ideal pure QHE systems our hierarchy structure suggests that the nested phase structure of the Fractional Quantum Hall (FQH) liquid occurs at any odd-denominator filling fraction. For a real system, however, weak disorder destroys all but some sufficiently stable FQHS and causes the Hall plateaus in the FQHS. Changing the magnetic field causes transitions between different Hall plateaus. Because of the onset of our hierarchy structure and the mapping relation between different filling fractions, we come to the ansatz first proposed by Jain and co-workers [84] that: the transition between FQHS at two different filling factors, which can generate filling factors of the next level FQH state between them, has the same scaling behavior as that of a transition between "adjacent" IQHS. Using our hierarchy structures, we can see that the transition critical point occurs at filling fraction which is the "critical fraction" of the generators (the Farey sum of the generators). For transitions between FQHS at filling factors which can not be generators, the hierarchy structure suggests there is no scaling behavior, and at low enough temperature the transition may show hysteresis.

For a more thorough scaling theory implied by our hierarchy structure, we propose the RG flow diagram for the FQHE illustrated in Fig.[3.3]. Here we are not presenting a rigorous scaling theory, but rather arguing on physical grounds. If a scaling theory exists which is consistent with our hierarchy structure, and if it can be projected onto the $\sigma_{xx} - \sigma_{xy}$ plane in a meaningful way, then our topologically simplest RG flow diagram shown in Fig.[3.3] will result. As with another recent proposal [85], our RG flow diagram only has

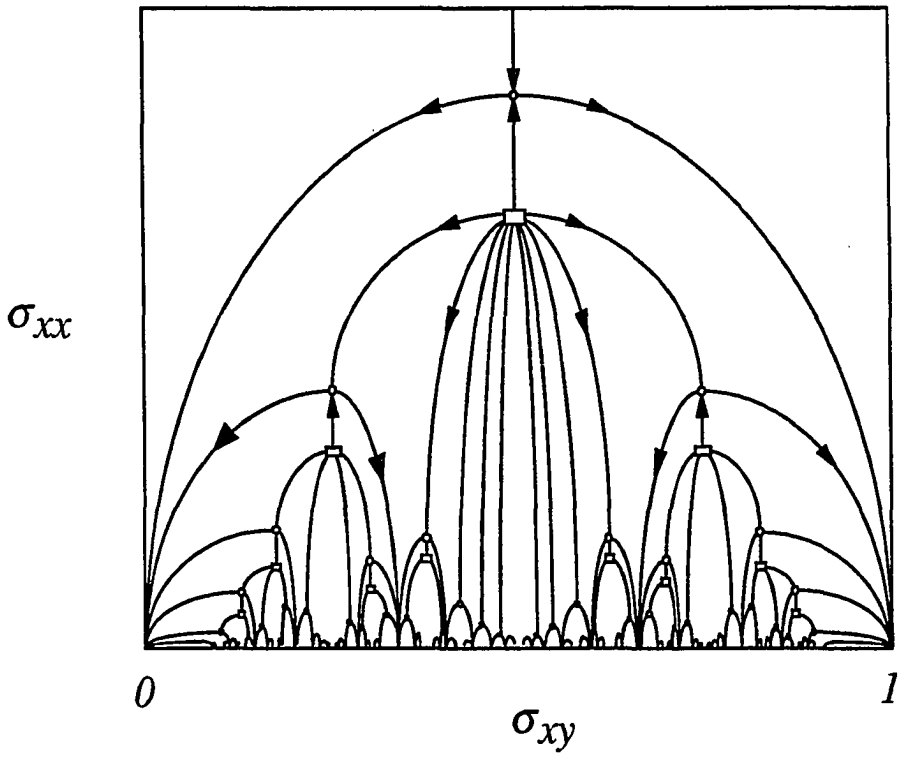

Figure 3.3: The RG flow diagram of the FQHE.
The fixed points corresponding to the critical-point transition are illustrated as circles and the fixed points corresponding to the gap closing transition are illustrated as boxes.

heuristic value. The Ansatze we have made to get this RG flow diagram are:

i) Our hierarchy structure, and the relation of the energy gap to this structure correctly describes the nested phase structure of FQHE;

ii) The transition between different FQHS is physically similar to transitions in the IQHS as connected by the mapping relation. All states at even-denominator filling factor can be obtained after an iterative mapping from $n+1/2$ [see Appendix A]. Thus such states are fixed points at $\sigma_{xy} = \nu_e$, and this corresponds to the critical point of the transition between QHS at filling fractions of the relevant generators in the presence of disorder;

iii) To get a topologically reasonable RG flow diagram, we should have another fixed point connected to each $\sigma_{xy} = \nu_e$, this fixed point is the gap-closing transition point [85, 3].

Given this RG diagram, let's discuss the scaling behavior of transitions between different Hall plateaus [75, 85].

There are several existing scaling theories of FQHE. Our construction of a RG flow diagram follows Laughlin *et al.* [85]. But our RG flow diagram is different because of our distinct hierarchy structure of FQHE [compare our Fig.[3.3] with Fig.1 of Ref.[85]. See Fig.[3.4]] For example, there is a continuous phase transition between $\nu = \frac{1}{3}$ and $\nu = \frac{2}{3}$ states according to Laughlin *et al.* [85], while there is no continuous phase transition according to our RG flow diagram. The RG flow diagram in the self-dual model [75] was constructed in conformity with the symmetry $SL(2, Z)$ which gives its hierarchy structure. In that diagram the even-denominator filling fraction phase is inherent in its RG flow diagram and is accessible in the Self-Dual

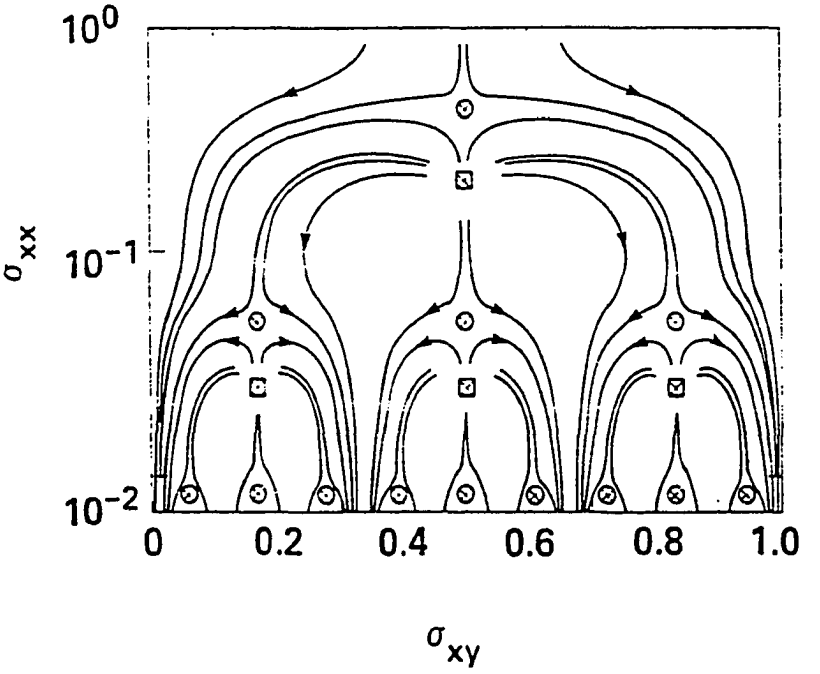

Figure 3.4: The RG flow diagram of the FQHE proposed by Laughlin *et al.*. Reproduced from Ref.[75].

scaling theory. The scaling behavior in phase transitions between different filling fractions was also proposed by Jain and co-workers [84] which is based on the idea of unification of IQHE and FQHE, and their prediction on transition behavior is consistent [2] with our predicted scaling behavior from our RG flow diagram Fig.[3.3].

[2]Their prediction in Ref.[84] that the transition between the $\nu = 3/2$ and $\nu = 1$ is not continuous is incorrect, they corrected this in an erratum to Ref.[84].

Chapter 4

Optical properties of FQHE systems

4.1 Gap excitations and Magneto-excitons

4.1.0 Introduction

The FQHE systems have a rich structure of their excitation spectra [3]. The excitations can be classified in following categories:

(i) inter-Landau level charge-density waves (CDW)— which are the magneto-plasmons due to inter-Landau level transitions [35, 36].

(ii) intra-Landau level charge density waves — the magneto charge density waves without (virtual) inter-Landau level transitions. They are also called gap-excitation or magneto-roton excitations [38, 39, 36].

(iii) spin density waves (SDW) — there are many kinds of spin density excitations such as the inter-subband SDW, inter-Landau level SDW and intra-Landau level SDW [78].

(iv) quasi-particles — the fractional statistical and fractional charged

quasi-hole and quasi-electron first introduced by Laughlin [8, 86].

(v) edge waves — the edge states at the boundary of the incompressible liquid in IQHE [7] and FQHE [87, 88, 22, 89] systems.

The intra-Landau level collective mode, also called the magneto-roton or gap excitation, is the most interesting one for studying the properties of FQHE systems [35, 36, 38, 39]. The low energy response functions due to an electromagnetic perturbation are closely related to the dynamics of this mode. Despite success in the study of the ground states of FQHE systems, the calculation of the value of the magneto-roton gap and the response functions using Chern-Simons field theory is still a challenge for theorists [26, 37].

A more complicated problem is the theoretical study of the optical properties of FQHE systems, such as the photoluminescence (PL) [31, 32, 33] and inelastic Raman scattering (RS) [34]. In the PL problem, the appearance of an injected valence hole will perturb the already strongly correlated electrons. In the resonance RS the resonance relation will in addition make analytical study more difficult than for the calculation of response functions of the "pure" electron systems away from resonance [90]. Fortunately, the numerical simulations of finite systems are very effective in the study of properties of FQHE system due to its incompressibility.

In this chapter, I will study the optical properties of FQHE using numerical diagonalization of the exact Hamiltonian with Coulomb electron-electron interaction in spherical geometry, in which finite size effects can be minimized. The results will be compared to experiment and will be used to predict experiments to be done.

4.1.1 Spherical geometry

In spherical geometry [9, 55], the electrons are on the surface of a sphere of radius R with a Dirac magnetic monopole in the center [91]. By Dirac's quantization condition, the magnitude of the (radial) magnetic field is: $B = \frac{\hbar S}{eR^2}$ ($2S$ is an integer). I will use the following gauge:

$$\vec{A} = -\frac{\hbar S}{eR}\cot\theta\vec{\varphi} \tag{4.1}$$

In this gauge, the single particle wave function in the lowest Landau level can be written as

$$\psi_{S,m} = \left[\frac{2S+1}{4\pi}\binom{2S}{S+m}\right]^{1/2} u^{S+m}v^{S-m} \quad \text{for } m = S, S-1, \cdots, -S \tag{4.2}$$

where $\binom{2S}{S+m}$ is the binomial coefficient, and $u = \cos(\theta/2)e^{i\varphi/2}$; $v = \sin(\theta/2)e^{-i\varphi/2}$, so (u, v) are spinor variables. The degeneracy of the lowest Landau level is $2S + 1$. Due to the non-zero curvature of the spherical surface, the filling fraction of N electrons in the sphere with flux $2S$ is $\nu = (N-1)/(2S)$. The formalism in spherical geometry is very similar to that in the disk geometry. The wave function $\psi_{S,m}$ in spherical geometry corresponds to z^k in disk geometry, with $k = S + m$. The Hamiltonian matrix elements of the Coulomb interaction can be written as follows:

$$\begin{aligned}&\langle m_1 m_2|V(r)|m_3 m_4\rangle_S \\ &= \textstyle\sum_{J=0}^{2S}\sum_{M=-J}^{J}\langle Sm_1Sm_2|JM\rangle\langle Sm_3Sm_4|JM\rangle V_J^S(d)/R\end{aligned} \tag{4.3}$$

where $\langle Sm_i Sm_j | JM \rangle$ are Clebsch-Gordan coefficients and $V(r) = e^2/(\epsilon r)$. And

$$V_J^S(d) = \langle JM \left| \frac{1}{\sqrt{|\vec{\Omega}_1 - \vec{\Omega}_2|^2 + (d/R)^2}} \right| JM \rangle$$
$$= \frac{R}{d} \frac{\sum_{k=0}^{J} {}_2F_1\left(\frac{1}{2}, 2S-k+1, 2S+2, -\left(\frac{2R}{d}\right)^2\right) \frac{(2S-k)!(J+k)!}{(J-k)!k!}}{\sum_{k=0}^{J} \frac{(2S-k)!(J+k)!}{(J-k)!k!}} \quad (4.4)$$

Here ${}_2F_1$ is the hypergeometric function [92], d is the electron-hole seperation, and $\vec{\Omega}_i$ is a unit vector in the radial direction denoting the electron (hole) position in the electron (hole) sphere. In the special case of $d = 0$, we have a very simple result for $V_J^S(0)$:

$$V_J^S(0) = 2 \frac{\binom{4S-2J}{2S-J}\binom{4S+2J+2}{2S+J+1}}{\binom{4S+2}{2S+1}} \quad (4.5)$$

In the above equations, we have used the magnetic length l_0 as the unit of length and $e^2/\epsilon l_0$ (ϵ is the dielectric constant) as the unit of energy. To satisfy the relation between magnetic flux and the density of electrons, we need to let $R = \sqrt{S}$.

In the spherical geometry, the symmetry operators are the z-component of angular momentum $\hat{L}_z$ and square of total angular momentum $\hat{L}^2$. Each subspace of L_z is an invariant subspace of the Hamiltonian. For numerical diagonalization studies, we only need to study the subspace: $L_z = 0$. Because of the $SU(2)$ symmetry of the Hamiltonian, each eigenstate with angular momentum L has degeneracy $2L + 1$. The subspace with $L_z = 0$ consists

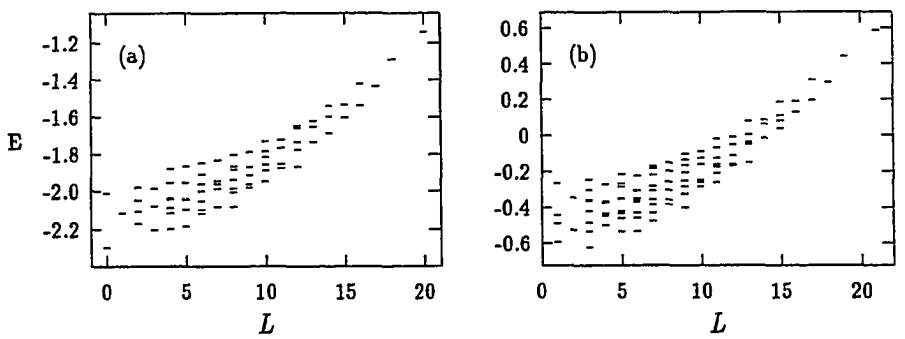

Figure 4.1: Spectrum of the FQHE system. (a) $N = 5$ and $2S = 12$ at $\nu = 1/3$; (b) $N = 6$ and $2S = 12$ with one extra electron added to the Laughlin state at $\nu = 1/3$.

of all the non-degenerate eigenstates, while all the other subspaces $L_z \neq 0$ consist of the multiplets of the eigenstates in subspace $L_z = 0$.

Fig.[4.1] shows the spectrum of the FQHE system for (a) $N = 5$ and (b) $N = 6$ with $2S = 12$. The spectrum was obtained by exact diagonalization of the Hamiltonian in Eq.[4.3]. For $N = 5$, the system is at $\nu = 1/3$. It is easy to see that the ground state is at $L = 0$, and has a large gap $\Delta \sim 0.093(e^2/\varepsilon l_0)$ from the excited states. From Section 2.2 we know this ground state is well approximated by the Laughlin wave function Ψ_3. It was observed by Haldane [79] that the lowest branch of excited states comprising $L = 2, 3, \cdots$ can be recognized as the dispersion relation of the neutral magneto-roton. At $N = 6$, we find that the ground state is at $L = 3$, and there are no $L = 0$ states. The gap between the ground state and excited states reduces to $\Delta \sim 0.026(e^2/\varepsilon l_0)$. We can speculate that the gap will vanish in the thermodynamic limit.

4.1.2 Magneto-Exciton

Before discussing the PL [31, 32, 33] and RS [34] of FQHE systems, let us study the many-body magneto-exciton [93, 94] first. A magneto-exciton is the "excitation" formed in the 2D correlated electron system in the presence of the strong magnetic field, plus a (suddenly) injected hole and one added electron. Here we will simplify the problem by assuming the valence hole is also in the lowest Landau level. In the experimental $GaAs/AlGaAs$ samples, the effective mass of the valence hole is five times of that of conduction electrons, so the cyclotron energy of the hole is $1/5$ that of an electron. The assumption that the hole is confined in the lowest Landau level might not be a good approximation, and requires further examination. In what follows we do assume for convenience lowest Landau confinement.

There are two equivalent ways to describe the valence hole: one is using the $2S$ electrons in the lowest Landau level (one electron is missing from a full Landau level); another is using a single hole with the wave function of the hole state taken as the time-reverse of the corresponding electron state. The difference is that using $2S$ electrons in the valence "layer" will introduce a trivial energy shift due to electron-electron intra-valence "layer" interaction. The second description will be used in my numerical calculations, while the first description will be used for analytical discussions.

In the first description, the magneto-exciton system is analogous to the spin-1/2 systems, if we assume the conduction electrons are spin-up and valence electrons are spin-down. From the results in Section 2.2, it is obvious that part of the eigenenergies making up the magneto-exciton are equal re-

spectively to each corresponding eigenenergy in the FQHE system in the symmetric model, here we are taking $d = 0$ in which case $V_{ee} = |V_{eh}$. The reason is as follows.

In a system of two "layers" with total number of electron $2S + 1 + N$, the electron wave functions with fixed number of electrons in each layer form a subspace of the whole Hilbert space. In the spin-1/2 language, these subspaces correspond to fixed total S_z. For N electrons in the conduction band layer, $S_z = (N - 2S - 1)/2$. For $N + 1$ electrons in the conduction band, (one hole in valence band), $S_z = (N - 2S + 1)/2$. In the symmetric model, each eigenstate $|\Psi_\alpha^e\rangle$ of the Hamiltonian in the N-electron system has a corresponding eigenstate $|\Psi_\alpha^{me}\rangle$ of the Hamiltonian in the $N+1$-electron and one 1-hole (magneto-exciton) system, which can be obtained by $\hat{S}_+|\Psi_\alpha^{me}\rangle = \sum_{m=-S}^{S} e_m^\dagger h_m^\dagger |\Psi_\alpha^e\rangle$. Here $e_m^\dagger$ and $h_m^\dagger$ are the creation operator of (conduction) electron and (valence) hole respectively, and we have used the α as an index of the quantum numbers of the eigenstate. If the Laughlin state is stable against the formation of a many-body magneto-exciton, the Laughlin wave functions should be one of the degenerate ground states in the whole Hilbert space, so the ground state of the magneto-exciton should have angular momentum $L = 0$. In this $d = 0$ limit, there is a direct relation between states of FQHE systems and that of magneto-exciton systems, However, it is doubtful that we can consider the corresponding states of the magneto-exciton to be *multiplicative* states of: Laughlin states plus one extra exciton state as suggested by Apalkov and Rashba [93].

In the spherical geometry, the electron-hole system can be modeled as

two concentric spheres with the same radius R. The electron-hole interaction can be written as $V_{eh} = 1/\sqrt{|\vec{\Omega}_1 - \vec{\Omega}_2|^2 + (d/R)^2}$ (see Eq.[4.4]), where d is the distance between electron-hole layers. In this geometry, the rotational symmetry $SU(2)$ exists in the magneto-exciton even for $d \neq 0$. So the subspace of $L_z^{me} \equiv L_z^e + L_z^h = 0$ contains all the non-degenerate eigenstates, and all the others can be derived by using $\hat{L}_\pm^{me} \equiv \hat{L}_\pm^e + \hat{L}_\pm^h$ to operate on the eigenstates of subspace $L_z^{me} = 0$.

In the study of optical properties, the transition probability $\left|\langle\Psi_\beta^e|\hat{\mathcal{L}}_i|\Psi_\alpha^{me}\rangle\right|^2$ is needed, where $|\Psi_\alpha^{me}\rangle$ is the wave function of the magneto-exciton, and $|\Psi_\beta^e\rangle$ is that for its FQHE system, and $\hat{\mathcal{L}}_i$ is the transition operator. We will show that for optical properties, only the calculation using subspaces with $L_z^{me} \equiv M = 0, \pm 1$ is necessary.

In the spin language, $\hat{\mathcal{L}}_0 = S_-$ and $\hat{\mathcal{L}}_{+1} = \sum_i s_-^i l_-^i$. It is easy to check that

$$\langle\Psi_m^e|\hat{L}_\pm^{me}\hat{\mathcal{L}}_i\hat{L}_\mp^{me}|\Psi_n^{ex}\rangle = const\langle\Psi_m^e|\hat{\mathcal{L}}_i|\Psi_n^{ex}\rangle \tag{4.6}$$

where *const* is a constant dependent on the transition process $\hat{\mathcal{L}}_i$ and value of L and M of the FQHE states or magneto-exciton states respectively, *i.e.* $const = (L \pm M)(L \mp M + 1)$ for $\hat{\mathcal{L}}_{\pm 1}$ and $M(M \mp 1)$ for $\hat{\mathcal{L}}_0$, where $\pm$ is for different operators $\hat{L}_\mp^{me}$ respectively. The renormalization of the transition probabilities for different M will not change the structure of the optical spectrum in the region of interest. So we can use the largest subspaces $M = 0, \pm 1$, which will give the most complete spectrum.

Fig.[4.2] shows the spectrum of the magneto-exciton consisting of 6 electrons (6e) and 1 hole (1h) with $2S = 12$ at different electron-hole distance

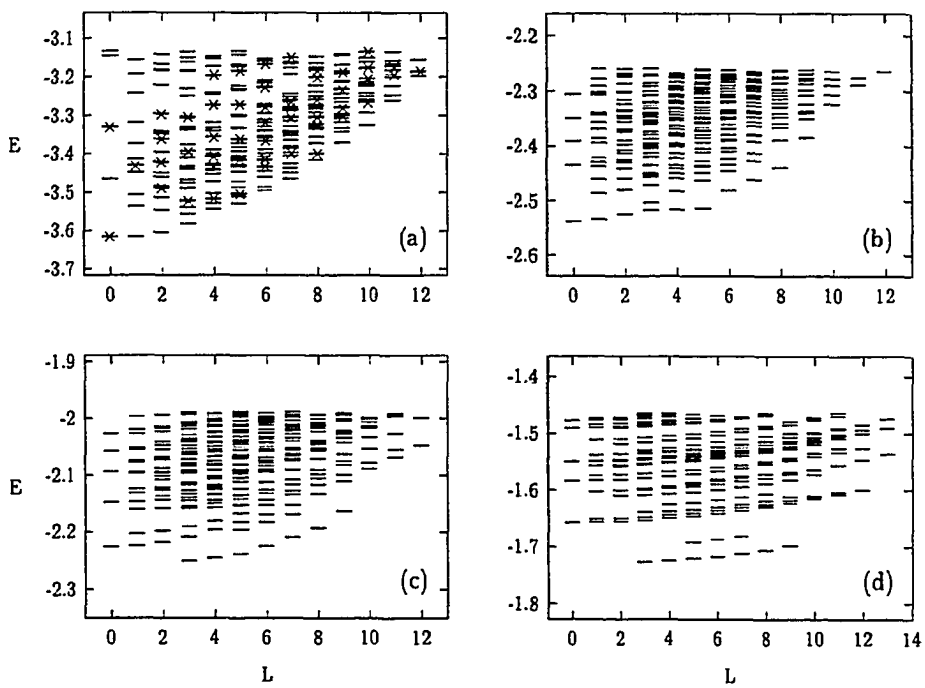

Figure 4.2: Spectrum of the magneto-exciton for $2S = 12$ and 6e plus 1h. x-axis: angular momentum L; y-axis: Energy ($e^2/\varepsilon l_0$). (a) $d = 0R$; (b) $d = 0.6R$; (c) $d = 0.9R$; (d) $d = 1.8R$. In (a), the crossed states correspond to FQHE states at $\nu = 1/3$ (see text).

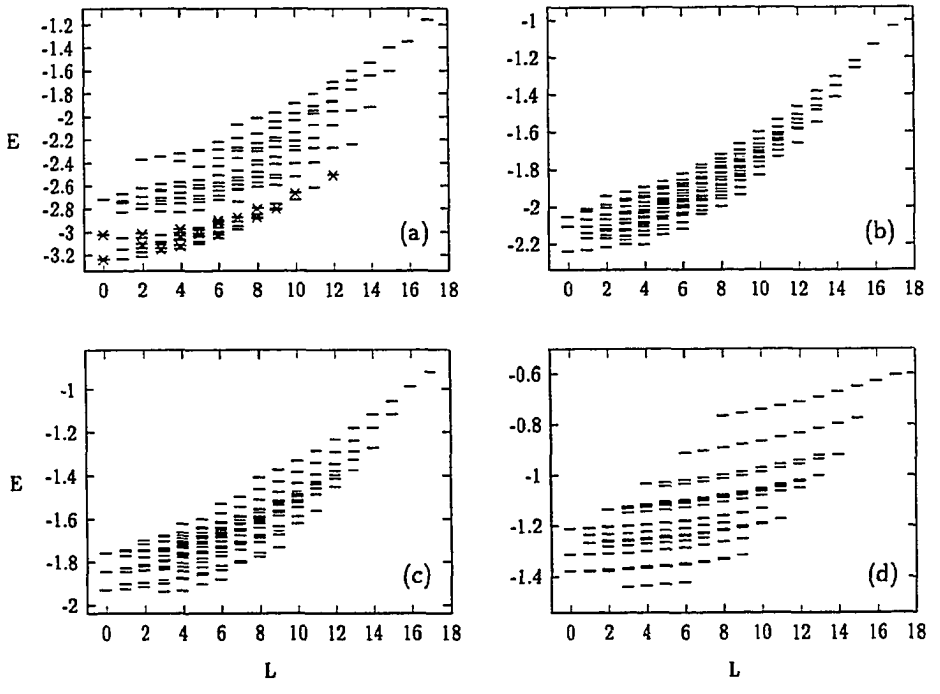

Figure 4.3: Spectrum of the magneto-exciton for $2S = 9$ and 5e plus 1h. x-axis: angular momentum L; y-axis: Energy $(e^2/\varepsilon l_0)$. (a) $d = 0R$; (b) $d = 0.6R$; (c) $d = 0.9R$; (d) $d = 1.8R$. In (a), the crossed states correspond to FQHE states at $\nu = 1/3$ (see text page 65).

d. This was calculated by diagonalize the full Hamiltonian using the matrix elements given by Eq.(4.4). For comparison the spectrum for 5e and 1h with $2S = 9$ is shown in Fig.[4.3]. One thing to be noted is that at $d = 0$ the ground state of a magneto-exciton of 6e and 1h has angular momentum $L = 1$, which means that the Laughlin state (with $N = 5$) is unstable against formation of a many-body magneto-exciton. However the energies of the ground state with $L = 1$ and Laughlin's multiplet state with $L = 0$ are almost degenerate. The Laughlin state of $N = 4$ is stable against the formation of a magneto-exciton.

4.1.3 Magneto-Exciton Spectrum As a Function of Electron-Hole Separation

The spectrum of the magneto-exciton shows an interesting dependence on the distance between electron and hole layers, and can be classified into two regions depending on the distance d. Recall that d enters the calculation by V_{eh}, which was given in Eq.(4.4).

We find that the results depend on whether $d \geq d_c$. Where $d_c \sim 0.9R$ (R is the radius of the sphere). In the region $d > d_c$, the spectrum of the magneto-exciton has low energy branches which have parabolic-like dispersion relations. With the increase of d, more and more eigenstates have a parabolic-like dispersion law and the dispersion becomes flatter. The origin of these magneto-exciton states can be understood most easily in the large d limit. At $d = \infty$, the electron and hole are decoupled. The eigenstates are the direct product of many-body electron states and hole states. If we fix

the total $L_z = M$, the Hilbert space $\mathcal{H}$ is

$$\mathcal{H} \equiv \sum_{m=-S}^{S} \varphi_m \mathcal{H}^e_{\{M-m\}} \tag{4.7}$$

where $\mathcal{H}^e_{\{M-m\}}$ is the subspace of the electron system with angular momentum $L^e_z = M - m$, and φ_m is the wave function of the hole with angular momentum $l^h_z = m$. Without losing generality, we can set $L_z = 0$. For each eigenstate of $N+1$ conduction band electrons with $L^e = l$, there are $2l+1$ multiplet states $L^e_z = -l, -l+1, \cdots, l-1, l$, and so the degeneracy for the many-body magneto-exciton states is $min(2l+1, 2S+1)$. Each many-body eigenstate of conduction electrons corresponds to a degenerate band for the many-body magneto-exciton at $d = \infty$. Turning on the electron-hole interaction adiabatically, the magneto-exciton obtains a finite renormalized mass due to the e-h interaction. In the sense of the correspondence $L \sim k$(momentum), the magneto-exciton has an approximately parabolic dispersion relation. This parabolic spectrum structure for low energy states survives with the increase of e-h interaction as d decreases, until up to d_c. For $M = 0$, the wave functions for these states can be approximated by

$$|\Psi^{me,L}_\alpha\rangle = \sum_m \langle S(-m)lm|L0\rangle \varphi_m |\Psi^{e,lm}_\alpha\rangle + \delta |\Psi^{me,L}_\alpha\rangle \tag{4.8}$$

Here $|\Psi^{e,lm}_\alpha\rangle$ is the eigenstate of the decoupled $N+1$ electron and 1 hole systems.

When d continue to decrease, after $d < d_c$, the magneto-exciton goes into the strongly correlated region of electron and hole. In this region, the effect of the e-h interaction is comparable to that of the e-e interaction. A new kind of magneto-exciton is formed (an example is the symmetric model [93, 41]

at $d = 0$ and $V_{ee} = |V_{eh})$. In this region, the eigenstates and eigenenergy (at least part of them as discussed above) are related to that in the N electrons system.

4.2 Photoluminescence

The PL experiments [31, 32, 33] showed very interesting energy anomalies and correlation between modulation of optical PL intensity with magnetic field and the modulation of transport coefficients σ_{xy} and σ_{xx} as function of applied magnetic field B (see Fig.[4.4]). Another interesting feature of the PL is the doublet structure in the PL spectra (see Fig.[4.5]), of which the physical origin is still unclear.

The behavior of PL intensity modulations was interpreted by Wang, Birman and Su [40] using a simple model of considering the magneto-exciton states as the perturbed Laughlin state times an excitonic-like entity. Although the energy anomalies have been investigated theoretically [41, 42, 43], the doublets (or triplets) structure and their temperature and magnetic field dependence are still not well understood. The main subject of this section is to study the energy anomalies in the approximation of taking the valence hole in the lowest Landau level.

In photoemission or PL, after excitation by the laser, the initial state is $N + 1$ electrons in the conduction band with 1 hole in the valence band denoted Ψ_n^{me} below; after recombination of a electron with the hole, the final state is the N electron FQHE system denoted Ψ_m^e. The coupling between electron (hole) and photon is from the $\vec{j} \cdot \vec{A}$ term. Decompose the vector

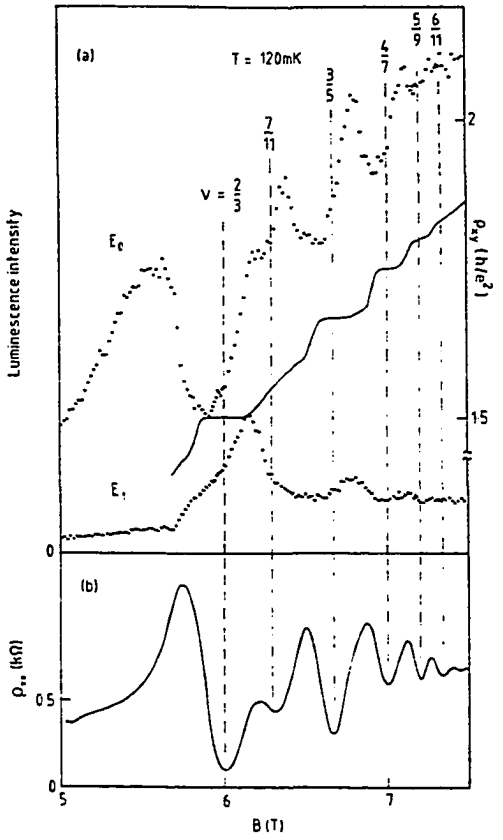

Figure 4.4: Dependence of the PL intensity as a function of the applied transverse magnetic field.
(a) Intensities of the E_0 and E_1 luminescence lines at $120mK$ as a function of magnetic field for $\nu \leq 1$. (b) Simultaneous ρ_{xx} data. Also shown in (a) is a ρ_{xy} trace from a Hall bar at a similar temperature in the absence of laser illumination. Reproduced from Fig.(3) of Ref.[32]

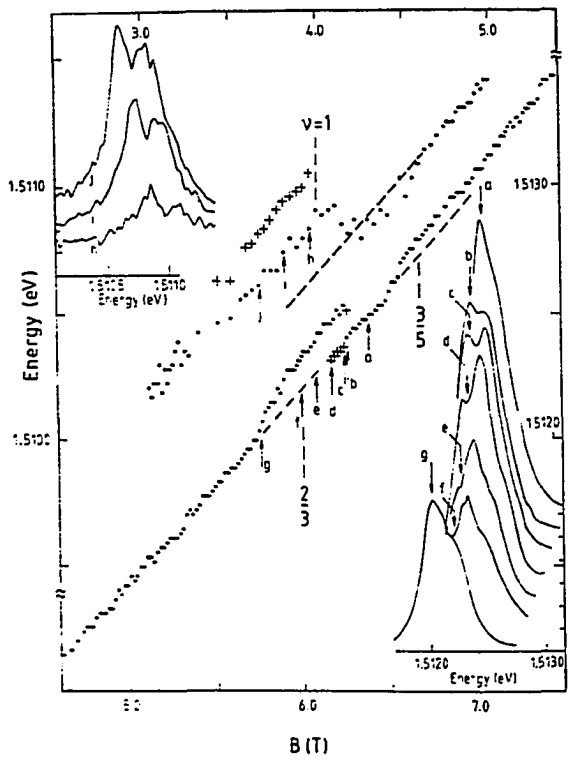

Figure 4.5: Dependence of the PL intensity as a function of the applied transverse magnetic field.
Magnetic-field dependence of the energy of the E_0 luminecence line. Bottom and rigth-hand axes refer to the lower section of the figure (spanning the $\nu = 2/3$ hierarchy), while top and left-hand axes refer to its low-field continuation (to the $\nu = 1$ region). Lower and upper insets: Spectra showing E_0 doublet structure resolved at $\nu = 2/3$ and 1. The weaker component is marked as +. Reproduced from Fig.(3) of Ref.[32]

potential as $\vec{A} = A_+\hat{e}_+ + A_-\hat{e}_- + A_0\hat{e}_0$, where $\hat{e}_+ = (\hat{e}_1 - i\hat{e}_2)/\sqrt{2}$, $\hat{e}_- = (\hat{e}_1 + i\hat{e}_2)/\sqrt{2}$, and $\hat{e}_0 \equiv \hat{e}_3$ are polarization vectors of the electromagnetic field. The electron-photon coupling term in the dipole approximation can be written as

$$H_{int} = c_1 A_+ \hat{\mathcal{L}}_{+1} + c_{-1} A_- \hat{\mathcal{L}}_{-1} + c_0 A_0 \hat{\mathcal{L}}_0 + h.c. \tag{4.9}$$

where c_i are constants and

$$\hat{\mathcal{L}}_i = \sum_m \hat{e}_m \hat{h}_{m+i} \tag{4.10}$$

and $\hat{e}_m$ and $\hat{h}_m$ are annihilation operators of the electron and hole respectively. Previous studies [41, 42, 43] used only $\hat{\mathcal{L}}_0$ as the transition operator. However, as $\hat{\mathcal{L}}_0$ only couples with $\vec{A}_3$, the electromagnetic fields with this polarization will propagate along the $x-y$ plane and cannot be measured in the experiments which are done in back emission. So the relevant transition operators are $\hat{\mathcal{L}}_{+1}$ and $\hat{\mathcal{L}}_{-1}$. However, we also will study the PL spectra due to $\hat{\mathcal{L}}_0$ just for comparison.

From the Fermi Golden rule, the intensity of the emission, called $P(\omega)$, in the PL spectra are given by

$$P(\omega) = M \sum_{m,n} e^{-\beta E_n^{me}} \left| \langle \Psi_m^e | \hat{\mathcal{L}}_i | \Psi_n^{me} \rangle \right|^2 \delta(\hbar\omega - E_n^{me} + E_m^e) \tag{4.11}$$

Where $\beta = (KT)^{-1}$ is the inverse temperature. Ψ_n^{me} (E_n^{me}) and Ψ_m^e (E_m^e) are eigen wave functions (energies) of the ME ($(N+1)$e plus 1h) and pure electron system (Ne) respectively. And For simplicity, we have assumed that only circularly polarized light is measured. Since $P_{-1}(\omega)$ is identical to $P_{+1}(\omega)$ we will use $P_1(\omega)$ in this paper to represent $P_{\pm 1}(\omega)$.

We calculate numerically the PL spectra using Eq.(4.11). The eigen functions and eigen energies are calculated exactly using exact diagonalization of Hamiltonian for (6e+1h) system and (5e) system respectively. We found that the spectra $P_{0,1}(\omega)$ has complex structure and interesting dependence on the e-h interaction (and specifically dependence on d), originating from the interesting dependence of magneto-exciton states on d. Before discussion of the general features of these d dependence photoemission spectra, let's first quote the previous result on the special limit $d = 0$. It is easy to prove that at $d = 0$, the PL spectra due to $\hat{\mathcal{L}}_0$ has a single peak $P_0(\omega) = \delta(\hbar\omega - E_h)$ where E_h is the "activation" energy of a single hole. In the analogous spin-1/2 system,

$$\begin{aligned} \hat{\mathcal{L}}_0|\Psi_n^{ex}\rangle &= S_t^+|n, S_t, (N-1)/2 - S\rangle \\ &= \sqrt{(S_t+1/2)^2 - (S-N/2)^2}|n, S_t, (N+1)/2 - S\rangle \quad (4.12) \end{aligned}$$

Since $|n, S_t, (N+1)/2 - S\rangle$ is a state of the FQHE, we have the above result about $P_0(\omega)$. This relation does not exist for $\hat{\mathcal{L}}_{\pm 1}$. So there are many peaks in $P_1(\omega)$ at $d = 0$ limit. However our numerical calculations show that there is a *dominant* single peak for $P_1(\omega)$. Other peaks are almost invisible although they are not zero.

From the last section, we know that there are three regions of d in which the enrgy level spectrum of the FQHE system and the magneto-exciton are distinct (see Fig.[4.2] & [4.3]). Then three regions of e-h separation d play a very significant role in classifying the optical emission spectra.

(i) In the large d region $d > d_c$, the magneto-exciton has a band-like structure. At finite temperature, $T \sim 0.003e^2/\varepsilon l_0(0.5K) - 0.01e^2/\varepsilon l_0(2K)$,

there should be a broad peak from the lowest branch of states of magneto-exciton. Because of angular-momentum (or momentum) conservation, this peak is due to transitions from the states in the lowest (parabolic) branches to the "dip" of magneto-roton states [see below].

(ii) In the small d limit, $d \ll d_c$. There is a sharp peak which comes from the transition $0 \to 0$ (for $P_0(\omega)$) or $1 \to 0$ (for $P_1(\omega)$) (ground state $\to$ Laughlin state).

(iii) Near the transition region $d \sim d_c$, there should be two peaks which are peaks of the same origin as those in (i) and (ii). The energy differences are around the gap energy of the Laughlin incompressible state.

The magnitude of the optical peaks depends on the density of states, population of the initial magneto-exciton states, and transition probability from the magneto-exciton to FQHE states. In this study, the effect of density of states (DOS) can be neglected, since for the two peaks discussed above, the initial states is either at $L \sim 0$ (or $k \sim 0$) or at the "dip" region of the magneto-roton, so the DOS is rather large. From Fig.[4.2], we see that in the region $d < d_c$, the lowest energy states have $L \sim 0$, and in the region $d > d_c$, the lowest energy states in the lowest branch have $L \sim 3$ for $\nu = 1/3$. In the transition region, the low energy states with $L \sim 0$ and $L \sim 3$ have competing energies. So we can relate this result to the above statement about the optical spectrum in these three regions at low temperature. To quantify the above scenario, we calculate the relevant transition probabilities and unrenormalized transition amplitudes thermally weighted by $e^{-\beta E_{ex}}$ ($\beta = 200(e^2/\varepsilon l_0)^{-1}$) in Table [4.1].

Distance d	Initial state E, L	ΔE	P_0	$P_0 e^{-\beta E_{ex}}$	ΔE	P_1	$P_1 e^{-\beta E_{ex}}$
0.00	-3.61464 ($L=0$)	-1.3171	8.00	6.85			
0.00	-3.61619 ($L=1$)	-1.4224	0.00	0.00	-1.3186	5.90	5.90
0.30	-2.53774 ($L=0$)	-0.2402	7.92	7.92			
0.30	-2.53365 ($L=1$)	-0.4200	0.00	0.00	-0.0187	6.34	6.34
0.30	-2.51696 ($L=3$)	-0.3125	0.65	0.80	-0.3125	0.43	0.08
0.30	-2.51580 ($L=4$)	-0.3162	0.00	0.00	-0.3162	1.319	0.22
0.40	-2.31954 ($L=0$)	-0.0220	7.04	2.09			
0.40	-2.31625 ($L=1$)	-0.2026	0.00	0.00	-0.0187	5.96	1.27
0.40	-2.33166 ($L=3$)	-0.1272	0.21	0.21	-0.1272	0.16	0.16
0.40	-2.32724 ($L=4$)	-0.1277	1.32	0.85	-0.1277	1.04	0.67
0.45	-2.22585 ($L=0$)	0.0717	6.71	0.58			
0.45	-2.22299 ($L=1$)	-0.1094	0.00	0.00	0.0746	5.72	0.38
0.45	-2.25024 ($L=3$)	-0.0458	0.17	0.17	-0.0458	0.13	0.13
0.45	-2.24520 ($L=4$)	-0.0456	1.78	0.71	-0.0456	0.95	0.57
0.90	-1.65807 ($L=0$)	0.6395	5.22	0.01			
0.90	-1.65725 ($L=1$)	0.4564	0.01	0.00	0.6403	4.62	0.00
0.90	-1.77274 ($L=3$)	0.4770	0.11	0.11	0.4770	0.10	0.10
0.90	-1.72483 ($L=4$)	0.4747	0.87	0.67	0.4747	0.74	0.57

Table 4.1: Calculation of transition probabilities. The unit of energy is $e^2/\varepsilon l_0$ and $\beta = 200$

Where $P_0 = \left|\langle \Psi_m^e | \hat{\mathcal{L}}_0 | \Psi_n^{ex} \rangle\right|^2$ and $P_1 = \left|\langle \Psi_m^e | \hat{\mathcal{L}}_1 | \Psi_n^{ex} \rangle\right|^2$

For the $P_0(\omega)$ transition, there is a selection rule $\Delta L = 0$ where L is the total angular momentum of the magneto-exciton (magneto-roton). For the $P_1(\omega)$ transition, no such selection rule exists. However, the largest transition probability occurs for transition $\Delta L = 0, \pm 1$, with the $(\pm)$ sign depending on the $P_{\pm 1}$ transition. In Table [4.1] we only give the most relevant transition probabilities. However we should remember that the states with larger L in the lowest branch of the magneto-exciton also contribute to the photoemission peak at large d. We neglect these states in Table [4.1] because they are similar to $L = 4$.

From Table [4.1] we see that the transition probability changes smoothly except at $d \leq d_c$ in which case the most relevant transition probability also changes smoothly. Due to the crossing of low energy levels with the change of d, the population of electrons will change drastically, so with the changing of d, the high energy peak will decrease, and the low energy peak will increase. In the crossover region $d \sim d_c$, the two peaks have comparable strength, *i.e.* we find doublets with energy splitting around the gap value of $\Delta \sim 0.1e^2/\varepsilon l_0$ (see Fig.[4.6] & Fig.[4.7]).

The PL spectra are shown in Fig.[4.6] and [4.7] for $P_0(\omega)$ and $P_1(\omega)$ respectively. For technical reason, regarding the plotting of our curves, the spectra in the figures were smoothed by hand using broadening of the delta functions to Lorentzian distributions with half-width $\gamma = 0.004e^2/\varepsilon l_0$. We have shifted the Photon energy by $\omega_0 = \Gamma_g + \mu_f$ (see Fig.4.8), where Γ_g is the semiconductor gap and μ_f is the chemical potential of the electrons.

The difference between the structure of $P_1(\omega)$ spectra and $P_0(\omega)$ spectra

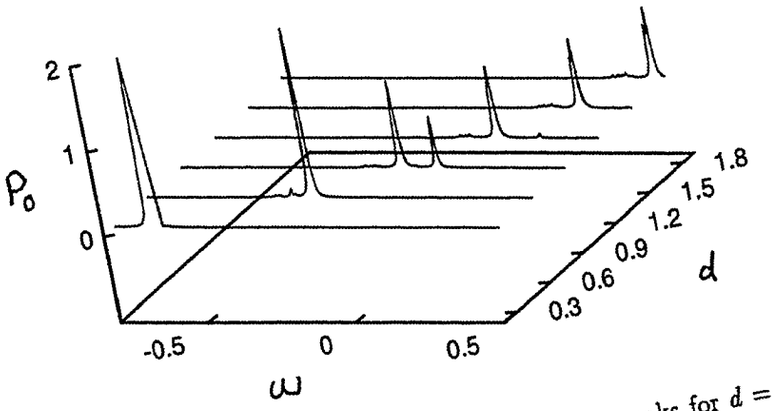

Figure 4.6: PL spectra $P_0(\omega)$ as function of d. The peaks for $d = 0.3$ has been reduced by factor of 4.

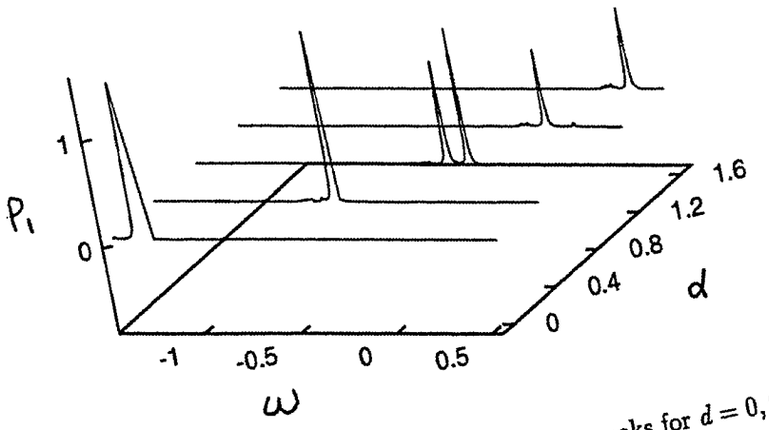

Figure 4.7: PL spectra $P_1(\omega)$ as function of d. The peaks for $d = 0, 0.4$ have been reduced by factor of 4.

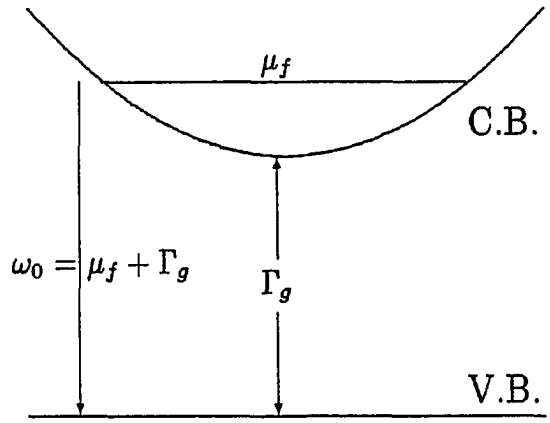

Figure 4.8: Illustration of the photon-frequency shift in energy band structrue diagram.

are rather small, as the $P_1(\omega)$ and $P_0(\omega)$ spectra are indistinguishable. A doublet structure appears in both $P_1(\omega)$ and $P_0(\omega)$. In this calculation using spherical geometry, the doublet structure occurs only in the transition region $d \sim 0.8R$. The reported experiments [33] are in plane geometry. We suggest that this critical region in spherical geometry corresponds to a very broad region in the flat plane geometry, and that most of the experiments in which the distance d between electron and valence hole is comparable to the magnetic length l_0 belong to this transition region, so the doublet structures can be observed. We should mention that doublets have different temperature behavior for $d < d_c$ and $d > d_c$. For example, in the experiment by Heiman *et al.* [33] the lower energy peak increases with the increase of temperature, this corresponds to $d < d_c$ [42]. If $d > d_c$, then the initial states for the low energy peak have lower energy than that of initial states for the

high energy peak, the lower energy peak should decrease with the increase of temperature. However, since the distance between the electron and hole might also depend on the temperature in some of the experiments, and the doublets are very sensitive to the distance d between electron and hole, the temperature dependence of the distance d can have important effects on the photoemission spectra.

4.3 Inelastic Raman Scattering

Recently Pinczuk *et al.* [34] found the magneto-roton resonance peak in RS experimentally at filling fraction $\nu = 1/3$. The measurement was done in backscattering at transferred wave-vector $Q = q_1 - q_2 = 0$ where q_1 (ω_1) and q_2 (ω_2) are the wave-vector (energy) of incident and scattered photons. They found three energy shift peaks around $\Omega \equiv \omega_1 - \omega_2 \approx 0.1E_c$. The central peak of energy shift peak (Ω) is unchanged with the changing of incident photon frequency (ω_1), while for two other peaks the "scattered" photon frequency ω_2 doesn't change with the changing of ω_1, *i.e.* the energy shift Ω of these two peaks changes with the change of ω_1. The conclusion is that the two side-peaks are *hot luminescence* peaks; and the central peak is the genuine RS peak. They found the magnitude of the RS peak is very sensitive to the incident photon frequency ω_1. The following parameters are typical for the samples they used: $l_0 \sim 100\mathring{A}$, $E_c \sim 14mev$, Temperature $T \sim 0.5K \sim 0.003E_c$, and the gap value they measured is $\Delta \sim 0.1E_c$ where $E_c = e^2/\varepsilon l_0$.

Usually, the RS efficiency is modeled so as to be proportional to the dy-

namic structure factor $S(Q,\Omega)$ of the conduction band electrons. From the results of approximating the entire optical strength by one mode, the so-called "Single Mode Approximation" or SMA [38, 39], and more basically from Kohn's theorem [77], which states that: in a translationally invariant electron gas subject to a magnetic field, the collective density mode has a zero-momentum gap ω_c (cyclotron frequency) which is independent of the electron-electron interaction, we know that the oscillator strength of the magneto-roton mode is proportional to Q^4, *i.e.* $S(Q,\Omega) \sim Q^4$. So the magneto-roton cannot be measured for $Q = 0$, and the magneto-roton cannot be measured in a usual RS experiment for $Q = 0$.

The reason it can be measured is because of the resonance enhancement and appearance of the valence hole [95] in the intermediate state. The magnitude of the RS peak from the magneto-roton mode is very sensitive to the incident photon energy ω_1, as found in the experiment [34]. I will now show this.

For numerical calculations for a finite system, the following equation for the RS efficiency ($Q = 0$) can be used:

$$\mathcal{W}(\Omega) = M \sum_{n,i,\mu,\nu} e^{-\beta E_i^e} \delta(\Omega - E_i^e - E_n^e) \times$$
$$\left| \sum_m \langle \Psi_i^e | \hat{\mathcal{L}}_\mu^\dagger | \Psi_m^{me} \rangle \frac{1}{\omega_1 + E_i^e - E_m^{me} - i\gamma} \langle \Psi_m^{me} | \hat{\mathcal{L}}_\nu | \Psi_n^e \rangle \right|^2 \qquad (4.13)$$

Here γ is the finite hole-lifetime broadening, and μ and ν are the index of the (circular) polarization $\mu, \nu = \pm$ for rh/lh polarization. We also renormalize (shift) the photon energy by the "activation" energy of the valence hole as

we did in last section. Since in the RS, the initial states are incompressible and $\Delta \gg T$, we will assume $T = 0$. Physically, the content of Eq.(4.13) is: the initial state of the system is N electrons in the ground state, (virtual) intermediate state is created by absorption of a photon, and the final state is again N electrons state, but with an "excitation" produced along with the scattered photon.

From section 4.2, we see that the PL spectrum depends on the electron-hole interaction (which is controled by the electron-hole separation d here). However, from Eq.[4.13] we can see that the positions of the resonance RS peaks are independent of the distance d between the electron-hole layers. Since the value of the transition probability $\left|\langle\Psi_m^e|\hat{\mathcal{L}}_1|\Psi_n^{ex}\rangle\right|^2$ is a smooth function of the distance d, we may expect that the magnitude of the peaks should not be very sensitive to the distance d.

Our calculation was again done using spherical geometry with $N = 5$ electrons in the initial states at $\nu = 1/3$, and $N + 1$ electrons plus 1 valence hole in the intermediate states. We use $\gamma = 0.03$ which is in the order of the energy level difference. The same calculation has been done for $N = 4$ and the RS spectrum is basically the same. We will only consider the $\hat{\mathcal{L}}_1$ process since the experiments are done in backscattering geometry. The calculated RS spectrum for the scattering process $\alpha \to \beta$ with $(\alpha \neq \beta)$ at different d is shown in Fig.[4.9]. We found that for this process, in which the circular polarization of the incident and scattered photon are opposite, the RS has a robust peak at an energy shift ($\Omega \sim 0.12E_c$) larger than the gap value

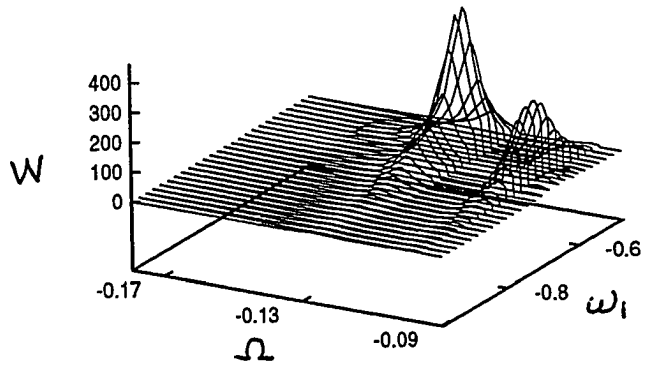

RS spectrum $W(\Omega, \omega_1)$ for $d = 0.3R$.

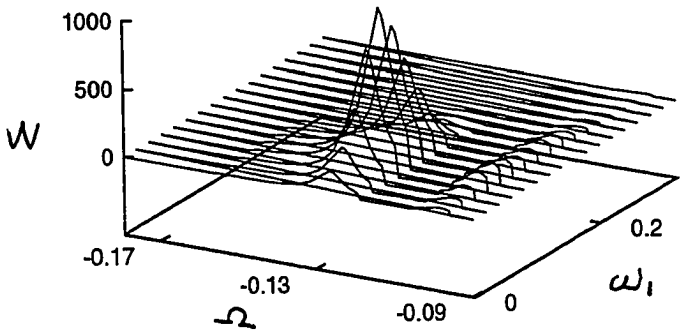

RS spectrum $W(\Omega, \omega_1)$ for $d = 0.9R$.

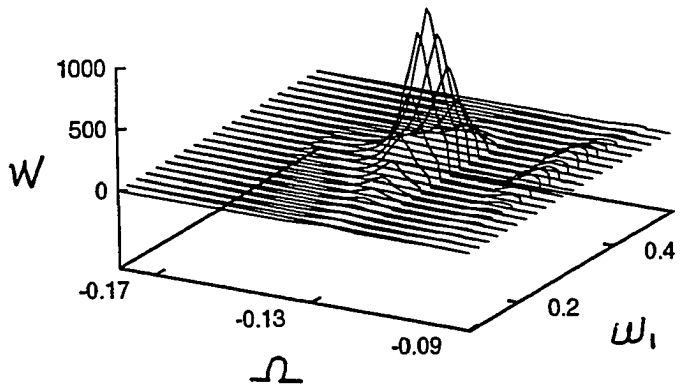

Figure 4.9: RS spectrum $W(\Omega, \omega_1)$ for $d = 1.2R$.

$\Delta \sim 0.09$ [1]. For $N = 5$, the gap is $\Delta = 0.09E_c$, while the resonance peak is at $\Omega = 0.12E_c$. This is not surprising since the magneto-roton at the minimum energy has wavevector around $k_0 \sim 1/(\nu l_0)$, and the resonance is at $Q = 0$. It is believed that the gap-excitation in the $k = 0$ limit can be approximated by a two-roton bound state [39]. Using the result of Haldane and Rezayi [96], $\Omega = 0.12E_c$ is around the gap value of gap-excitation at $k = 0$. Another feature in Fig.[4.9] is that the resonance only occurs in a narrow frequency region of the incident photon frequency. This agrees with the experiments [34]. For the process that the incident and out scattered photon has the same (circular) polarization ($\alpha = \beta$), there is only an *elastic* peak.

The resonance RS at $\nu = 2/5$ has also been calculated [see Fig 4.10] and no robust resonance peak close to the gap value can be found. The absence of the resonance peak of the gap excitation is in agreement with Pinczuk's experiment [97].

[1] In Fig[4.9], the weak peak around gap value is due to finite size effect and is not a robust peak

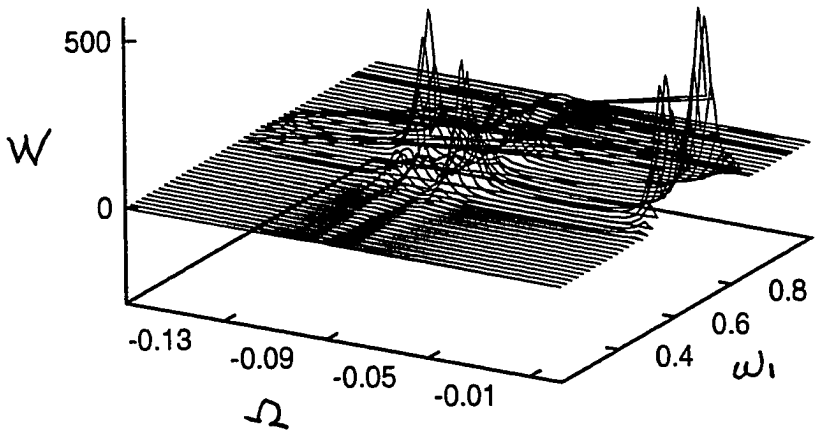

Figure 4.10: RS spectrum $W(\Omega, \omega_1)$ for $d = 1.2R$ at $\nu = 2/5$.

Chapter 5

Fermi Edge Singularity in Double Layer FQHE Systems

5.0 Introduction

In semiconductors, a double layer (DL) 2-dimensional electron gas (2DEG) can be realized in a wide $GaAs/AlGaAs$ quantum well (QW) or in a double $GaAs/AlGaAs$ quantum well (DQW). The separation between the two layers can be various from $30\mathring{A}$ (DQW) to $400\mathring{A}$ (QW).

In the double layer FQHE systems, novel quantum effects can be revealed [44, 45, 46, 47, 48, 49, 50], due to interplay of inter-layer electron-electron interaction, intra-layer electron-electron interaction, and interlayer tunneling. One interesting phenomenon is that the FQHE occurs at *even*-denominator filling fraction [47, 48] $\nu = 1/2$. Due to the interaction and tunneling between electrons in different layers, the ground state can have strongly correlated states well approximated by the trial wavefunction proposed by Halperin

[64]

$$\Psi_m(z_1, z_2, \cdots, z_N) = \mathcal{N} \prod_{i<j}^{N} (z_i - z_j)^m \prod_{i<j}^{N} (z_{i'} - z_{j'})^m \prod_{i',j}^{N} (z_{i'} - z_j)^n \\ e^{-(\sum_i |z_i|^2)/4l_0} e^{-(\sum_{i'} |z_{i'}|^2)/4l_0} \quad (5.1)$$

Here i $(i = 1, \cdots, N)$ and i' $(i' = 1, \cdots, N)$ represent the index of electrons at different layers. It was recently found that a new quantum phase occurs in the presence of magnetic field parallel to the layers [50, 54].

The collective excitation spectra of the double layer FQHE systems are also very interesting, recalling the rich structure in the single layer FQHE systems. Single mode approximation (SMA) [98] as well as Chern-Simons field theoretical approach [52, 53, 99] have been used to study the inter-Landau and intra-Landau collective charge excitations, and discrepancies exist in these theories [98].

In this chapter, I will use the Chern-Simons field theoretical approach to show that the Fermi edge singularity (FES) [100, 101] exists in the double layer FQHE systems due the presence of a neutral gapless mode [52, 53, 99]. Since the FES is sensitive to the oscillator strength as well as the energy gaps of the collective charge density modes, we propose that the FES experiments of FES in these systems would be able to resolve the discrepancies in the literature about the nature of the neutral gapless excitations [98].

5.1 Double Layer FQHE: Chern Simons Field Theory Approach

The double layer FQHE (DLQHE) systems have two parallel layers of 2-dimensional (2D) electrons with layer separation d. The filling fractions for the DLQHE is defined as $n_{tot}/(eB/hc)$, where n_{tot} is the total electron density of two layers and B is the magnitude of the magnetic field perpendicular to the plane of 2D electron gas. The Lagrangian for the DLQHE system without term for interlayer electron tunneling, in Euclidian space is:

$$\mathcal{L} = \sum_{\alpha} \bar{\Psi}_{\alpha}\partial_0\Psi_{\alpha} + \sum_{\alpha}\frac{1}{2m}|\vec{D}\Psi_{\alpha}|^2 + \sum_{\alpha,\beta}\frac{1}{2}(\bar{\Psi}_{\alpha}\Psi_{\alpha} - \bar{\rho_{\alpha}})V_{\alpha\beta}(\bar{\Psi}_{\beta}\Psi_{\beta} - \bar{\rho_{\beta}}) \quad (5.2)$$

where α, $\beta = 1, 2$ is the index of layers, $\vec{D} = -i\vec{\partial} - \vec{A}$ ($\vec{A}$ is the external vector potential) and $V_{\alpha\beta}$ represents both interlayer and intralayer Coulomb interactions

$$V_{\alpha\beta}(\vec{x},\vec{y}) = \frac{V_0}{[|\vec{x}-\vec{y}|^2 + d^2\delta_{\alpha\beta}]^{1/2}} \quad (5.3)$$

Where d is the interlayer separation.

To study the FQHE for a double layer system with equal layer-density $\bar{\rho}_1 = \bar{\rho}_2$, we transform Fermions to Bosons using a singular gauge transformation [18, 52]:

$$\Psi^{\dagger}_{\alpha}(\vec{x}) = e^{-i\int d^2\vec{x}'\Theta(z-z')[k_1\phi^{\dagger}_{\alpha}(z')\phi_{\alpha}(z')+k_2\phi^{\dagger}_{\beta}(z')\phi_{\beta}(z')]}\phi_{\alpha}(\vec{x}) \quad (\beta \neq \alpha) \quad (5.4)$$

$$= e^{-i\int_{\infty}^{\vec{x}} d\vec{x}'\cdot\vec{a}_{\alpha}(\vec{x}')}\phi^{\dagger}_{\alpha}(\vec{x}) \quad (5.5)$$

Here k_1, k_2 are odd-integers, $z = x_1 + ix_2$ with $\vec{x} = x_1\hat{e}_1 + x_2\hat{e}_2$ and in Eq.(5.5) the integration path $\infty \rightarrow \vec{x}$ means the path begins from $(r = \infty, \theta = 0)$.

The condition for the statistical gauge field $\vec{a}_\alpha$ in Eq.(5.5) is:

$$\vec{\partial} \times \vec{a}_\alpha(\vec{x}) = k_1 \phi^\dagger_\alpha(\vec{x})\phi_\alpha(\vec{x}) + k_2 \phi^\dagger_\beta(\vec{x})\phi_\beta(\vec{x}) \tag{5.6}$$

Using the Coulomb gauge for $\vec{a}_\alpha(\vec{x})$,

$$\vec{a}_\alpha(x) = \hat{e}_3 \times \int d^2\vec{x}' \frac{\vec{x}-\vec{x}'}{|\vec{x}-\vec{x}'|^2}[k_1 \phi^\dagger_\alpha(\vec{x}')\phi_\alpha(\vec{x}') + k_2 \phi^\dagger_\beta(\vec{x}')\phi_\beta(\vec{x}')] \tag{5.7}$$

for $\alpha \neq \beta$.

Define

$$\vec{b}_1 = \frac{k_1\vec{a}_1 - k_2\vec{a}_2}{(k_1+k_2)(k_1-k_2)}; \quad \vec{b}_2 = \frac{k_1\vec{a}_2 - k_2\vec{a}_1}{(k_1+k_2)(k_1-k_2)} \tag{5.8}$$

then

$$\vec{\partial} \times \vec{b}_\alpha(\vec{x}) = \phi^\dagger_\alpha(\vec{x})\phi_\alpha(\vec{x}) \tag{5.9}$$

After the transformation and separating the modulus and phase degrees of freedom $\phi_\alpha = \rho_\alpha^{1/2} e^{i\eta^\alpha}$, we get:

$$\begin{aligned} \mathcal{L} &= \sum_\alpha i\rho_\alpha(\partial_0\eta^\alpha + b^0_\alpha) + \sum_\alpha \frac{\rho_\alpha}{2m}|\vec{\partial}\eta^\alpha + \vec{a}_\alpha - \vec{A}|^2 + \sum_\alpha \frac{1}{2m}(\vec{\partial}\rho_\alpha^{1/2})^2 \\ &\quad + \sum_{\alpha,\beta}\frac{1}{2}(\rho_\alpha - \bar{\rho}_\alpha)V_{\alpha\beta}(\rho_\beta - \bar{\rho}_\beta) - \sum_\alpha i\underline{b_\alpha}\cdot\underline{\nabla}\times\underline{b_\alpha} \end{aligned} \tag{5.10}$$

Here ρ_α is the electron density in layer α, and the three-component vector symbol $\underline{C} \equiv (C_0, \vec{C})$ is used. In Eq.(5.10) the CS term is introduced from the condition Eq.(5.9) and by doing a gauge transformation to an arbitrary gauge for $\underline{b_\alpha}$ [18, 19]. The DLQHE states are described by the mean field solution of the theory taking $\bar{\rho}_1 = \bar{\rho}_2$:

$$\begin{aligned} (\vec{\partial} \times \langle\vec{a_1}\rangle) = (\vec{\partial} \times \langle\vec{a_2}\rangle) = (\vec{\partial} \times \langle\vec{A}\rangle) = (k_1+k_2)(\bar{\rho}_1+\bar{\rho}_2)/2 \\ \bar{\eta}_\alpha = 0 \end{aligned} \tag{5.11}$$

The filling fraction of this DLQHE state is $\frac{2}{k_1+k_2}$. For $k_1 = 3$, $k_2 = 1$, the even-denominator filling fraction $\nu = 1/2$ is obtained, and the mean-field solution of the wavefunction is just Eq.[5.1] with $m = 3$ and $n = 1$. For $k_1 = k_2$, the electrons in the different layers are strongly coupled, so that the DLQHE state is equivalent to the single layer FQHE state at $\nu = 1/k_1$. When $k_1 = k_2 = 2$, a different double layer FQHE state takes place at $\nu = 1/2$.

5.2 Density Fluctuations, Photoemission and Fermi Edge Singularity in 1/k States

5.2.1 Density Fluctuations and Neutral Gapless Mode

Now we will study the dynamics of a core hole coupled with the DLFQH system. For the core hole is in symmetrical position or in asymmetrical position, the dynamics of the core hole will be drastically changed.

The dynamics of the core hole and coupling with the fluctuations around the mean field solution $(1/k)$ can be described by the Lagrangian [see Appendix B]:

$$\begin{aligned}
\mathcal{L}_t &= \mathcal{L}^+ + \mathcal{L}^- + \bar{d}(\partial_0 + \varepsilon_d)d + \bar{d}d(\lambda^+\rho^+ + \lambda^-\rho^-) \\
\mathcal{L}^+ &= -\frac{m}{2\bar{\rho}}(\partial_0\rho^+)\frac{1}{\partial^2}(\partial_0\rho^+) - \frac{(2k)^2\bar{\rho}}{2m}(\rho^+)\frac{1}{\partial^2}(\rho^+) + \frac{1}{8m\bar{\rho}}(\vec{\partial}\rho^+)^2 + \frac{1}{2}\rho^+V^+\rho^+ \\
\mathcal{L}^- &= i\rho^-\partial_0\eta^- + \frac{\bar{\rho}}{2m}(\vec{\partial}\eta^-)^2 + \frac{1}{8m\bar{\rho}}(\vec{\partial}\rho^-)^2 + \frac{1}{2}\rho^-V^-\rho^- \qquad (5.12)
\end{aligned}$$

Here d, $\bar{d} \equiv \hat{d}^\dagger$ are variables of the core hole, $\rho^+ = (\delta\rho_1 + \delta\rho_2)/\sqrt{2}$, and $\rho^- = (\delta\rho_1 - \delta\rho_2)/\sqrt{2}$. $\mathcal{L}^+$ describes the fluctuation of the total charge density (TCD) which is the same as the charge fluctuation in FQHE in $\nu = 1/k$ states [23]. $\mathcal{L}^+$ is obtained using a duality transformation [23, 102].

$\eta^+ = (\delta\eta^1 + \delta\eta^2)/\sqrt{2}$ has been absorbed into the gauge field $\underline{a}$, while $\eta^- = (\delta\eta^1 - \delta\eta^2)/\sqrt{2}$ appears in $\mathcal{L}^-$, which Lagrangian describes the fluctuation of the difference charge density (DCD) which in turn is the neutral gapless excitation [52], ε_d is the renormalized site energy of the core hole. In Fourier space, $V^+(q) = V_0(1 + e^{-qd})/q$ and $V^-(q) = V_0(1 - e^{-qd})/q$. λ^+ (λ^-) are the symmetrized (antisymmetrized) coupling constants of the core hole with the density fluctuations. It is easy to see that $\lambda^+ < 0$, while either $\lambda^- < 0$ or $\lambda^- > 0$ can occur. In the case the core hole is in the middle of the two layers, $\lambda^- = 0$.

We now integrate out η^- in $\mathcal{L}^-$ and are left with an effective action $S_{\rho d}$ describing the core hole coupled with a fluctuating plasmon field ρ^+ and ρ^-.

$$S_{\rho d} = \int \bar{d}(\partial_0 + \varepsilon_d)d + \int \bar{d}d(\lambda^+\rho^+ + \lambda^-\rho^-)_{\vec{x}=0} + \frac{1}{2}\int \rho^+\chi_+^{-1}\rho^+ + \frac{1}{2}\int \rho^-\chi_-^{-1}\rho^- \tag{5.13}$$

where in Fourier space:

$$\begin{aligned} \chi_+ &= \frac{\bar{\rho}}{m}\frac{q^2}{\omega^2 + \epsilon_+^2} \\ \chi_- &= \frac{\bar{\rho}}{m}\frac{q^2}{\omega^2 + \epsilon_-^2} \end{aligned} \tag{5.14}$$

Where $\epsilon_- = \sqrt{\frac{\bar{\rho}}{m}V^-(q)q^2 + \frac{q^4}{4m^2}}$, and $\epsilon_+ = \sqrt{\omega_c^2 + \frac{\bar{\rho}}{m}V^+(q)q^2 + \frac{q^4}{4m^2}}$ with $\omega_c = eB/(m^*c)$ is the electron cyclotron frequency. In Eq.(5.14), χ_- is the density susceptibility of the DCD mode, and χ_+ is the density susceptibility of the TCD mode.

We should mention here that χ_+ in Eq.(5.14) has only the contribution from the inter-Landau level magnetoplasmon mode. It was shown by several authors [35, 39, 26, 25] that the magnetoplasmon mode will saturate

the f-sum rule in the limit $q = 0$ because of Kohn's theorem [77]. Lopez and Fradkin showed [26] that this is also true in the long wavelength limit ($q \ll 1/l_0$) except for $\nu = 1/3$ with short range interactions. Here we are considering long range (Coulomb) interaction [1]. So the χ_+ we used in Eq.[5.14] will be the principal part of the density susceptibility of the TCD mode. We will show later that the TCD mode will not contribute to FES (which is our main concern here) if there is a gap in the dispersion of this mode (or modes). Since the dispersion of this mode has a finite gap ($\sim \omega_c/15$ is estimated for FQHE system), the portion left out of χ_+ in Eq.[5.14] does not contribute to the FES. So we believe that using χ_+ in Eq.[5.14] will not change the essential result of our theory.

5.2.2 Green's Functions, Photoemission and FES

We now calculate the Green's function for the core hole

$$G_d(\tau - \tau') = -i\langle T[\hat{d}(\tau)\hat{d}^\dagger(\tau')]\rangle. \tag{5.15}$$

Using Eq.(5.14), the Green's Function can be calculated in the deep-hole limit (the core hole energy is far below the Fermi surface) [103, 104] $G_d(\tau) = G_d^0(\tau)e^{-Q_{oc}^+ - Q_{oc}^-}$ with

$$Q_{oc}^i = -\frac{\tilde{\rho}(\lambda^i)^2}{2m}\int_0^\Lambda dq \frac{q^2}{\varepsilon_i^2(q)}[\tau - \frac{1-e^{-\varepsilon_i\tau}}{\varepsilon_i}] \tag{5.16}$$

where $G_d^0(\tau) = e^{-\varepsilon_d\tau}$ is the Green's function of a bare hole, and Λ is the momentum cutoff. We have used the assumption that coupling between core

[1] Since the gapless mode is neutral, the Coulomb interaction cannot be screened out and then become short-range

hole and density-fluctuation involves only s-wave scattering. So instead of using $\int d\vec{q}$, we should use $\int_0^\infty dq$ whenever doing the Fourier transform of the core site $\vec{x} = 0$.

Because of the energy gap in the dispersion $\varepsilon_+(q)$, Q_{oc}^+ converges. It also can be seen that $\varepsilon_-(q) = (V_0 d\bar{\rho}/m)^{1/2} q$ $(q \to 0)$ has a linear dispersion for the gapless excitation. As is well known [103, 104], this gapless mode will introduce an infrared divergence in Eq.[5.16]: $Q_{oc}^- \sim \frac{\bar{\rho}(\lambda^-)^2}{2m(V_0 d\bar{\rho}/m)^{3/2}} \log(\tau)$. And this will give the *orthogonality catastrophe* [105] contribution to FES $|\omega - E_0|^{\beta^{oc}}$ with $\beta^{oc} = (\lambda^-)^2/[2(\bar{\rho}/m)^{1/2}(V_0 d)^{3/2}]$

Now we turn to the transitions between the core hole state and the electrons at $\nu = 1/k$ states. The absorption (or emission) cross-section is given by the Fermi-Golden rule. The relevant correlation function to consider for this process is

$$F_\alpha(\tau - \tau') = \langle T[\hat{d}(\tau)\hat{\Psi}_\alpha(0,\tau)\hat{\Psi}_\alpha^\dagger(0,\tau')\hat{d}^\dagger(\tau')]\rangle \tag{5.17}$$

and we can calculate the intensity of the optical spectra using

$$I(\omega) \propto Im \int_0^\infty dt[\mathcal{F}_1(t) + \mathcal{F}_2(t)]e^{i\omega t}. \tag{5.18}$$

Here $\mathcal{F}_\alpha$ is a real-time analog of F_α after a Wick rotation. To change the Fermion field $\hat{\Psi}_\alpha$ to a Boson field ϕ_α in F_α, we recall the procedure in deriving Lagrangian [5.12] [see Appendix B]: using the Fermion-Boson transformation Eq.(5.5)and after a gauge transformation of $\underline{b_\alpha}$ to absorb the phase η^+, then integrating out $\underline{b_\alpha}$, we are left with Lagrangian [5.12]. The Fermion variable $\hat{\Psi}_\alpha(0,\tau)\hat{\Psi}_\alpha^\dagger(0,\tau')$ can be approximately written as

$$\bar{\rho} e^{if_\alpha \frac{\eta^-(0,\tau) - \eta^-(0,\tau')}{\sqrt{2}}} e^{ik\int d^2\vec{x}'\Theta(-\vec{x}')[\rho^+(\vec{x}',\tau) - \rho^+(\vec{x}',\tau')]} \tag{5.19}$$

where $f_1 = 1$ and $f_2 = -1$ and we have neglected the fluctuation of the amplitude field $\delta\rho$.

Then we can separate the correlation function into TCD mode and DCD mode part. It can be shown that there is no infrared divergence contribution from TCD mode part because of the gap ω_c in the mode dispersion (There is no infrared divergence in the integral of Eq.[5.16] and Eq.[5.20] if $\varepsilon_i(q = 0) \neq 0$). So there is no contribution to the FES from the TCD mode.

We now use the Lagrangian [5.12] to calculate the DCD mode part of the correlation function. First integrate out η^- then integrate out ρ^-, and combining with the TCD mode part, we get $F_\alpha(\tau) = G_d(\tau)G_\rho(\tau)e^{-Q^\alpha_{exc}}$ where $G_\rho(\tau)$ is the Green function when the electrons are not coupled with the core hole. The contribution to $G_\rho(\tau)$ from the TCD mode having the form $\int d\vec{q}\frac{\varepsilon_-(q)}{q^2}(1 - e^{-\varepsilon_-(q)\tau})$ is convergent because the space dimension is 2. While the well known infrared divergence in Q_{oc} and Q^α_{exc} originates from that in calculating Q_i^-'s we have an effective space dimension 1 in the summation on momentum because the coupling between core hole and electrons involves only *s-wave* scattering. The FES contribution from the exciton effect [106, 100] is found to be:

$$Q^\alpha_{exc}(\tau) = -\frac{f_\alpha\lambda^-}{\sqrt{2}}\int_0^\Lambda dq\frac{1}{\varepsilon_-(q)}(1 - e^{-\varepsilon_-(q)\tau}) \tag{5.20}$$

This gives long time behavior $Q^\alpha_{exc}(\tau) = \frac{f_\alpha\lambda_-}{(2V_0d\bar{\rho}/m)^{1/2}}\log(\tau)$. So the contribution to the FES is $|\omega - E_0|^{\beta_{exc}}$ with $\beta^\alpha_{exc} = f_\alpha\lambda_-/(2V_0d\bar{\rho}/m)^{1/2}$.

Recalling that $f_1 = 1$ and $f_2 = -1$, we can see that for $\alpha \neq \alpha'$, $\beta^\alpha_{exc} = -\beta^{\alpha'}_{exc}$. Two "excitonic" exponents exist for each localized core hole.

5.2.3 Discussion

Now let us turn to discuss the effect of interlayer hopping. It is easy to show that if $\varepsilon_{-}(q)$ has a small gap Δ ($\Delta << \tau^{-1}$) in Eq.[5.16,5.20] the gap can be neglected in calculating Q_{oc} and Q_{exc}. So if the limit of experimental time for measurements is T_{exp}, the "long time behavior" of Q_{oc} and Q_{exc} are the same as that in the absence of interlayer hopping, providing $T_{res} << T << T_{exp}$ ($T_{exp} << \Delta^{-1}$), where T_{res} is the response time of the density-fluctuation to the perturbation of the presence of the core hole. In the above argument, the estimated gap Δ is extremely small. Hence, in order to measure the *power law anomaly* (exponents β^{α}) of the FES the interlayer hopping probability must be strongly suppressed.

To summarize, we discussed here for the first time the optical FES of double-layer quantum Hall systems in a simplified model of a static core hole (infinite mass) with infinite life-time, coupled with an electron of a DLQHE systems. Similar to the usual Fermi-liquid behavior, we obtained the exponent $\beta^{\alpha} = \beta^{\alpha}_{exc} + \beta_{oc}$ of the *power law anomaly* with $\beta_{oc} > 0$ and $\beta^{\alpha}_{exc} = -\beta^{\alpha'}_{exc}$ ($\alpha \neq \alpha'$), where α is layer index. Using our calculations, $|\beta_{oc}/\beta_{exc}| = |\lambda^{-}|/(\sqrt{2}V_0 d)$. We believe our predicted FES in DLQHE systems is a promising phenomena to be discovered in experiments, which can be used to study the properties of the neutral gapless excitations.

Chapter 6

Conclusion to Part I: Summary and Remaining Problems

In conclusion I have studied the properties of FQHE systems in this part of my thesis.

The Laughlin wave function was studied in the disk geometry. In contrast to the belief by some authors that the Laughlin wave function is not a good approximation to the exact ground state wave function, I found numerically that the Laughlin wave function is a very good approximation in the disk geometry. More generally, I showed that the Laughlin wave function has a large overlap with the exact ground state for reasonable *natural* short range or long range repulsive interactions.

I studied the hierarchy structure of FQHE using the Farey series. We proposed a heuristic RG flow diagram of the FQHE systems based on our hierarchy structure. Our phase diagram is consistent with that of Kivelson *et al.* [24] which was independently derived using the Chern-Simons field

theory.

The magneto-exciton in the FQHE systems was studied numerically. I found the spectrum of the magneto-exciton can be characterized into two phases according to the distance of the injected hole from the plane of the 2D electron gas. In one phase, the distance between electron and hole d is smaller than a critical value d_c, and the electron and valence hole are strongly correlated. The limiting case is $d = 0$ when electron and hole are in the same plane, a case already treated by other authors. In another phase, $d > d_c$, the valence hole is "weakly" coupled to an (strongly correlated) electron gas in the FQHE regime. The photoluminescence (PL) of the FQHE system can be understood from the properties of the magneto-exciton. The doublets in the PL were found to strongly depend on the distance d between the electron and hole. The resonance Raman scattering was calculated and one resonance peak around the gap value was found which confirmed Pinczuk *et al.*'s experiment [34].

I also studied the excitation spectra in the double layer FQHE systems using the Chern-Simons field theoretical method. I calculated the Fermi edge singularities (FES) in these systems due to the neutral gapless density mode. The FES exponents due to recombination of electrons in different layer with core hole are different. Since there is no FES in the *incompressible* FQHE systems without this neutral gapless mode, we proposed that the FES experiment can be used to detect the gapless mode in photoluminescence or Raman scattering.

There are many important questions in this subject which remain unan-

swered. It was found in this research that some of the arguments about the Laughlin wave function in the literature are insufficient. One of them is that the Laughlin wave function is just a mean-field or semi-classical solution of the Chern-Simons field theory (CSFT). However, we have shown that ground state in FQHE systems is specific for different interactions. So the stability of the mean-field solutions in the CSFT depends on the interaction potentials of the model. A more rigorous understanding of the Laughlin wave function in the framework of CSFT approach is still needed.

Although the global phase diagram of the FQHE has been proposed based on different approaches, the rigorous understanding of the impurity effects or the disorder driven phase transition between incompressible and compressible phases is still an open question.

To have a solid understanding of the PL of FQHE systems, we need an accurate understanding of the quantum states of the valence hole in different experimental situations. This subject might be able to give critical understanding of the current experimental results. Although I have shown numerically there is a resonance peak around the gap value, the physical origin of this peak is still unclear at present time. Is it due to the two-roton bound state, or due to a single magneto-roton at $k = 0$? And why is the RS in FQHE systems at $\nu = 2/5$ different from that at $\nu = 1/3$? Further numerical studies based on the computer programs used in Section 4.3 would be able to answer some of these questions.

This is just a selection of important and interesting questions remaining for future study.

Part II

Transport Theory in Nanostructures

Chapter 7

Introduction to Transport Theory

7.1 Introduction

Due to advances in the manufacturing techniques of semiconductor devices, and the need to understand fundamental quantum mechanical processes in order to improve these devices, quantum transport of electrons through ultrasmall structures has become the subject of active research during the last decade [107, 108]. There has been great progress in the understanding of transport in systems with dimensions small compared to an equilibration length (length needed for carriers to randomize their phases and break the coherence), *i.e.* in a mesoscopic system [109]. Because of the importance of both technological applications and issues of basic physics, resonant tunneling in double-barrier heterostructures (DBH) as well as in multiple-barrier heterostructures has been extensively studied experimentally and theoretically [107, 108].

The first attempts at modeling the resonant tunneling utilized simple

quantum tunneling [110, 111, 112, 113, 114, 115, 116, 117]. For a given potential $V(x)$ of the barrier, the tunneling probability can be calculated as function of the energy $T(E)$ using the WKB approximation or the transfer matrix method. The current through the device then can be calculated using the Landauer formula [118, 119, 120]. Other approaches such as classical kinetic rate equation approach [121] and Wigner function method [122, 123, 124] have also been used. For studies of the elastic and inelastic effects, the many-body Green's function method [125, 126, 127, 128, 129], especially the non-equilibrium Green's function method has been extensively used [130, 131, 132, 133, 134, 135, 136, 137, 138, 139, 140, 141, 142, 143].

The traditional theoretical tools for the transport theory are classical Boltzmann equations and quantum Kubo's formula [100]. The limitations of these theories in the above problems are apparent — the mesoscopic systems are usually far from thermal equilibrium and the quantum effects are important, and also the transport processes are not necessary linear, which is beyond the scope of the Kubo's formula. The non-equilibrium Green's function [144, 145, 146, 147, 148] can naturally describe the non-thermal-equilibrium systems and non-linear response as well as many-body effects systematically, so there are advantages to the use of non-equilibrium Green's function in study of transport properties in mesoscopic systems. The technical advantage is that quantum kinetic equations can be easily obtained [148, 149], from which the semi-classical Boltzmann equations can be derived, while at the same time the many-body Green's function techniques [150] and path integral techniques can be used [151].

In this part of my dissertation research, I studied the resonant tunneling by use of the non-equilibrium Green's function method. The work described here was published already [139, 140]. The organization of the rest of this part is as following:

In the rest of Chapter 7, I will briefly review the non-equilibrium Green's function method and summarize the results which are frequently used in the study of the resonant tunneling, and then give some general formal results of resonant tunneling obtained by using the non-equilibrium Green's function method. The results described here are known in the literature, although some derivations are new.

In Chapter 8, we studied the electron-electron interaction effects in the resonant tunneling through double barrier diodes. The intrinsic bistability phenomena was first studied by us using the non-equilibrium Green's function method. We also found that the "tri-stability" was claimed by Coon *et al.* [113] is a computational artifact.

In Chapter 9, we studied the resonant tunneling through a multi-barrier structure. The traditional approach for this problem is the transfer matrix method [152, 153, 154, 155]. Using the non-equilibrium Green's function method, we are able to derive an exact Breit-Wigner formula for the resonant current. The analytical results were used to explain an experiment [156] reporting conductance fluctuations in the transport through a strongly disordered quantum wire.

7.2 Non-equilibrium Green's Function

There exist several excellent reviews of the non-equilibrium Green's function method in the literature [150, 149, 151]. Here I will give a brief review of the non-equilibrium Green's function method and summarize the results which I will use in the later chapters. Since these results can not be obtained from a single source and the notations are different in different places, I think my effort here will be helpful.

Define the S-matrix for a system with Hamiltonian $H = H_0 + H_1$ as:

$$S(t,t') = T\exp\{-\frac{i}{\hbar}\int_{t'}^{t} H(\tau)d\tau\} \tag{7.1}$$

where T is the chronological time-ordering operator. Then in Heisenberg representation, $\hat{A}(t) = S(-\infty,t)\hat{A}_0 S(t,-\infty)$, where $\hat{A}_0$ is any time-independent operator. Assume the initial density matrix of the system at $t = -\infty$ is ρ_0, then the average value of the T-product of two operators A, B can be written as [1]:

$$\begin{aligned}\langle TA(t)B(t')\rangle &= Tr\{\rho_0 TS(-\infty,t)A_0 S(t,t')B_0 S(t',-\infty)\} \\ &= Tr\{\rho_0 T_C A(t)B(t')\} \\ &= \langle T_C A(+,t)B(+,t')\rangle \end{aligned} \tag{7.2}$$

Where label C is on contour of the closed time path [148, 149] shown in Fig.7.1, and T_C is the generalized chronological time-ordered operator on contour C. Here "+" means the t (or t') is in the "+" (upper) branch of contour T_c. We can use this contour C to define the average value of products

[1] I will omit the factor $[Tr\rho_0 S(-\infty,\infty)]^{-1}$ in the thermal average in the thesis.

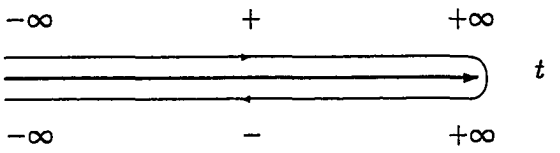

Figure 7.1: Closed time path T_c.

$A(t)B(t')$ and $B(t')A(t)$ in a similar fashion. Since we assume the initial state of the system at $t = -\infty$ is unimportant, we can chose an arbitrary initial density matrix ρ_0, such as $\rho_0 = e^{-\beta H_0}$, which is time-independent, *i.e.* at $t = -\infty$ take the system at equilibrium and with Hamiltonian H_0.

Then we can define the nonequilibrium Green's functions:

$$G(\tau,\tau') = -i\langle T_C\{\psi(\tau)\psi^\dagger(\tau')\}\rangle \,, \tag{7.3}$$

where $\tau \equiv (\beta, t)$ $\beta = +, -$ is in the contour C. In matrix form:

$$\hat{G}(\tau,\tau') \equiv \begin{pmatrix} G^{++}(t,t') & G^{+-}(t,t') \\ G^{-+}(t,t') & G^{--}(t,t') \end{pmatrix} \tag{7.4}$$

The four elements of the matrix Green's function $\hat{G}(\tau,\tau')$ are not linearly independent, and the following relations exist:

$$\begin{aligned} G^{++}(t,t') &= \theta(t-t')G^{-+}(t,t') + \theta(t'-t)G^{+-}(t,t') \\ G^{--}(t,t') &= \theta(t-t')G^{+-}(t,t') + \theta(t'-t)G^{-+}(t,t') \end{aligned} \tag{7.5}$$

where $\theta(x)$ is the step function. The Green's function $\hat{G}$ can be transformed into the Keldysh space by a rotation $R = (1+i\hat{\sigma}_y)/\sqrt{2}$, where $\hat{\sigma}_y$ is the Pauli matrix. In the Keldysh space, the Green's function matrix is:

$$\bar{G}(\tau,\tau') \equiv \begin{pmatrix} 0 & G^a(t,t') \\ G^r(t,t') & G^K(t,t') \end{pmatrix} \tag{7.6}$$

Here G^a (G^r) is the usual advanced (retarded) Green's function and G^K is the (Keldysh) correlation function

$$G^K(t,t') = -i\langle[\psi(t),\psi^\dagger(t')]_\pm\rangle \tag{7.7}$$

The relations between the elements of $\hat{G}$ and $\bar{G}$ are as following:

$$\begin{aligned} G^r &= G^{++} - G^{+-} = -G^{--} + G^{-+} \\ G^a &= G^{++} - G^{-+} = -G^{--} + G^{+-} \\ G^K &= G^{++} + G^{--} = G^{+-} + G^{-+} \end{aligned} \tag{7.8}$$

The diagrammatic formulation of the nonequilibrium Green's function is identical in form to standard diagrammatic theory, except that both propagators and vertices are tensors with row/colum indices $\pm$. The tensor structure results in the need to carry out internal sums over branch indices in addition to the usual integration over internal variables when evaluating diagrams.

Summation of diagrams for the complete Green's function leads to the (left and right) Dyson's equation

$$G = G_0 + G_0\Sigma G \qquad\qquad G = G_0 + G\Sigma G_0 \tag{7.9}$$

Here G_0 is the zeroth order Green's function. Where in matrix form the self-energy is

$$\hat{\Sigma} = \begin{pmatrix} \Sigma^{++} & \Sigma^{+-} \\ \Sigma^{-+} & \Sigma^{--} \end{pmatrix} \quad \text{and} \quad \bar{\Sigma} = \begin{pmatrix} \Sigma^K & \Sigma^r \\ \Sigma^a & 0 \end{pmatrix} \tag{7.10}$$

The relation between four elements in $\hat{\Sigma}$ and $\bar{\Sigma}$ is as following:

$$\begin{aligned} \Sigma^r &= \Sigma^{++} + \Sigma^{+-} = -(\Sigma^{--} + \Sigma^{-+}) \\ \Sigma^a &= \Sigma^{++} + \Sigma^{-+} = -(\Sigma^{--} + \Sigma^{+-}) \\ \Sigma^K &= \Sigma^{++} + \Sigma^{--} = -(\Sigma^{+-} + \Sigma^{-+}) \end{aligned} \tag{7.11}$$

The Dyson's equation provides an exact description of the system. Since G^r and G^a characterize the states, and G^K essentially carries the information of the distribution function, the Dyson's equation for G^K is a quantum kinetic equation. So the quantum or semi-classical Boltzmann's equation can be derived from these Dyson's equations [148, 149].

Before closing this section, let me give some useful operator identities here [150].

1) If $A = \int_C BC$, *i.e.* in matrix form

$$\begin{aligned}\hat{A}(t,t') &= \int_{-\infty}^{\infty} dt_1 \hat{B}(t,t_1)\hat{\sigma}_3\hat{C}(t_1,t') \\ \bar{A}(t,t') &= \int_{-\infty}^{\infty} dt_1 \bar{B}(t,t_1)\hat{\sigma}_1\bar{C}(t_1,t')\end{aligned} \tag{7.12}$$

The equations for the elements are:

$$\begin{aligned}A^{r,a}(t,t') &= \int dt_1 B^{r,a}(t,t_1)C^{r,a}(t_1,t') \\ A^K(t,t') &= \int dt_1 [B^r(t,t_1)C^k(t_1,t') \\ &\quad + B^k(t,t_1)C^a(t_1,t')] \\ A^{+-}(t,t') &= \int dt_1 [B^r(t,t_1)C^{+-}(t_1,t') \\ &\quad + B^{+-}(t,t_1)C^a(t_1,t')]\end{aligned} \tag{7.13}$$

Where A, B, and C are Green's functions. The difference between Green's function and self-energy in the matrix form can be clarified by noting that $\hat{\Sigma} = \hat{\sigma}_3\hat{G}\hat{\sigma}_3$.

2) For the Dyson's equations, the following equations can be derived using the above equations:

$$G^{r,a} = G_0^{r,a} + G_0^{r,a}\Sigma^{r,a}G^{r,a}$$

$$G^{r,a} = G_0^{r,a} + G^{r,a}\Sigma^{r,a}G_0^{r,a} \tag{7.14}$$

$$\begin{aligned} G^{+-} &= G_0^{+-} + G_0^r\Sigma^r G^{+-} + G_0^r\Sigma^{+-}G^a + G_0^{+-}\Sigma^a G^a \\ G^{+-} &= G_0^{+-} + G^r\Sigma^r G_0^{+-} + G^r\Sigma^{+-}G_0^a + G^{+-}\Sigma^a G_0^a \end{aligned} \tag{7.15}$$

Using Eq.[7.14][7.15], the following equations can be derived:

$$\begin{aligned} G^{+-} &= (1 + G^r\Sigma^r)G_0^{+-}(1 + \Sigma^a G^a) + G^r\Sigma^{+-}G^a \\ G^K &= (1 + G^r\Sigma^r)G_0^K(1 + \Sigma^a G^a) + G^r\Sigma^K G^a \end{aligned} \tag{7.16}$$

7.3 Resonant Tunneling Model: General Solution

7.3.1 Model Hamiltonian

In this section, we discuss some general results obtained by using the nonequilibrium Green's function method for resonant tunneling. In resonance tunneling through a quantum well or quantum dot structure, we can separate the system into three region: left lead, right lead, and the central region within which the electronic states are localized. The Hamiltonian for the general tunneling model then can be written as

$$H = H_L + H_R + H_T + H_c \tag{7.17}$$

Where H_L and H_R are Hamiltonians of the left and right leads; H_T is the coupling (tunneling) of the electrons between the leads and the central region; and H_c is the Hamiltonian of the central region. The Hamiltonian of the

central region can be generally written as

$$H_c = \sum_n \epsilon_n \hat{c}_n^\dagger \hat{c}_n + H_i \tag{7.18}$$

here $\hat{c}_n$ ($\hat{c}_n^\dagger$) is the annihilation (creation) operator of electrons in the central region, H_i describes the general scattering terms. Since the system is open, the response of the electrons in the leads is much faster than that in the sample region. So following the idea of Buttiker [157] in his model for a multi-terminal conductor, we assume that in the leads there is substantial inelastic electron scattering so the leads can be treated as quasi-equilibrium reservoirs with chemical potentials μ_L and μ_R; *i.e.* we take it that the level broadening of leads introduced by the coupling to the central states is much smaller than that introduced by inelastic scattering. In the steady state, we can model the leads as two Fermi seas of quasi-particles, so

$$H_{\alpha \in L,R} = \sum_{k\alpha \in L,R} \epsilon_k \hat{a}_{k\alpha}^\dagger \hat{a}_{k\alpha} \tag{7.19}$$

In the *weak* link between the central region and the two leads, the coupling term can be approximated as a tunneling Hamiltonian

$$H_T = \sum_{\substack{k,\alpha \in L,R \\ n}} [V_{k\alpha,n} \hat{a}_{k\alpha}^\dagger \hat{c}_n + h.c.] \tag{7.20}$$

Here $\hat{a}_{k\alpha \in L,R}$ ($\hat{a}_{k\alpha \in L,R}^\dagger$) is the the annihilation (creation) operator of electrons in the left (L) or right (R) lead [2]. In this model, the Green's functions are defined as following:

$$G_{n,k\alpha}(\tau, \tau') \equiv -i\langle \hat{a}_{k\alpha}^\dagger(\tau') \hat{c}_n(\tau) \rangle \tag{7.21}$$

[2]Notice that I have used α as index of both leads ($\alpha \in \{L, R\}$) and branches ($\alpha \in \{+, -\}$) in closed-time-path under different context.

$$G_{k\alpha,n}(\tau,\tau') \equiv -i\langle \hat{c}_n^\dagger(\tau')\hat{a}_{k\alpha}(\tau)\rangle \quad (7.22)$$

$$G_{n,m}(\tau,\tau') \equiv -i\langle \hat{c}_m^\dagger(\tau')\hat{c}_n(\tau)\rangle \quad (7.23)$$

$$G_{k\alpha,k\alpha}(\tau,\tau') \equiv -i\langle \hat{a}_{k\alpha}^\dagger(\tau')\hat{a}_{k\alpha}(\tau)\rangle \quad (7.24)$$

7.3.2 Elimination of Degrees of Freedom of Electrons in the Leads

Since the Hamiltonian has only bilinear terms in $\hat{a}_{k\alpha\in L,R}$ ($\hat{a}^\dagger_{k\alpha\in L,R}$), we can do the path integral of $\hat{a}_{k\alpha\in L,R}$ ($\hat{a}^\dagger_{k\alpha\in L,R}$) exactly. Define $H_0 = H_c + H_L + H_R$ and $H_I = H_T$, and $\rho_0 = e^{-\beta H_0}$. Then in the interaction picture, the "thermal average" of a function $f(c,c^\dagger)$ of the operator variables c_n and $c_m^\dagger$ becomes

$$\langle T_C f(c,c^\dagger)\rangle = Tr\left[\rho_0 T_C \exp\left(-i\int_C d\tau_1 H_T(\tau_1)\right) f(c,c^\dagger)\right]$$
$$Tr\Big[\rho_0 T_C \exp\Big(-i\int_C d\tau_1 d\tau_2 \sum_{\substack{k,\alpha\in L,R\\ m,n}} V^*_{k\alpha,m} V_{k\alpha,n} g_{k\alpha,k\alpha}(\tau_1,\tau_2)$$
$$c_m^\dagger(\tau_1)c_n(\tau_2)\Big) f(c,c^\dagger)\Big] \quad (7.25)$$

Where $g_{k\alpha,k\alpha}(\tau_1,\tau_2)$ is the Green's function in the leads without coupling to the central region:

$$\bar{g}_{k\alpha,k\alpha}(\omega) = \begin{pmatrix} 0 & \frac{1}{\omega-\epsilon_{k\alpha}-i\gamma_\alpha} \\ \frac{1}{\omega-\epsilon_{k\alpha}+i\gamma_\alpha} & \frac{2\pi i[2f_\alpha(\omega)-1]}{(\omega-\epsilon_{k\alpha})^2+\gamma_\alpha^2} \end{pmatrix} \quad (7.26)$$

Here γ_α is the energy level broadening of the electrons in the leads, and $f_\alpha(\omega)$ is the Fermi-Dirac distribution function $f_\alpha(\omega) = \{\exp[\beta(\omega-\mu_\alpha)]+1\}^{-1}$ with the difference of chemical potential of the two leads $\mu_L - \mu_R = eV_{ext}$.

Using Eq.[7.25], the Green's functions $G_{n,k\alpha}(\tau,\tau')$ and $G_{k\alpha,n}(\tau,\tau')$ can be

readily expressed by $G_{n,m}(\tau,\tau')$ and $g_{k\alpha,k\alpha}(\tau,\tau')$. For example:

$$\begin{aligned} G_{n,k\alpha}(\tau,\tau') &= i\frac{\delta}{\delta[V_{k\alpha,m}c_m](\tau')}\langle T_C c_n(\tau)\rangle \\ &= \int_C d\tau_1 \sum_m V^*_{k\alpha,m} G_{n,m}(\tau,\tau_1) g_{k\alpha,k\alpha}(\tau_1,\tau') \\ G_{k\alpha,n}(\tau,\tau') &= i\frac{\delta}{\delta[V^*_{k\alpha,m}c^\dagger_m](\tau)}\langle T_C c^\dagger_n(\tau')\rangle \\ &= \int_C d\tau_1 \sum_m V_{k\alpha,m} G_{m,n}(\tau_1,\tau') g_{k\alpha,k\alpha}(\tau,\tau_1) \end{aligned} \tag{7.27}$$

7.3.3 Tunneling Current: Formal Solution

The current from the left lead through left barrier to the central region can be calculated from the time evolution of the occupation number operator for electrons of the left lead:

$$J_L(t) = -e\langle \dot{N}_L\rangle = -\frac{ie}{\hbar}\langle[\hat{H},\hat{N}_L]\rangle\,, \tag{7.28}$$

where $\hat{N}_L = \sum_{k,\alpha\in L}\hat{a}^\dagger_{k\alpha}\hat{a}_{k\alpha}$. Since H_c and $H_{\alpha\in L,R}$ commute with N_L, one readily finds

$$\begin{aligned} J_L &= \frac{ie}{\hbar}\sum_{\substack{k,\alpha\in L\\ n}}\left[V_{k\alpha,n}\langle\hat{a}^\dagger_{k\alpha}\hat{c}_n\rangle - V^*_{k\alpha,n}\langle\hat{c}^\dagger_n\hat{a}_{k\alpha}\rangle\right] \\ &= \frac{2e}{\hbar}Re\left\{\sum_{\substack{k,\alpha\in L\\ n}} V_{k\alpha,n}G^{+-}_{n,k\alpha}(t,t)\right\} \end{aligned} \tag{7.29}$$

Where we have used the relation $G^{+-}_{k\alpha,n}(t,t') = -\left[G^{-+}_{k\alpha,n}(t',t)\right]^*$.

Define the self-energy of electrons in the central region due to coupling to the leads as following:

$$[\Sigma_\alpha(\tau,\tau')]_{mn} = \sum_k V^*_{k\alpha,m}V_{k\alpha,n}g_{k\alpha}(\tau,\tau') \tag{7.30}$$

Using Eq.[7.13,7.27,7.29], we can obtain the following formula for the currents

$$\begin{aligned} J_{\alpha\in L,R} &= \frac{ie}{\hbar}\sum_{\substack{k\alpha \\ m,n}}\int dt_1 V^*_{k\alpha,m}V_{k\alpha,n} \\ &\quad [G^r_{nm}(t,t_1)g^{+-}_{k\alpha}(t_1,t)+G^{+-}_{nm}(t,t_1)g^a_{k\alpha}(t_1,t) \\ &\quad -G^a_{nm}(t_1,t)g^{+-}_{k\alpha}(t,t_1)-G^{+-}_{nm}(t_1,t)g^r_{k\alpha}(t,t_1)] \\ &= \frac{ie}{\hbar}\int\frac{d\epsilon}{2\pi}Tr\Gamma^\alpha(\epsilon)\{G^{+-}(\epsilon)+f_\alpha(\epsilon)[G^r(\epsilon)-G^a(\epsilon)]\} \quad (7.31) \end{aligned}$$

We have defined the broadening of the energy level due to coupling to the leads as

$$\begin{aligned} [\Gamma^\alpha(\epsilon)]_{mn} &= [\Sigma^r_\alpha(\epsilon)]_{mn}-[\Sigma^a_\alpha(\epsilon)]_{mn} \\ &= \sum_k V^*_{k\alpha,m}V_{k\alpha,n}\frac{2i\gamma_\alpha}{(\omega-\epsilon_{k\alpha})^2+\gamma^2_\alpha} \quad (7.32) \end{aligned}$$

Finally, using the conservation of the total current $J = J_L = -J_R$, we can obtain the resonant tunneling symmetrized current equation and a constraint for the Green's functions due to current conservation

$$\begin{aligned} J = &\frac{ie}{2\hbar}\int\frac{d\epsilon}{2\pi}Tr\{[\Gamma^L(\epsilon)-\Gamma^R(\epsilon)]G^<(\epsilon) \\ + &[f_L(\epsilon)\Gamma^L(\epsilon)-f_R(\epsilon)\Gamma^R(\epsilon)][G^r(\epsilon)-G^a(\epsilon)]\} \quad (7.33) \end{aligned}$$

$$\begin{aligned} 0 = &\int\frac{d\epsilon}{2\pi}Tr\{[\Gamma^L(\epsilon)+\Gamma^R(\epsilon)]G^<(\epsilon) \\ + &[f_L(\epsilon)\Gamma^L(\epsilon)+f_R(\epsilon)\Gamma^R(\epsilon)][G^r(\epsilon)-G^a(\epsilon)]\} \quad (7.34) \end{aligned}$$

The Eq.(7.33) & Eq.(7.34) are formal solution of general Hamiltonian (7.17). These results will be used in Chapter 8 and Chapter 9.

Chapter 8

Intrinsic Bistability in DBRTS

8.1 Introduction

Since the pioneering work of Esaki and Tsui [110], resonant tunneling (RT) of electrons through double barrier structures (DBS) has been a subject of great interest, both for potential applications and also for the challenging physical questions which arise. In connection with digital circuit applications, intrinsic bistability (IB) in devices which possess ultraspeed switching is of considerable interest [158, 159, 160, 111, 121, 112, 113, 122, 123, 161]. This IB effect is caused by the electrostatic feedback of space charge dynamically stored in the quantum well. A simple understanding may be obtained by taking account of the charge buildup using a sequential approach [121], or the global transmission coefficient approach [111, 112, 113]. Using a linear theory of resonant tunneling including charge buildup, Coon *et al.* [113] claimed existence of a tristable *I-V* regime. Also, the Wigner distribution function method was used to simulate time-evolution, including dynamical bistability [161] in the negative-differential-resistance (NDR) range. The

results in Ref.[161] were mainly numerical, and somewhat controversial, since their I-V curve in the NDR range has a different character from what was found in the experiments and previous theoretical calculations.

Since the electron distribution in the central well is highly non-equilibrium, we will use the non-equilibrium Green's function method. From section 7.3.3 we know that the resonance tunneling current is given by Eq.(7.33), and all many-body interactions can be treated systematically to any order in perturbation theory. If there is no scattering in the central region, the resonant tunneling current can be calculated exactly, and the result is just the Breit-Wigner formula (A generalized proof will be given in Chapter 9). Taking into account any general scattering mechanism in the central region, such as the electron-electron interaction, impurity scattering, and phonon-electron scattering, the main task is to calculate the Green's function and then use Eq.(7.33) to calculate the current. Although the results in the last chapter can be readily generalized to dynamic currents, here we will restrict our attention to the steady-state (time-independent) properties of the system. We will include in the present work only the direct Coulomb interaction effects, but discuss semi-quantitatively the effects of other than direct-Coulomb interactions. Finally we give results which show that the reported tristability [113] in these system is a computational artifact.

8.2 Hartree Approximation

As in section 7.3.1 Eq.(7.17), we take the total Hamiltonian of our system to be $H = H_L + H_R + H_T + H_c$. The definition of $H_{L,R}$ and H_T is the same as

that in section 7.3.1. To emphasize the electron-electron interaction, which is responsible for the intrinsic bistability, we write H_c as follows

$$H_c = \sum_n \epsilon_n \hat{c}_n^\dagger \hat{c}_n + \sum_{m \neq n} V_c \hat{c}_m^\dagger \hat{c}_m \hat{c}_n^\dagger \hat{c}_n + H_s \tag{8.1}$$

We have replaced H_i in Eq.(7.18) by $H_s + \sum_{m \neq n} V_c \hat{c}_m^\dagger \hat{c}_m \hat{c}_n^\dagger \hat{c}_n$ which separates the electron-electron interaction from other scatterings H_s. In this specific model, we assume there is only one quantized (resonant) level in the tunneling direction, which is chosen as the x-axis, then the index n denotes the quantum numbers of the transverse mode (including spin), $n = \{K_y, K_z, \sigma\}$, the index k for the leads is $k = \{p, n\}$, where $p \equiv K_x$. Considering the effect of the bias voltage $eV_{ext} = \mu_L - \mu_R$, in the Hamiltonian $H_{L,R}$, single particle energies can be written as $\epsilon_{kL} = E_n + p^2/2m^*$ for the left (emitter) and $\epsilon_{kR} = E_n + p^2/2m * -eV$ for the right (collector) leads, respectively. We used $E_n = (K_y^2 + K_z^2)/2m^*$ as the transverse mode energy and take $\hbar = 1$. If E_r is the subband energy in the quantum well, the single particle energy of electrons in the central quantum well is $\epsilon_n = E_n + E_r - \chi e V_{ext}$ (χ is a coefficient depending on the structure of the quantum well). Electrostatically, the DBS is equivalent to capacitors connected in series, so we have [128] $E_c = e^2/(C_L + C_R)$ and $\chi = C_R/(C_L + C_R)$.

Here we assume the tunneling conserves transverse momentum, *i.e.* $V_{k\alpha,n} = V_{(m,p)\alpha,n}\delta(m,n) \equiv V_{mp\alpha}\delta(m,n)$. The energy level broadening due to tunneling then is $[\Gamma^\alpha(\epsilon)]_{mn} = \delta(m,n)\Gamma_m^\alpha(\epsilon)$ where

$$\Gamma_m^\alpha(\epsilon) = \sum_p V_{mp\alpha}^* V_{mp\alpha} \frac{2i\gamma_\alpha}{(\omega - \epsilon_{mp\alpha})^2 + \gamma_\alpha^2} \tag{8.2}$$

For the whole system, we write the self-energy due to scattering as $\bar{N}E_c + \sigma_n(\epsilon)$. Where $\bar{N}$ is the total space charge in the well. We have written the direct Coulomb interaction self-energy separately, and similarly we define $\gamma_n = -Im\sigma_n^r$. Then the Green's function $G_{n,m}(\tau,\tau')$ in the Keldysh space can be obtained using a formal Dyson-equation:

$$\begin{aligned} G_m^a(\omega) &= \frac{1}{\omega - \epsilon_m - \bar{N}E_c - \Sigma_m^a - \sigma_m^a} \\ G_m^{+-}(\omega) &= -iF_m(\omega)S_m(\omega) \end{aligned} \tag{8.3}$$

Here $S_m(\omega) = i[G_m^r - G_m^a(\omega)]$ is the spectral function, and the distribution function F_m is

$$F_m(\omega) = \frac{2\Gamma_m(\omega)F_m^0(\omega) + \sigma_m^{+-}(\omega)}{2\Gamma_m(\omega) + \gamma_m(\omega)} \tag{8.4}$$

where $F_m^0(\omega)$ is the noninteracting system F-function, which is the weighted average of Fermi functions $f_L(\omega)$ and $f_R(\omega)$ of the two leads:

$$F_m^0(\omega) = \frac{f_L(\omega)\Gamma_m^L(\omega) + f_R(\omega)\Gamma_m^R(\omega)}{\Gamma_m^L(\omega) + \Gamma_m^R(\omega)} \tag{8.5}$$

Let $\bar{\epsilon}_m(\omega) = \epsilon_m + Re(\Sigma_m^r + \sigma_m^r)$ be the renormalized resonant energy. The space charge buildup is given by the non-linear integral equation

$$\bar{N} = \sum_m \int \frac{d\omega}{2\pi} \frac{2\Gamma_m F_m^0 + \sigma_m^{+-}}{2\Gamma_m + \gamma_m} \frac{2\Gamma_m + \gamma_m}{[\omega - \bar{\epsilon}_m(\omega) - \bar{N}E_c]^2 + (\Gamma_m + \gamma_m)^2} \tag{8.6}$$

From Eq.(7.33) & Eq.(7.34), the average tunneling current J, and current conservation condition $J_L - J_R = 0$, are given by:

$$\begin{aligned} J &= e\sum_m \int \frac{d\omega}{2\pi} \frac{4\Gamma_m^L\Gamma_m^R}{\Gamma_m^L + \Gamma_m^R}[f_L - f_R]S_m(\omega) \\ &+ e\sum_m \int \frac{d\omega}{2\pi} \frac{\Gamma_m^L - \Gamma_m^R}{\Gamma_m^L + \Gamma_m^R}[G_m^{-+}\sigma^{+-} + [G_m^{+-}\sigma^{-+}] \end{aligned} \tag{8.7}$$

$$0 = \int \frac{d\omega}{2\pi}[G_m^{-+}\sigma^{+-} + [G_m^{+-}\sigma^{-+}] \tag{8.8}$$

Eq.(8.6)-(8.8) are general for all kinds of scattering. And in principle we can use non-equilibrium perturbation theory to calculate the self-energy. As discussed previously, the level broadening of electrons in the leads is much larger than that in the well, hence we can approximately use $\Gamma_m^\alpha(\omega) = \Gamma^\alpha$ ($\alpha = R, L$). So the second term in Eq.(8.8) vanishes because of the detailed current-conservation Eq.(8.8). Since intrinsic bistability is mainly caused by the electron charging effect, and our present objective is to derive the most immediate consequences of the theory, here we will use a Hartree-Approximation, *i.e.* we let $\sigma_m(\tau, \tau') = 0$. Later we will discuss the effect of adding electron-electron exchange interaction and other scattering effects. Further, as we are interested in the NDR range, $\tilde{\epsilon}_m \gg \mu_R$, we can safely set $f_R(\omega) = 0$, i.e. suppose that all collector electron states are empty. In this approximation $I = \Gamma^R e\bar{N}$. The integral Eq.(8.6) can be simplified as

$$\bar{N} = N_0 \frac{1}{\beta\mu_L} \int \frac{d\omega}{2\pi} \frac{2\Gamma}{[\omega - (E_r - \chi eV_{ext}) - \bar{N}E_c]^2 + \Gamma^2} \ln[1 + e^{-\beta(\omega-\mu_L)}] \quad (8.9)$$

where $N_0 = \Gamma^L m^* A\mu_L/(\Gamma\pi)$, μ_L is Fermi energy of electrons in the emitter.

8.3 Numerical Calculations: Bistability

Eq.(8.9) is a useful and important result of the theory, in the steady state approximation. It expresses the non-linear current in terms of $\bar{N}$ and includes in an accurate fashion the feed-back due to charging effects. In order to examine features of the solutions of Eq.(8.9), we draw the graph of

$$Y(\bar{N}) = N_0 \frac{1}{\beta\mu_L} \int \frac{d\omega}{2\pi} \frac{2\Gamma}{[\omega - (E_r - \chi eV_{ext}) - \bar{N}E_c]^2 + \Gamma^2} \ln[1 + e^{-\beta(\omega-\mu_L)}] \quad (8.10)$$

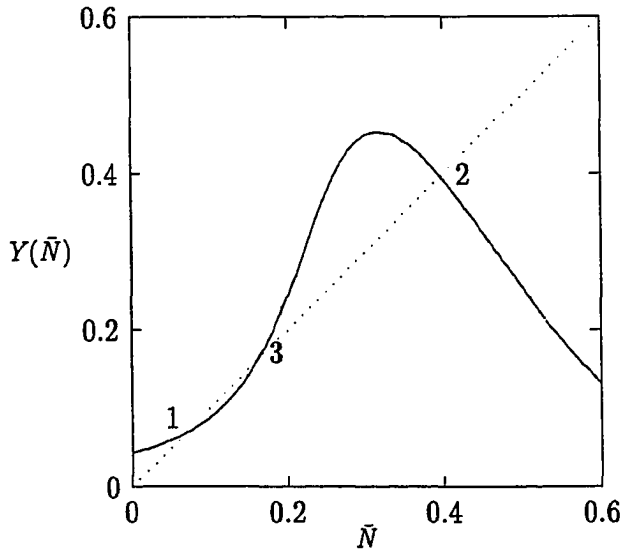

Figure 8.1: Behavior of $Y(\bar{N})$ as a function of $\bar{N}$, in a typical GaAs/(AlGa)As DBS.
see Eq.(8.10) for the definition of $y(\bar{N})$. The parameter of GaAs/(AlGa)As DBS is the same as that in Fig.8.2. $\Gamma = 4meV$, $V = 240mV$, $T = 25K$. It can be seen easily that solution 1 is stable and 3 is unstable. And solution 2 is unstable locally and oscillate globally.

as a function of $\bar{N}$. Here $Y(\bar{N})$ is just the "induced charge buildup" in the well as a function of the average charge $\bar{N}$ in the well. In equilibrium, $Y(\bar{N}) = \bar{N}$. We have illustrated in Fig.8.1 & 8.2 the content of this expression using values of physical parameters approximate to realistic systems [158, 159, 160, 111, 121, 112, 113]. In Fig.8.1, it can be seen clearly that we have three solutions in the bistability range, which means that in this range we have three stationary states. We calculate the I-V curves for a typical DBRTS, as in Fig.8.2. Refer to the curves in NDR range numbered in the inset of Fig.8.2. Curve 1 and

2 are well known [158, 159, 160, 111, 121, 112, 113], while curve 3 is just the third solution of Coon *et al.* [112, 113]. To check the stability of every solution, we solve Eq.(8.9) iteratively using an initial $\bar{N}$ very near to the exact one. In the dynamical process, the charge buildup at time t_{i+1} is induced by the charge buildup at t_i, so this iteration process using Eq.(8.10) in some sense mimics the forward time evolution of the system. We find: the first solution is stable and the third is unstable in the NDR range (see Fig.8.1). This result is independent of the level-broadening and temperature. The stability behavior of the second solution is complicated and sensitive to the level-broadening and temperature. For small level-broadening and low temperature, near V_1 (V_1 is the lower bound of NDR range) the second solution is unstable, near V_2 (V_2 is the upper bound of NDR range) the second solution is stable. In the range between them, the solution will oscillate (see Fig.8.1). The oscillation comes from the existence of the third unstable solution. With the increase of level-broadening or temperature, the unstable range will disappear and the oscillation range will dominate the NDR range. From these result, we suggest that the third solution is not stable. We think that the oscillation behavior of the second solution has the same physical origin as that of the "high-frequency" dynamic bistability of Jensen and Buot [161]. Another result needing mention is the controversial character of Fig.1 in Ref.[161]. This can be understood in our calculation (Fig.8.1): the oscillation around the second solution is asymmetric, the averaged current has different a character.

The scattering term $\sigma_m^{+-}(\omega)$ in the F-function is the correction to the elec-

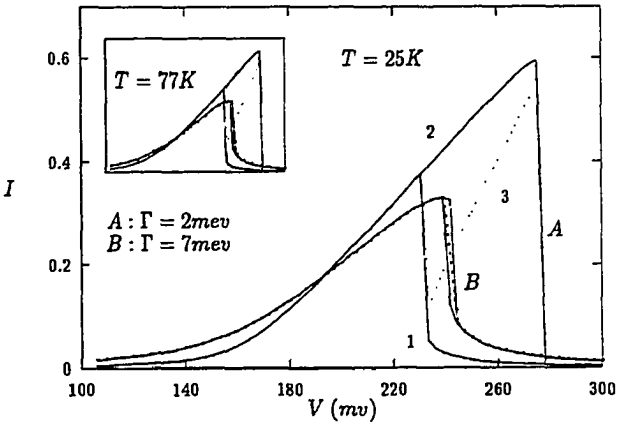

Figure 8.2: Current I as a function of applied bias V, in a typical GaAs/(AlGa)As DBS.
The potential barrier is $0.4eV$, the width of well is $56nm$; $E_r \approx 85meV$ in the well, $E_f \approx 18meV$ in the leads. A) $T = 25K$, $\Gamma = 2meV$, B) $T = 25K$, $\Gamma = 7meV$; Inset: $T = 77K$; it has the same I,V-axis scale.

tron distribution in the well. From physical considerations, it will not differ qualitatively from a Fermi-function or the effective-Fermi-function $F_m^0(\omega)$. So we may assume the σ-term in the F-function in Eq.(8.6) only gives a global factor after integration, and moreover, we assume the direct Coulomb-interaction dominates the resonant energy renormalization (which seems reasonable in the NDR range). Then we anticipate that including the self-energy of electron-electron exchange interaction (and higher order contribution) and other impurity and phase breaking scattering, mainly produces changes in the energy level broadening, and does not change the phenomenon qualitatively, if the scattering is weak.

Now we will discuss the effect of temperature and level-broadening on

the static intrinsic bistability without taking into account their effect on the stability of the solutions. Bound-state level broadening Γ (we take it as $\Gamma+\gamma$ afterwards) can be due for example to inhomogeneity of the quantum well, tunneling to the leads, and elastic and inelastic (phase breaking) scattering. We use Eq.(8.9) to calculate the I-V curves for different level broadening Γ, [see curves A and B in Fig.8.2]. It is seen that the bistability is very sensitive to the level broadening: that is a few meV of broadening will destroy the bistability, as can be seen from curves in Fig.8.2B. For the effect of temperature, there are several aspects which come in. First, higher temperature will make scattering (impurity or phase breaking) effects important and this contributes to the level broadening. Second, when the temperature is different from zero, the Fermi-Dirac distribution will change, as well as the chemical potential. To see how the bistability effect depends on the latter temperature effect, we calculate the I-V curves for $T = 77K$ comparing to $25K$ without changing level broadening, [Inset of Fig.8.2]. It can been seen that it does not influence the IB very much. So we believe that the effect of temperature on influence of the IB occurs mainly by introducing level broadening.

Chapter 9

Multi-Barrier Resonant Tunneling

9.1 Introduction

Resonant tunneling phenomena through multiple barrier structures have not been as extensively studied in the literature as that through double barrier structures. Most theoretical work has been devoted to the conductance fluctuations due to resonant tunneling through strongly disordered mesoscopic systems. In that case, the numerical transfer matrix method is used. Analytically an approximation of single-localized-state resonant tunneling has been used. Based on the work of M. Ya. Azbel [162, 163], it is believed [156, 155] that resonant tunneling via a single localized state (or single quantum well) can dominate the whole tunneling process. Assuming this, the resonant tunneling of the whole system can approximately be treated using the resonant tunneling via a single localized state. Then, the Breit-Wigner formula is

postulated to express the transmission coefficient

$$t(E) = \frac{\Gamma^L \Gamma^R}{(E - E_r)^2 + (\Gamma^L/2 + \Gamma^R/2)^2} \tag{9.1}$$

Here E_r is the energy of the localized state and Γ^L, Γ^R are the leak rates of an electron from the localized state to the left and right leads, respectively taken as: $\Gamma^L \propto \exp[-2x/\xi]$ and $\Gamma^R \propto \exp[-2(L-x)/\xi]$ where L is the sample length, x is the position of the resonant well, and ξ is the localization length. This approximation (which we will call single-localized-state-approximation or SLSA) was used to explain the experimental results [156]. However, the occurrence of resonant tunneling and the magnitude of the tunneling current should depend on the configuration of the mesoscopic system. The change of any single localized state will change the current magnitude or destroy the condition needed for the resonant tunneling. So this single-localized-state-approximation (SLSA) can not describe the detailed physics in these systems.

Generally these systems can be modeled as multi-level double barrier systems, thus principlely Eq.[7.33] can be used. However, there are some technical difficulties to use Eq.[7.33] directly. In this chapter, we model the multiple-barrier structure using the traditional tight-binding Hamiltonian. Using the nonequilibrium Green's function method, we obtain an exact Breit-Wigner formula for the conductance (or transmission) which is directly related to the site energies and tunneling matrix element of different resonance level. Based on this formula which we obtained, we calculate the conductance structure for some special systems. For comparison we also calculate the conductance using the SLSA at the same time. We find that the conductance

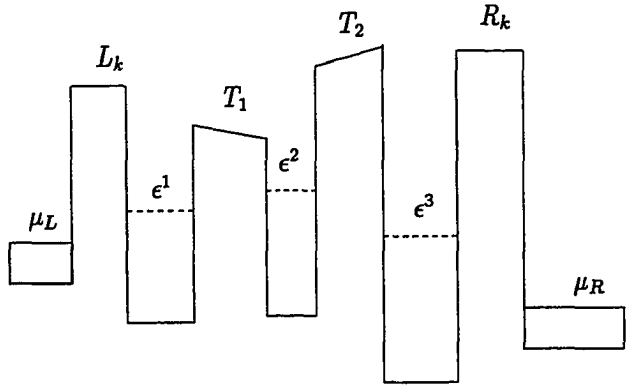

Figure 9.1: Schematic of the system described by our Hamiltonian for N=4.

calculated in the SLSA has a somewhat similar fluctuation structure, but the detailed conductance versus energy dependence for our exact method versus SLSA is both qualitatively and quantitatively different as shown below.

9.2 Resonant Tunneling in the Tight Banding Model

Let us consider a nearest neighbor tight-binding model in a one-dimensional system containing a finite sample region of N sites and two leads (left and right) connected with it [see Fig.9.1]. We take the Hamiltonian to be $H = H_0 + H_i$

$$H_0 = \sum_{n=1}^{N} \epsilon^n \hat{c}_n^\dagger \hat{c}_n + \sum_k \epsilon_k^L \hat{a}_k^\dagger \hat{a}_k + \sum_k \epsilon_k^R \hat{b}_k^\dagger \hat{b}_k + \sum_{n=1}^{N-1} T_n \hat{c}_n^\dagger \hat{c}_{n+1} + h.c. \quad (9.2)$$

$$H_i = \sum_k L_k \hat{c}_1^\dagger \hat{a}_k \sum_k R_k \hat{c}_N^\dagger \hat{b}_k + h.c. \quad (9.3)$$

Here $\hat{c}_n$ ($\hat{c}_n^\dagger$) is the annihilation (creation) operator for the electron state

at the nth site (localized state). $\hat{a}_k$ ($\hat{a}_k^\dagger$) and $\hat{b}_k$ ($\hat{b}_k^\dagger$) are annihilation (creation) operators for the electron state in left and right leads respectively. The single electron energy parameters ϵ^n of the nth site are random compared to the chemical potential μ_L and μ_R. The hopping elements T_n between different sites are random in the range $[-V,V]$. The bias voltage (or electric field) will change the difference of the chemical potential $(\mu_l - \mu_R)$ as well as the site energy. We have absorbed this site energy change into ϵ^n. When the difference $\mu_l - \mu_R$ is much smaller than the randomness of the site energy, the effect of the the bias on the site energy can be neglected completely.

The Green's function can be obtained exactly by using the equation-of-motion-method. We take the time derivative of the Green's functions and find:

$$\begin{aligned} i\partial_{t_1} G^{\alpha\beta}_{m,n}(t_1,t_2) &= \epsilon^m G^{\alpha\beta}_{m,n}(t_1,t_2) + T_m G^{\alpha\beta}_{m+1,n}(t_1,t_2) + T_m^* G^{\alpha\beta}_{m-1,n}(t_1,t_2) \\ &+ \frac{1}{2}(\eta^\alpha + \eta^\beta)\delta(t_1,t_2)\delta_{m,n} \end{aligned} \tag{9.4}$$

where $\eta^+ = -\eta^- = 1$ and we have used the relation:

$$\begin{aligned} \partial_{t_1}\langle A_1(\alpha t_1)A_2(\beta t_2)\rangle &= \frac{1}{i}\langle [A_1(\alpha t_1), H]_- A_2(\beta t_2)\rangle \\ &+ \frac{1}{2}(\eta^\alpha + \eta^\beta)\delta(t_1,t_2)\langle [A_1(\alpha t_1), -A_2(\beta t_2)]_\epsilon\rangle \end{aligned} \tag{9.5}$$

where $\varepsilon = +(-)$ for the fermion (boson) case.

In the present work, our interest is in the steady state behavior of the mesoscopic system, so we can take the time-Fourier-transformation of Eq.(9.4).

$$(\omega - \epsilon^m)G^{\alpha\beta}_{m,n}(\omega) = T_m G^{\alpha\beta}_{m+1,n}(\omega) + T_m^* G^{\alpha\beta}_{m-1,n}(\omega) + \frac{1}{2}(\eta^\alpha + \eta^\beta)\delta_{m,n} \tag{9.6}$$

For $m = 1$ and $m = N$, we can use Eq.[7.27] to eliminate the degree of freedom of the reservoirs. In this fashion we have obtained the starting and final equations for our system of $4N$ matrix equations:

$$(\omega - \epsilon^1)G^{\alpha\beta}_{1,n}(\omega) = T_1 G^{\alpha\beta}_{2,n}(\omega) + \sum_\nu \vec{\Sigma}^{\alpha\nu}_1 \eta^\nu G^{\nu\beta}_{1,n}(\omega) + \frac{1}{2}(\eta^\alpha + \eta^\beta)\delta_{1,n} \quad (9.7)$$

$$(\omega - \epsilon^N)G^{\alpha\beta}_{N,n}(\omega) = T^*_N G^{\alpha\beta}_{N-1,n}(\omega) + \sum_\nu \vec{\sigma}^{\alpha\nu}_N \eta^\nu G^{\nu\beta}_{N,n}(\omega) + \frac{1}{2}(\eta^\alpha + \eta^\beta)\delta_{N,n} \quad (9.8)$$

Here, $\vec{\Sigma}^{\alpha\nu}_1(\omega) = \sum_k |L_k|^2 A^{\alpha\beta}_k(\omega)$ is the left-self-energy of the 1st site, and $\vec{\sigma}^{\alpha\nu}_N = \sum_k |R_k|^2 B^{\alpha\beta}_k(\omega)$ is the right-self-energy of the Nth site. Here $A^{\alpha\beta}_k$ and $B^{\alpha\beta}_k$ are zeroth order Green's functions of the leads. Now we eliminate the leads-correlated Green's functions[1] from the system of matrix equations. The group of coupled equations is then closed and becomes a group of $4N \times 4N$ algebraic equations. Although these equations can be solved straightforwardly, it is a tedious task to solve $4N \times 4N$ equations. To make the solution more transparent, we shall use a "trick". We solve the system of matrix equations in the Keldysh space [148]. Then the system of matrices Eqs.(9.7),(9.8) becomes :

$$\begin{pmatrix} -\vec{\Sigma}^K_1 & \omega - \epsilon^1 - \vec{\Sigma}^r_1 \\ \omega - \epsilon^1 - \vec{\Sigma}^a_1 & 0 \end{pmatrix} \begin{pmatrix} 0 & G^a_{1,n} \\ G^r_{1,n} & G^K_{1,n} \end{pmatrix} = T_1 \sigma_x \begin{pmatrix} 0 & G^a_{2,n} \\ G^r_{2,n} & G^K_{2,n} \end{pmatrix} + \delta_{1,n} \quad (9.9)$$

$$(\omega - \epsilon^m)\sigma_x \begin{pmatrix} 0 & G^a_{m,n} \\ G^r_{m,n} & G^K_{m,n} \end{pmatrix} \begin{pmatrix} 0 & G^a_{1,n} \\ G^r_{1,n} & G^K_{1,n} \end{pmatrix} = T_1 \sigma_2 \begin{pmatrix} 0 & G^a_{m+1,n} \\ G^r_{m+1,n} & G^K_{m+1,n} \end{pmatrix} + \begin{pmatrix} 0 & G^a_{m-1,n} \\ G^r_{m-1,n} & G^K_{m-1,n} \end{pmatrix} + \delta_{m,n} \quad (9.10)$$

[1] I formally use index $n = 0$ and $N + 1$ referring to the index of the two leads in the equation-of-motion.

$$\begin{pmatrix} -\vec{\sigma}_N^K & \omega-\epsilon^N-\vec{\sigma}_N^r \\ \omega-\epsilon^N-\vec{\sigma}_N^a & 0 \end{pmatrix}\begin{pmatrix} 0 & G_{N,n}^a \\ G_{N,n}^r & G_{N,n}^K \end{pmatrix} = T_{N-1}^*\sigma_x\begin{pmatrix} 0 & G_{N-1,n}^a \\ G_{N-1,n}^r & G_{N-1,n}^K \end{pmatrix} + \delta_{N,n} \quad (9.11)$$

Where σ_x are Pauli matrix, $n = 1, 2, \cdots, N$, $m = 2, 3, \cdots, N-1$. Starting from Eq.(9.9),(9.11), we can iterate inwards from the two ends using the Eq.(9.10), and we then solve the Green's Functions at the site chosen for joining them (which can be chosen arbitrarily). By introducing left-self-energy and right-self-energy for each site, which is defined later, then Eq.(9.10) can be changed to two recursion equations similar to Eq.(9.9) and (9.11:

$$\begin{pmatrix} -\vec{\Sigma}_m^K & \omega-\epsilon^m-\vec{\Sigma}_m^r \\ \omega-\epsilon^m-\vec{\Sigma}_m^a & 0 \end{pmatrix}\begin{pmatrix} 0 & G_{m,n}^a \\ G_{m,n}^r & G_{m,n}^K \end{pmatrix} = T_m\sigma_x\begin{pmatrix} 0 & G_{m+1,n}^a \\ G_{m+1,n}^r & G_{m+1,n}^K \end{pmatrix} + \delta_{1,n} \quad (9.12)$$

$$\begin{pmatrix} -\vec{\sigma}_m^K & \omega-\epsilon^m-\vec{\sigma}_m^r \\ \omega-\epsilon^m-\vec{\sigma}_m^a & 0 \end{pmatrix}\begin{pmatrix} 0 & G_{m,n}^a \\ G_{m,n}^r & G_{m,n}^K \end{pmatrix} = T_{m-1}^*\sigma_x\begin{pmatrix} 0 & G_{m-1,n}^a \\ G_{m-1,n}^r & G_{m-1,n}^K \end{pmatrix} + \delta_{N,n} \quad (9.13)$$

The left(right)-self-energy can be defined and calculated using Eq.(9.12) & (9.13) respectively in a recursive way:

$$-\vec{\Sigma}_{n+1} = \begin{pmatrix} -\vec{\Sigma}_{n+1}^K & -\vec{\Sigma}_{n+1}^r \\ -\vec{\Sigma}_{n+1}^a & 0 \end{pmatrix} = |T_n|^2\begin{pmatrix} \frac{-\vec{\Sigma}_n^K}{(\omega-\epsilon^n-\vec{\Sigma}_n^r)(\omega-\epsilon^n-\vec{\Sigma}_n^a)} & \frac{1}{(\omega-\epsilon^n-\vec{\Sigma}_n^r)} \\ \frac{1}{(\omega-\epsilon^n-\vec{\Sigma}_n^a)} & 0 \end{pmatrix} \quad (9.14)$$

$$-\vec{\sigma}_n = \begin{pmatrix} -\vec{\sigma}_n^K & -\vec{\sigma}_n^r \\ -\vec{\sigma}_n^a & 0 \end{pmatrix} = |T_n|^2\begin{pmatrix} \frac{-\vec{\sigma}_{n+1}^K}{(\omega-\epsilon^{n+1}-\vec{\sigma}_{n+1}^r)(\omega-\epsilon^{n+1}-\vec{\sigma}_{n+1}^a)} & \frac{1}{(\omega-\epsilon^{n+1}-\vec{\sigma}_{n+1}^r)} \\ \frac{1}{(\omega-\epsilon^{n+1}-\vec{\sigma}_{n+1}^a)} & 0 \end{pmatrix} \quad (9.15)$$

For clarity and comparison, we write out the starting point for the recursion of Eqs.(9.14) and (9.15), which is the left(right)-self-energy of 1st(Nth) site.

$$\begin{aligned} -\vec{\Sigma}_1 &= \sum_k |L_k|^2 \begin{pmatrix} A_k^K & A_k^r \\ A_a^r & 0 \end{pmatrix} \\ -\vec{\sigma}_N &= \sum_k |R_k|^2 \begin{pmatrix} B_k^K & B_k^r \\ B_a^r & 0 \end{pmatrix} \end{aligned} \tag{9.16}$$

All the Green's functions (diagonal and off-diagonal) can be calculated straightforwardly by using the Eqs.(9.12),(9.13) recursively, and the self-energies can be obtained by using recursion relation [9.14]-[9.15]. For example:

$$\begin{pmatrix} 0 & G_{n,n}^a \\ G_{n,n}^r & G_{n,n}^K \end{pmatrix} = \begin{pmatrix} 0 & \frac{1}{\omega-\epsilon^n-\vec{\Sigma}_n^r-\vec{\sigma}_n^r} \\ \frac{1}{\omega-\epsilon^n-\vec{\Sigma}_n^a-\vec{\sigma}_n^a} & \frac{\vec{\sigma}_n^K+\vec{\Sigma}_n^K}{(\omega-\epsilon^n-\vec{\Sigma}_n^r-\vec{\sigma}_n^r)(\omega-\epsilon^n-\vec{\Sigma}_n^a-\vec{\sigma}_n^a)} \end{pmatrix} \tag{9.17}$$

The steady electrical current flowing in the system can be obtained by averaging the current operator at an arbitrary site i:

$$j_i = \int d\omega j_i(\omega) = \int d\omega [T_i G_{i+1,i}^{+-}(\omega) - T_i^* G_{i,i+1}^{-+}(\omega)] \tag{9.18}$$

Using the relation $G^{+-} = (G^K + G^a - G^r)/2$, the current can be obtained as [see Appendix C]

$$j_n(\omega) = \frac{1}{2} \frac{(\vec{\Sigma}_n^r - \vec{\Sigma}_n^a)(\vec{\sigma}_n^r - \vec{\sigma}_n^a)}{(\omega - \epsilon^n - \vec{\Sigma}_n^r - \vec{\sigma}_n^r)(\omega - \epsilon^n - \vec{\Sigma}_n^a - \vec{\sigma}_n^a)} \times \left(\frac{\vec{\Sigma}_n^K}{\vec{\Sigma}_n^r - \vec{\Sigma}_n^a} - \frac{\vec{\sigma}_n^K}{\vec{\sigma}_n^r - \vec{\sigma}_n^a} \right) \tag{9.19}$$

We have proved in Appendix C that the current is independent of site n as it should be because of current conservation at each site. Using the

nonequilibrium Green's functions (zeroth order) in the leads we get the exact formula for the current [Appendix C]

$$j_i = \int d\omega \frac{(\vec{\Sigma}_n^r - \vec{\Sigma}_n^a)(\vec{\sigma}_n^r - \vec{\sigma}_n^a)}{(\omega - \epsilon^n - \vec{\Sigma}_n^r - \vec{\sigma}_n^r)(\omega - \epsilon^n - \vec{\Sigma}_n^a - \vec{\sigma}_n^a)}[f_L(\omega) - f_R(\omega)] \quad (9.20)$$

Where f_L, f_R are the Fermi-Dirac distribution functions of the left lead and right lead, which has chemical potential μ_L, μ_R respectively. Now define $\Gamma_n^L = i(\vec{\Sigma}_n^r - \vec{\Sigma}_n^a)$ and $\Gamma_n^R = i(\vec{\sigma}_n^r - \vec{\sigma}_n^a)$ is the coupling constant (partial width of site energy level) of site n to the left and right neighbor. Define the renormalized nth site energy as $\epsilon_{eff}^n = \epsilon^n + \Delta\epsilon^n$ with $\Delta\epsilon^n = Re(\sigma_n^a + \Sigma_n^a)$. For small applied voltage, the difference of the chemical potential of the two leads is small, and the conductance of the system is:

$$\sigma_{cond} = -\frac{e^2}{\hbar}\int d\omega \frac{\Gamma_n^L\Gamma_n^R}{(\omega - \epsilon^n - \Delta\epsilon^n)^2 + \left(\frac{\Gamma_n^L+\Gamma_n^R}{2}\right)} \frac{\partial f_L(\omega)}{\partial\omega} \quad (9.21)$$

Eq.(9.21) has exactly the same form as the widely used Breit-Wigner formula for the resonant tunneling transmission of a double barrier structure. For first time, we have derived the exact generalized Breit-Wigner formula for the transmission (or conductance) of multi-barrier (multi sites) structure resonant tunneling in 1D Anderson Model from a microscopic treatment. Notice that in Eq.[9.21] we calculate the global transmission (conductance) using the "local" coupling constants and renormalized site energy of one particular site n. This reflects the coherence property of the system: the coupling constants and renormalized site energies are no longer "local", they are dependent on the whole system. It is clearly shown in the Appendix C that the current calculated in Eq.(9.20) is independent of site label n.

At low temperature, Eq.(9.21) can be simplified using $\frac{\partial f_L(\omega)}{\partial \omega} = \delta(\omega - \mu_L)$, and so

$$\sigma_{cond} = \frac{\Gamma_n^L \Gamma_n^R}{(\mu_L - \epsilon^n - \Delta\epsilon^n)^2 + \left(\frac{\Gamma_n^L + \Gamma_n^R}{2}\right)^2} \tag{9.22}$$

From Eq.(9.22) we can understand the transport due to resonant tunneling of electrons transport through multi-barrier structure. There are generally N "channels" for the electrons resonantly tunneling through a $(N+1)$-barrier (N site) structure: the resonant tunneling will occur whenever $\mu_f = \epsilon^n - \Delta\epsilon^n$ $(n = 1, 2, \cdots, N)$. The peak magnitude for the transmission in each resonant tunneling case is different and strongly dependent on the coupling constants Γ_n^L and Γ_n^R of site n: if $\mu_f = \epsilon^n - \Delta\epsilon^n$, Eq.(9.22) immediately yields:

$$\sigma_{cond} = \frac{4e^2 \Gamma_n^L \Gamma_n^R}{\hbar(\Gamma_n^L + \Gamma_n^R)^2} \tag{9.23}$$

9.3 Numerical Results and Discussion

To illustrate the reproducible conductance structure, we use Eq.(9.22) to evaluate the conductance as a function of chemical potential. We have assumed that the site energies ϵ^n are uniformly distributed between $[0, W]$, and tunneling matrix T_n uniformly distributed between $V + xV$ $(-0.5 < x < 0.5)$. In our calculation, we take $W/V \sim 5$ to 10, $W/\Gamma_0 \sim 10$ to 50. N is chosen as 10 to 20, which we believe is appropriate for the experiments in the literature [156]. For comparison, we have also calculated the possible reproducible conductance peaks using SLSA. In Fig.9.1 we illustrate the model 1D system. From the conductance structure shown in Fig.9.2-9.3 (solid curve),

we can see there exist n visible conductance peaks, and generally, $n < N$. This is because the magnitude of other (if any) peaks are too small to be visible. The conductance using the SLSA approach for the same parameters in the same sample shown in Fig.9.2 (dotted curve) has qualitatively the same structure but is quantitatively completely different. Generally, we obtain larger coupling constants Γ_n^L and Γ_n^R than that in SLSA if we have the same initial and final constants Γ_1^L and Γ_N^R respectively. So in the figures, the half-widths of the peaks calculated using our method (solid curves) are larger than that calculated in SLSA (dashed curves). To demonstrate the sensitivity of the conductance structure to the change of single localized state (site), we change one localized state energy for each configuration of the system to calculate the conductance (Fig.(9.2b) and (9.3b)). It can be seen from Fig.(9.2b),(9.3b), the conductance changes drastically for all the peaks in our models by comparing to Fig.(9.2a),(9.3a) respectively, while in SLSA, only one peak (if any) changes from Fig.(9.2a),(9.3a). As discussed previously, in our tight-binding model, because of the coherence property of the system, the coupling constants and the renormalized site energies depend on the whole system. So changing *one* localized state energy for each configuration of the system will change all the coupling constants and the renormalized site energies, and change the whole low temperature reproducible conductance structure. In the usual SLSA model, however, the coupling constants and all other site energies will not change. This is the main physical difference between our model and the SLSA model. We demonstrated it here clearly by our numerical calculations.

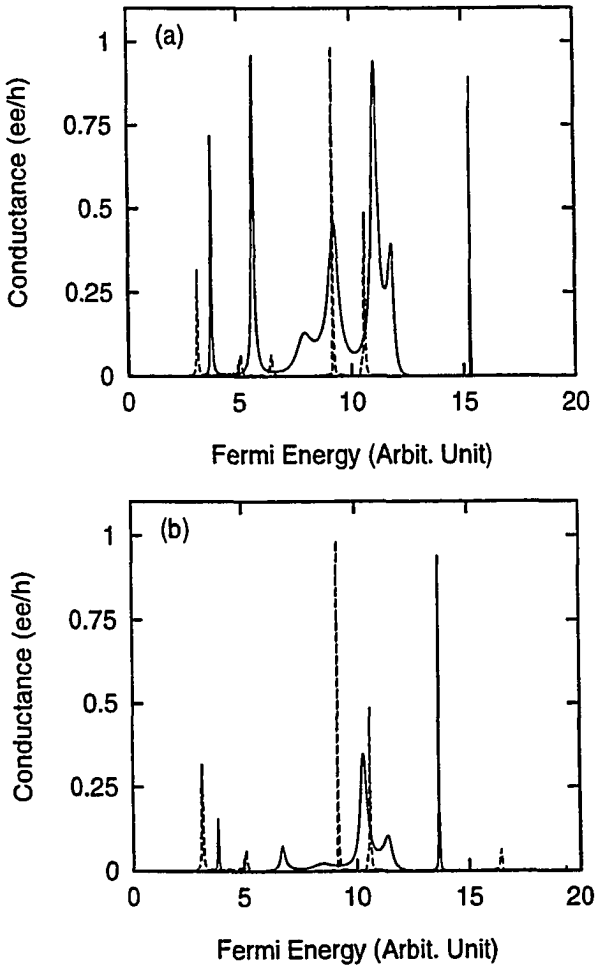

Figure 9.2: Conductance characteristics for a disordered quantum wire. Configuration (a): DASHED LINE–calculated using our formula; SOLID LINE–calculated using SLSA approach. Configuration (b) has a different site energy for a single localized state from (a).

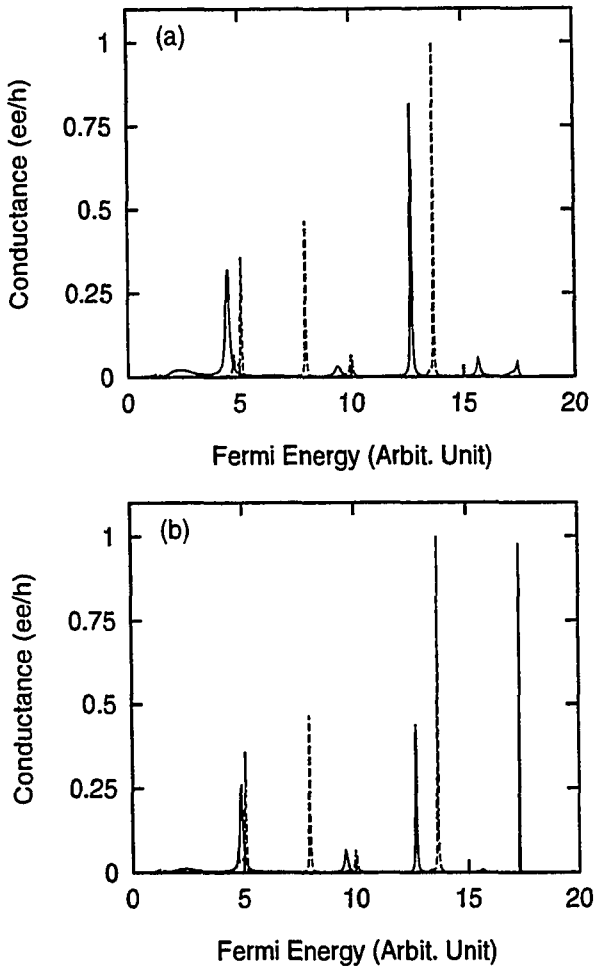

Figure 9.3: Conductance characteristics for a disordered quantum wire. The same as Fig.9.2 with a different system configuration. Configuration (b) has a different site energy for a single localized state from (a).

Chapter 10

Conclusion to Part II

In conclusion, I have studied the resonant tunneling in nanostructures using the nonequilibrium Green's function approach.

The electron-electron interaction effect in the resonant tunneling through the double barrier quantum well structure was investigated. In this system, the electron-electron interaction causes intrinsic bistability. We studied this intrinsic bistability using the non-equilibrium Green's function method for the first time. The "tri-stability" claimed by Coon *et al.* [113] was shown by us to be a computational artifact.

The resonant tunneling through a multiple-barrier structure was studied using the non-equilibrium Green's function method and a generalized exact Breit-Wigner formula was derived. The analytical results have been used to explain experiments [156] on conductance fluctuations in strongly disordered quantum wires.

My studies in this part of dissertation research are just a few examples demonstrating that the nonequilibrium Green's function approach has important advantages in transport problems in nanostructures. And there are

many very interesting open questions that can be studied using this approach, such as the electron-electron interaction in coupled quantum dots (multiple-barrier resonant tunneling), quantum Blockades in small superconductor-semiconductor-superconductor (S-Se-S) junctions, the dynamic (time-dependent) transport formulation in mesoscopic systems, and others. The non-equilibrium Green's function approach will certainly contribute to many important achievements in this very active field.

Appendix A

Equivalence of the Two Construction Rules R1 in Sec.3.1 and R2 in Sec.3.2

In this Appendix, we will give a proof of the equivalence between the construction rules described in Sec. 3.1.2 (R1) and in Sec. 3.2 (R2). Using the fact that $\nu = 1-(2+1/\mu)^{-1} = 1/[2-1/(\mu+1)]$, the filling fractions constructed using R1 can be written as:

$$\nu = \cfrac{1}{2\Delta_1 - \cfrac{1}{n_1+\alpha_1+\cfrac{1}{2\Delta_2-\cfrac{1}{n_2+\alpha_2+\cfrac{1}{\ddots\cfrac{}{}\cfrac{1}{2\Delta_k-\cfrac{1}{n_k+\alpha_k}}}}}}} \tag{A.1}$$

Where $\Delta_i = \pm$ and

$$\alpha_i = \begin{cases} 0, & \text{if } \Delta_i = +; \\ 1, & \text{if } \Delta_i = -. \end{cases}$$

For later convenience, we will denote this fraction by $\nu \equiv [n_1\Delta_1, n_2\Delta_2, \cdots, n_k\Delta_k]$ and we will denote

$$\nu = \cfrac{1}{2\Delta_1 \cfrac{1}{n_1 + \alpha_1 + \cfrac{1}{2\Delta_2 \cfrac{1}{n_2 + \alpha_2 + \cfrac{1}{\ddots \cfrac{1}{\cfrac{1}{2\Delta_k \cfrac{1}{n_k + \alpha_k + \mu}}}}}}}} \qquad \text{(A.2)}$$

by $\nu \equiv [n_1\Delta_1, n_2\Delta_2, \cdots, n_k\Delta_k, \mu]$ where μ is an odd-denominator fraction.

Before proving the equivalence of R1 and R2, we start from a theorem and certain conjectures.

Theorem (T1): If

$$h < k, \quad (h,k) = 1;$$

$$\bar{h}/\bar{k} = [n\Delta, h/k], \quad (\bar{h}/\bar{k}) = 1$$

then

$$\bar{h} = nk + h \quad \bar{k} = 2(nk + h) + k \quad \text{for } \Delta = +$$

$$\bar{h} = (n-1)k - h \quad \bar{k} = 2(nk - h) + 3k \quad \text{for } \Delta = -$$

The proof is as follows:

Proof For $\Delta = +$,

$$\begin{aligned} \bar{h}/\bar{k} &= 1/[2 + 1/(n + h/k)] \\ &= (nk + h)/[2(nk + h) + k], \end{aligned}$$

since $(nk + h, 2(nk + h) + k) = (h, k) = 1,$

so $\bar{h} = nk + h,\ \bar{k} = 2(nk + h) + k$ Q.E.D.

Using this theorem, the proof of the following conjectures is straightforward.

Conjecture (C1): Denote $\nu_i = [n\Delta, \nu_i^*]$ if $\nu_1^* \oplus \nu_2^* = \nu_3^*$

then $\nu_1 \oplus \nu_2 = \nu_3$

Conjecture (C2):

$$[n_1\Delta_1, n_2\Delta_2, \cdots, n_k\Delta_k, (0)(+)] = [n_1\Delta_1, n_2\Delta_2, \cdots, n_k\Delta_k] \quad (A.3)$$

$$[n_1\Delta_1, n_2\Delta_2, \cdots, n_k\Delta_k, (0)(-)] = [n_1\Delta_1, n_2\Delta_2, \cdots, (n_k + 1)\Delta_k] \quad (A.4)$$

$$[n_1\Delta_1, n_2\Delta_2, \cdots, n_k\Delta_k, (\infty)(\pm)] = [n_1\Delta_1, n_2\Delta_2, \cdots, n_k\Delta_k, 1/2] \quad (A.5)$$

Now we can prove the equivalence of R1 and R2. The proof is as follows:

(i) The first-level fraction constructed by R1 are $[n+]$ and $[n-]$, which are $n/(2n+1)$ and $(n+1)/(2n+1)$. They are just the two Farey series generated by $(0/1, 1/1)$ constructed by R2.

(ii) Up to the kth level in hierarchy structure constructed by R2, the fraction can be written as $[n_1\Delta_1, n_2\Delta_2, \cdots, n_k\Delta_k]$. Using $(A1)$ and $(A2)$, we see that when $n_k = 0$, the fractions $\Delta_k = \pm$ in the above expression are adjacent two fractions up to the $(k-1)$th level, and are the generators of fractions in the kth level [which is result of C1 and proof (i)]. Q.E.D.

Above we have proved the equivalence of R1 and R2. It is well known that the fractions $(\nu - 1)$ constructed by R2 will cover all the odd-denominator fractions and the convergence points of the farey series will cover all the even-denominator fractions $(\nu < 1)$. Using (A3) we can see that any even-denominator fraction can be obtained after iterative mapping from $n + 1/2$.

Appendix B

Proof for the Lagrangian of Density Fluctuations

For $k_1 = k_2 = k$ states, the Lagrangian can be written as:

$$\begin{aligned}\mathcal{L} &= \sum_\alpha i\rho_\alpha(\partial_0\eta^\alpha + a_0) + \sum_\alpha \frac{\rho_\alpha}{2m}|\vec{\partial}\eta^\alpha + \vec{a} - \vec{A}|^2 + \sum_\alpha \frac{1}{2m}(\vec{\partial}\rho_\alpha^{1/2})^2 \\ &+ \sum_{\alpha,\beta}\frac{1}{2}(\rho_\alpha - \bar{\rho}_\alpha)V_{\alpha\beta}(\rho_\beta - \bar{\rho}_\beta) - \frac{i}{2k}\underline{a}\cdot\underline{\nabla}\times\underline{a} \qquad \text{(B.1)}\end{aligned}$$

Define $\rho_\alpha = \bar{\rho} + \delta\rho_\alpha$, $\underline{a} = \langle\underline{a}\rangle + \delta\underline{a}$, in the Gaussian approximation of the fluctuations around the mean-field-approximation, the Lagrangian becomes

$$\begin{aligned}\mathcal{L} &= \sum_\alpha i\delta\rho_\alpha(\partial_0\eta^\alpha + \delta a_0) + \sum_\alpha \frac{\bar{\rho}}{2m}|\vec{\partial}\eta^\alpha + \delta\vec{a}|^2 + \sum_\alpha \frac{1}{8m\bar{\rho}}(\vec{\partial}\delta\rho_\alpha)^2 \\ &+ \sum_{\alpha,\beta}\frac{1}{2}\delta\rho_\alpha V_{\alpha\beta}\delta\rho_\beta - \frac{i}{2k}\delta\underline{a}\cdot\underline{\nabla}\times\delta\underline{a} + \bar{d}(\partial_0 + \varepsilon_d)d + \bar{d}d(\lambda_1\delta\rho_1 + \lambda_2\delta\rho_2) \qquad \text{(B.2)}\end{aligned}$$

where we have included the core hole degree of freedom $d(\hat{d})$, $\bar{d}(\hat{d}^\dagger)$.

Define $\rho^+ = (\delta\rho_1 + \delta\rho_2)/\sqrt{2}$, and $\rho^- = (\delta\rho_1 - \delta\rho_2)/\sqrt{2}$, and $\mathcal{A} = \sqrt{2}\delta a$, then

$$\mathcal{L}_t = \mathcal{L}^+ + \mathcal{L}^- + \bar{d}(\partial_0 + \varepsilon_d)d + \bar{d}d(\lambda^+\rho^+ + \lambda^-\rho^-)$$

$$\mathcal{L}^- = i\rho^-\partial_0\eta^- + \frac{\bar{\rho}}{2m}(\vec{\partial}\eta^-)^2 + \frac{1}{8m\bar{\rho}}(\vec{\partial}\rho^-)^2 + \frac{1}{2}\rho^- V^-\rho^- \qquad \text{(B.3)}$$

and

$$\begin{aligned}\mathcal{L}^+ &= i\rho^+(\partial_0\eta^+ + \mathcal{A}_0) + \frac{\bar{\rho}}{2m}(\vec{\partial}\eta^+ + \vec{\mathcal{A}})^2 + \frac{1}{8m\bar{\rho}}(\vec{\partial}\rho^+)^2 \\ &+ \frac{1}{2}\rho^+ V^+\rho^+ - \frac{i}{4k}\underline{\mathcal{A}}\cdot\underline{\nabla}\times\underline{\mathcal{A}} \qquad \text{(B.4)}\end{aligned}$$

Now we need to integrate out $\underline{\mathcal{A}}$ to obtain Eq.(5.12). This can be done using the Hubbard-Stratonorich transformation of $\mathcal{L}^+$:

$$\begin{aligned}\mathcal{L}^+ &= i\underline{J}\cdot(\underline{\nabla}\eta^- + \underline{\mathcal{A}}) + \frac{m}{2\bar{\rho}}|\vec{J}|^2 + \frac{1}{8m\bar{\rho}}(\vec{\partial}\rho^+)^2 + \frac{1}{2}\rho^+ V^+\rho^+ \\ &- \frac{i}{4k}\underline{\mathcal{A}}\cdot\underline{\nabla}\times\underline{\mathcal{A}} \qquad \text{(B.5)}\end{aligned}$$

Assuming there are no vortex-excitations, then we can absorb η^+ to the gauge field $\underline{\mathcal{A}}$, providing a constraint on $\underline{J}$: $\underline{\nabla}\cdot\underline{J} = 0$. This constraint can be satisfied by defining $\underline{J} = \underline{\nabla}\times\underline{b}$. Then we can integrate out $\underline{\mathcal{A}}$, obtain

$$\mathcal{L}^+ = \frac{m}{2\bar{\rho}}|\vec{J}|^2 + \frac{1}{8m\bar{\rho}}(\vec{\partial}\rho^+)^2 + \frac{1}{2}\rho^+ V^+\rho^+ + ik\underline{b}\cdot\underline{\nabla}\times\underline{b} \qquad \text{(B.6)}$$

In the Coulomb gauge $\vec{\partial}\times\vec{b} = 0$, $\vec{\partial}\times\vec{\partial}\times\vec{b} = -\partial^2\vec{b} = \vec{\partial}(\rho^+\hat{z})$ and $|\vec{J}|^2 = |\partial_0\vec{b}|^2 + |\vec{\partial}b_0|^2$. After integrating out b_0, we obtain

$$\begin{aligned}\mathcal{L}^+ = -\frac{m}{2\bar{\rho}}(\partial_0\rho^+)\frac{1}{\partial^2}(\partial_0\rho^+) - \frac{(2k)^2\bar{\rho}}{2m}(\rho^+)\frac{1}{\partial^2}(\rho^+) + \frac{1}{8m\bar{\rho}}(\vec{\partial}\rho^+)^2 \\ + \frac{1}{2}\rho^+ V^+\rho^+ \qquad \text{(B.7)}\end{aligned}$$

Appendix C

Proof of Current Eqs.(9.19)&(9.20)

In this Appendix, we will give the details of the derivation of Eqs.[9.19],[9.20]. From Eq.[9.12]-[9.15], and using $G_{n,n}$, we can calculate $G_{n,n+1}$ and $G_{n+1,n}$. Then substituting into Eq.[9.18], we get

$$j_n(\omega) = \frac{1}{2}\frac{|T_n|^2(\vec{\Sigma}^r_n - \vec{\Sigma}^a_n)}{[(\omega - \epsilon^n - \vec{\Sigma}^a_n)(\omega - \epsilon^{n+1} - \vec{\sigma}^a_{n+1}) - |T_n|^2]}$$
$$\frac{(\vec{\sigma}^r_{n+1} - \vec{\sigma}^a_{n+1})}{[(\omega - \epsilon^n - \vec{\Sigma}^r_n)(\omega - \epsilon^{n+1} - \vec{\sigma}^r_{n+1}) - |T_n|^2]} \times \left(\frac{\vec{\Sigma}^k_n}{\vec{\Sigma}^r_n - \vec{\Sigma}^a_n} - \frac{\vec{\sigma}^k_{n+1}}{\vec{\sigma}^r_{n+1} - \vec{\sigma}^a_{n+1}}\right) \tag{C.1}$$

Using the recursion relations for the self-energies [9.14] & [9.15], we have

$$\frac{\vec{\Sigma}^k_n}{\vec{\Sigma}^r_n - \vec{\Sigma}^a_n} = \frac{\vec{\Sigma}^k_{n+1}}{\vec{\Sigma}^r_{n+1} - \vec{\Sigma}^a_{n+1}} \quad \frac{\vec{\sigma}^k_n}{\vec{\sigma}^r_n - \vec{\sigma}^a_n} = \frac{\vec{\sigma}^k_{n+1}}{\vec{\sigma}^r_{n+1} - \vec{\sigma}^a_{n+1}} \tag{C.2}$$

and

$$\begin{aligned} \vec{\Sigma}^r_{n+1} - \vec{\Sigma}^a_{n+1} &= \frac{\vec{\Sigma}^r_n - \vec{\Sigma}^a_n}{(\omega - \epsilon^n - \vec{\Sigma}^a_n)(\omega - \epsilon^n - \vec{\Sigma}^r_n)}|T_n|^2 \\ \vec{\sigma}^r_n - \vec{\sigma}^a_n &= \frac{\vec{\sigma}^r_{n+1} - \vec{\sigma}^a_{n+1}}{(\omega - \epsilon^{n+1} - \vec{\sigma}^a_{n+1})(\omega - \epsilon^{n+1} - \vec{\sigma}^r_{n+1})}|T_n|^2 \end{aligned} \tag{C.3}$$

This relation can be used to prove straightforwardly that

$$
\begin{aligned}
j_n(\omega) &= \frac{1}{2}\frac{(\vec{\Sigma}_n^r - \vec{\Sigma}_n^a)(\vec{\sigma}_n^r - \vec{\sigma}_n^a)}{(\omega - \epsilon^n - \vec{\Sigma}_n^a - \vec{\sigma}_n^a)(\omega - \epsilon^n - \vec{\Sigma}_n^r - \vec{\sigma}_n^r)} \times \left(\frac{\vec{\Sigma}_n^k}{\vec{\Sigma}_n^r - \vec{\Sigma}_n^a} - \frac{\vec{\sigma}_n^k}{\vec{\sigma}_n^r - \vec{\sigma}_n^a}\right) \\
&= \frac{1}{2}\frac{(\vec{\Sigma}_{n+1}^r - \vec{\Sigma}_{n+1}^a)(\vec{\sigma}_{n+1}^r - \vec{\sigma}_{n+1}^a)}{(\omega - \epsilon^{n+1} - \vec{\Sigma}_{n+1}^a - \vec{\sigma}_{n+1}^a)(\omega - \epsilon^{n+1} - \vec{\Sigma}_{n+1}^r - \vec{\sigma}_{n+1}^r)} \\
&\times \left(\frac{\vec{\Sigma}_{n+1}^k}{\vec{\Sigma}_{n+1}^r - \vec{\Sigma}_{n+1}^a} - \frac{\vec{\sigma}_{n+1}^k}{\vec{\sigma}_{n+1}^r - \vec{\sigma}_{n+1}^a}\right) \\
&= \frac{1}{2}\frac{(\vec{\Sigma}_n^r - \vec{\Sigma}_n^a)(\vec{\sigma}_n^r - \vec{\sigma}_n^a)}{(\omega - \epsilon^n - \vec{\Sigma}_n^a - \vec{\sigma}_n^a)(\omega - \epsilon^n - \vec{\Sigma}_n^r - \vec{\sigma}_n^r)} \times \left(\frac{\vec{\Sigma}_1^k}{\vec{\Sigma}_1^r - \vec{\Sigma}_1^a} - \frac{\vec{\sigma}_N^k}{\vec{\sigma}_N^r - \vec{\sigma}_N^a}\right)
\end{aligned}
\tag{C.4}
$$

So we have proved the the current is independent of site n. For the zeroth order Greens functions of the leads, we have

$$
\begin{aligned}
\vec{\Sigma}_1^k &= [2f_L(\omega) + 1](\vec{\Sigma}_1^a - \vec{\Sigma}_1^r) \\
\vec{\sigma}_N^k &= [2f_R(\omega) + 1](\vec{\sigma}_N^a - \vec{\sigma}_N^r)
\end{aligned}
\tag{C.5}
$$

Finally we get equation [9.20].

Bibliography

[1] K. v. Klitzing, G. Dordaand, and M. Pepper, Phys. Rev. Lett. **45**, 494 (1980).

[2] D. C. Tsui, H. L. Stőrmer, and A. C. Gossard, Phys. Rev. Lett. **48**, 1559 (1982).

[3] *The Quantum Hall Effect*, edited by R. E. Prange and S. M. Girvin (Springer-Verlag, New York, 1990).

[4] H. Levine, S. B. Libby, and A. M. M. Pruisken, Phys. Rev. Lett. **51**, 1915 (1983).

[5] A. M. M. Pruisken, in *The Quantum Hall Effect*, edited by R. E. Prange and S. M. Girvin (springer-Verlag, New York, 1990).

[6] R. Laughlin, Phys. Rev. B **23**, 5632 (1981).

[7] B. I. Halperin, Phys. Rev. B **25**, 2185 (1982).

[8] R. Laughlin, Phys. Rev. Lett. **50**, 1395 (1983).

[9] F. D. M. Haldane, Phys. Rev. Lett. **51**, 605 (1983).

[10] R. B. Laughlin, Surf. Sci. **141**, 11 (1984).

[11] B. I. Halperin, Phys. Rev. Lett. **52**, 1583 (1984).

[12] J. K. Jain, Phys. Rev. Lett. **63**, 199 (1989).

[13] J. K. Jain, Phys. Rev. B **40**, 8079 (1989).

[14] J. K. Jain, Phys. Rev. B **41**, 7653 (1990).

[15] R. R. Du *et al.*, Phys. Rev. Lett. **70**, 2944 (1993).

[16] S. Chern, *Complex Manifolds without Potential Theory* (Springer-Verlag, Berlin, 1979).

[17] S. Deser, R. Jackiw, and S. Templeton, Ann. Phys. **140**, 372 (1982).

[18] S. C. Zhang, T. H. Hansson, and S. A. Kivelson, Phys. Rev. Lett. **62**, 82 (1989).

[19] N. Read, Phys. Rev. Lett. **62**, 86 (1989).

[20] N. Read, Phys. Rev. Lett. **65**, 1502 (1990).

[21] B. Blok and X. G. Wen, Phys. Rev. B **42**, 8133, 8145 (1990).

[22] X. G. Wen, Phys. Rev. B **44**, 5704 (1991).

[23] D. H. Lee and S. Zhang, Phys. Rev. Lett. **66**, 1220 (1991).

[24] S. Kivelson, D. H. Lee, and S. C. Zhang, Phys. Rev. B **47**, 2223 (1993).

[25] B. I. Halperin, P. A. Lee, and N. Read, Phys. Rev. B **47**, 7312 (1993).

[26] A. Lopez and E. Fradkin, Phys. Rev. B **47**, 7080 (1993).

[27] D. V. Khveshchenko, Phys. Rev. B **49**, 10514 (1994).

[28] B. Sakita, D. N. Sheng, and Z. B. Su, Phys. Rev. B **44**, 11510 (1991).

[29] R. Ray and B. Sakita, Ann. Phys. **230**, 131 (1994).

[30] Z. S. Ma and Z. B. Su, Phys. Rev. B **48**, 2347 (1993).

[31] H. Buhmann *et al.*, Phys. Rev. Lett. **65**, 1065 (1990).

[32] A. J. Tuberfield *et al.*, Phys. Rev. Lett. **65**, 637 (1990).

[33] B. B. Goldberg *et al.*, Phys. Rev. Lett. **1065**, 641 (1990).

[34] A. Pinczuk, B. S. Dennis, L. N. Pfeiffer, and K. West, Phys. Rev. Lett. **70**, 3983 (1993).

[35] C. Kallin and B. I. Halperin, Phys. Rev. B **30**, 5655 (1984).

[36] S. M. Girvin, in *The Quantum Hall Effect*, edited by R. E. Prange and S. M. Girvin (springer-Verlag, New York, 1990).

[37] S. H. Simon and B. I. Halperin, Phys. Rev. B **48**, 17368 (1993).

[38] S. M. Girvin, A. H. MacDonald, and P. M. Platzman, Phys. Rev. Lett. **54**, 581 (1985).

[39] S. M. Girvin, A. H. MacDonald, and P. M. Platzman, Phys. Rev. B **33**, 2481 (1986).

[40] B. S. Wang, J. L. Birman, and Z. B. Su, Phys. Rev. Lett. **68**, 1605 (1992).

[41] A. H. MacDonald, E. H. Rezayi, and D. Keller, Phys. Rev. Lett. **68**, 1939 (1992).

[42] V. M. Apalkov and E. I. Rashba, Phys. Rev. B **48**, 18312 (1993).

[43] X. M. Chen and J. J. Quinn, Surf. Sci. **305**, 71 (1994).

[44] T. Chakraborty and P. Pietilainen, Phys. Rev. Lett. **59**, 2784 (1987).

[45] D. Yoshioka, A. H. MacDonald, and S. M. Girvin, Phys. Rev. B **39**, 1932 (1989).

[46] S. He *et al.*, Phys. Rev. B **43**, 9339 (1991).

[47] Y. W. Suen *et al.*, Phys. Rev. Lett. **68**, 1379 (1992).

[48] J. P. Eisenstein *et al.*, Phys. Rev. Lett. **68**, 1383 (1992).

[49] J. Eisenstein *et al.*, Phys. Rev. Lett. **69**, 3804 (1992).

[50] S. Murphy *et al.*, Phys. Rev. Lett. **72**, 732 (1974).

[51] A. H. MacDonald, Surface Science **2229**, 1 (1990), for a brief review of the FQHE in double-layer systems.

[52] X. G. Wen and A. Zee, Phys. Rev. Lett. **69**, 1811 (1992).

[53] F. Ezawa and A. Iwasaki, Phys. Rev. B **47**, 7295 (1993).

[54] K. Yang *et al.*, Phys. Rev. Lett. **72**, 732 (1994).

[55] G. Fano, F. Ortolani, and E. Comombo, Phys. Rev. B **34**, 2670 (1986).

[56] C. Kane, S. kivelson, D. H. Lee, and S. C. Zhang, Phys. Rev. B **43**, 3255 (1991).

[57] A. Lopez and E. Fradkin, Phys. Rev. Lett. **69**, 2126 (1992).

[58] A. Lopez and E. Fradkin, Phys. Rev. B **44**, 5246 (1991).

[59] T. Chakraborty and P. Pietilainen, *The Fractional Quantum Hall Effect: Properties of an incompressible quantum fluid* (Springer-Verlag, New York, 1988).

[60] V. Bargmann, Rev. Mod. Phys. **34**, 829 (1962).

[61] S. Girvin and T. Jach, Phys. Rev. B **29**, 5617 (1984).

[62] This equation for the filling factor can be derived using the relation between the flux carried by electron i and factors $\prod_i (z_i - z_j)^{m_{ij}}$.

[63] In the stereographic mapping between disk and spherical geometry, the correspondence of the total angular momentum S here is $N\bar{S}$, where $2\bar{S}$ is the flux number across the sphere, and the angular momentum of the center of the mass is included in this correspondence.

[64] B. I. Halperin, Helv. Phys. Acta **56**, 75 (1983).

[65] R. Tao, J. Phys. C **17**, L53 (1984).

[66] R. Morf and B. I. Halperin, Phys. Rev. B **33**, 2221 (1986).

[67] S. Mitra and A. H. MacDonald, Phys. Rev. B **48**, 2005 (1993).

[68] G. Dev and J. K. Jain, Phys. Rev. B **45**, 1223 (1992).

[69] A. Govari, A. Mann, and J. Katriel, Phys. Rev. B **48**, 11404 (1993).

[70] G. Dunne, Int. J. Mod. B **999**, 999x (1994).

[71] S. M. Girvin and T. Jach, Phys. Rev. B **28**, 4506 (1983).

[72] D. Yoshiokoa, B. I. Halperin, and P. A. Lee, Phys. Rev. Lett. **50**, 1219 (1983).

[73] W. Lai, K. Yu, Z. Su, and L. Yu, Solid Stat. Comm. **52**, 339 (1984).

[74] J. Zang and J. L. Birman, Phys. Rev. B **47**, 16305 (1993).

[75] C. A. Lutken and G. G. Ross, Phys. Rev. B **45**, 11837 (1992).

[76] F. C. Chang and T. Chakraborty, Phys. Rev. B **30**, 7320 (1985).

[77] W. Kohn, Phys. Rev. **123**, 1242 (1961).

[78] J. P. Longo and C. Kallin, Phys. Rev. B **47**, 4429 (1993).

[79] F. D. M. Haldane, in *The Quantum Hall Effect*, edited by R. E. Prange and S. M. Girvin (springer-Verlag, New York, 1990).

[80] J. Jain and V. Goldman, Phys. Rev. B **45**, 1255 (1992).

[81] E. Fradkin, *Gauge Field Theory in Condensed Matter Physics* (Addison-Wesly, New York, 1991).

[82] G. H. Hardy and E. M. Wright, *An Introduction to the Theory of Numbers* (Clarendon, Oxford, 1954).

[83] R. B. Laughlin, Surf. Sci. **152**, 163 (1984).

[84] J. K. Jain, S. A. Kivelson, and N. Trivedi, Phys. Rev. Lett. **64**, 1297 (1990).

[85] R. B. Laughlin *et al.*, Phys. Rev. B **32**, 1311 (1985).

[86] R. B. Laughlin, in *The Quantum Hall Effect*, edited by R. E. Prange and S. M. Girvin (springer-Verlag, New York, 1990).

[87] C. W. J. Beenakker, Phys. Rev. Lett. **64**, 216 (1990).

[88] A. H. MacDonald, Phys. Rev. Lett. **64**, 220 (1990).

[89] Z. S. Ma, Y. X. Chen, and Z. B. Su, Phys. Rev. B **50**, 2232 (1994).

[90] J. Zang and J. L. B. Z.-B. Su, to appear in Solid State Comm. (1994) (unpublished).

[91] D. Huang and G. Gumbs, Phys. Lett. A **167**, 396 (1992), notice that the problem of electron in a sphere with uniform external field has also been studied.

[92] E. T. Whittaker and G. N. Watson, *A Course of Modern Analysis* (Cambridge University Press, New York, 1965).

[93] V. M. Apalkov and E. I. Rashba, Phys. Rev. B **46**, 1628 (1992).

[94] X. M. Chen and J. J. Quinn, Phys. Rev. Lett. **70**, 2130 (1993).

[95] P. M. Platzman and S. He, Phys. Rev. B **49**, 13674 (1994).

[96] F. D. M. Haldane and E. H. Rezayi, Phys. Rev. Lett. **54**, 237 (1985).

[97] A. Pinczuk, (private communication).

[98] A. H. MacDonald and S. C. Zhang (unpublished).

[99] J. Zang, D. Schmeltzer, and J. L. Birman, Phys. Rev. Lett. **71**, 773 (1993).

[100] G. D. Mahan, *Many-Particle Physics*, 2nd ed. (Plenum, New York, 1981).

[101] K. Ohtaka and Y. Tanabe, Rev. Mod. Phys **62**, 929 (1990).

[102] D. Schmeltzer, Phys. Rev. B **47**, 11980 (1993).

[103] K. D. Schotte and U. Schotte, Phys. Rev. **182**, 479 (1969).

[104] S. Doniach and E. H. Sondheimer, *Green's Function for Solid State Physicists* (Addison-Wesley, New York, 1978).

[105] P. W. Anderson, Phys. Rev. Lett. **18**, 1049 (1967).

[106] G. D. Mahan, Phys. Rev. **153**, 882 (1967).

[107] in *Electronic Properties of Multilayers and Low-Dimensional Semiconductor Structures*, edited by J. Chamberlain, L. Eaves, and J. Portal (Plenum, New York, 1989).

[108] *Nanostructures and Mesoscopic Systems*, edited by W.P.Kirk and M.A.Reed (Academic Press, San Diego, 1992).

[109] *Mesoscopic Phenomena in Solids*, edited by B. L. Altshuler, P. A. Lee, and R. A. Webb (Elsevier, Amsterdam, 1991).

[110] L. Esaki and R. Tsui, IBM J. Res. Develop **14**, 61 (1970).

[111] H. L. Berkowitz and R. A. Lux, J. Vac. Sci. Technol. B **5**, 967 (1987).

[112] K. M. S. V. Bandara and D. Coon, Appl. Phys. Lett. **53**, 1865 (1988).

[113] D. D. Coon, K. M. S. V. Bandara, and H. Zhao, Appl. Phys. Lett. **54**, 2115 (1989).

[114] W. Cai *et al.*, Phys. Rev. Lett. **63**, 418 (1989).

[115] W. Cai *et al.*, Phys. Rev. Lett. **65**, 104 (1990).

[116] W. Cai and M. Lax, Phys. Rev. B **47**, 4096 (1993).

[117] M. Y. Sumetskii and M. Fel'shtyn, JETP Lett. **53**, 24 (1991).

[118] R. Landauer, IBM J. Res. Dev. **1**, 233 (1957).

[119] R. Landauer, Philos. Mag. **21**, 863 (1970).

[120] M. Büttiker and R.Landauer, Phys. Rev. Lett. **49**, 1739 (1982).

[121] F. W. Sheard and G. A. Toombs, Appl. Phys. Lett. **52**, 1228 (1988).

[122] W. R. Frensley, Phys. Rev. B **36**, 1570 (1987).

[123] N. Kluksdahl, A. Kriman, D. Ferry, and C. Ringhofer, Phys. Rev. B **39**, 7720 (1989).

[124] F. A. Buot and K. L. Jensen, Phys. Rev. B **42**, 9429 (1990).

[125] N. S. Wingreen, K. W. Jacobsen, and J. W. Wilkins, Phys. Rev. B **40**, 11834 (1989).

[126] Y. Meir, N. Wingreen, and P. Lee, Phys. Rev. Lett. **70**, 2601 (1993).

[127] S. Datta, Phys. Rev. B **45**, 1347 (1992).

[128] A. Groshev, T. Ivanov, and V. Valtchinov, Phys. Rev. Lett. **66**, 1082 (1991).

[129] H. Pastawski, Phys. Rev. B **46**, 4053 (1992).

[130] C. Caroli, R. Combescot, P. Nozieres, and D. Saint-James, J.Phys. C: Solid. St. Phys. **4**, 916, 2598, 2611 (1971).

[131] C. Caroli, R. Combescot, P. Nozieres, and D. Saint-James, J.Phys. C: Solid. St. Phys. **5**, 21 (1972).

[132] L. Y. Chen and C. S. Ting, Phys. Rev. B **41**, 8533 (1990).

[133] L. Y. Chen and C. S. Ting, Phys. Rev. B **43**, 2097, 4534 (1990).

[134] L. Y. Chen and C. S.Ting, Phys. Rev. B **44**, 5916 (1991).

[135] E. V. Anda and F. Flores, J. Phys. C: Cond. Matt. **3**, 9087 (1991).

[136] E. Runge and H. Ehrenreich, Annals of Physics **219**, 55 (1992).

[137] E. Runge and H. Ehrenreich, Phys. Rev. B **45**, 9145 (1992).

[138] R. Lake and S. Datta, Phys. Rev. B **45**, 6670 (1992).

[139] J. Zang and J. L. Birman, Phys. Rev. B **46**, 5020 (1992).

[140] J. Zang and J. L. Birman, Phys. Rev. B **47**, 10654 (1993).

[141] J. H.Davies, S. Hershfield, P. Hyldgaard, and J. W. .Wilkins, Phys. Rev. B **47**, 4603 (1993).

[142] N. Wingreen, A. Jauho, and Y. Meir, Phys. Rev. B **47**, 8487 (1993).

[143] in *Physics of Hot-electron Transport in Semiconductor*, edited by C. S. Ting (World Scientific, New Jersey, 1992).

[144] P. Martin and J. Schwinger, Phys. Rev. **115**, 1342 (1959).

[145] J. Schwinger, J. Math. Phys. **2**, 407 (1961).

[146] L. P. Kadanoff and G.Baym, *Quantum Statistical Mechanics* (Benjamin, New York, 1962).

[147] P. M. Bakshi and K. T. Mahanthappa, J. Math. Phys. **4**, 1,12 (1963).

[148] L. V. Keldysh, Sov. Phys. JETP **20**, 1018 (1965).

[149] J. Rammer and H. Smith, Rev. Mod. Phys. **58**, 323 (1986).

[150] D.C.Langreth, in *Linear and Nonlinear Electron Transport in Solids*, edited by J.T.Devreese and V. Doren (Plenum, New York, 1976).

[151] K. C. Chou, Z. B. Su, B. L. Hao, and L. Yu, Phys. Rep. **118**, 1 (1985).

[152] I. Lifshitz and V. Kirpichenko, Sov. Phys. JETP **50**, 499 (1979).

[153] D. Thouless and S. Kirkpatrick, J. Phys. C: Solid State Phys. **14**, 235 (1981).

[154] A. Stone and P. Lee, Phys. Rev. Lett. **54**, 1196 (1985).

[155] W. Xue and P. Lee, Phys. Rev. B **38**, 3913 (1988).

[156] A. B. Fowler, J. Wainer, and R. A. Webb, IBM J. Res. Develop. **32**, 372 (1989).

[157] M. Buttiker, Phys. Rev. Lett. **57**, 1761 (1986).

[158] V. Goldman, D. Tsui, and J. Cunningham, Phys. Rev. Lett. **58**, 1256 (1987).

[159] A. Zaslavsky, V. Goldman, D. Tsui, and J. Cunningham, Appl. Phys. Lett. **53**, 1408 (1988).

[160] T. Sollner, Phys. Rev. Lett. **59**, 1622 (1987).

[161] K. L. Jensen and F. A. Buot, Phys. Rev. Lett. **66**, 1078 (1991).

[162] M. Y. Azbel and P. Soven, Phys. Rev. B **27**, 831 (1983).

[163] B. Ricco and M. Azbel, Phys. Rev. B **29**, 1970 (1984).

List of Publications

1. *Theory of Intrinsic Bistability in Double Barrier Resonant Tunneling Structure*, Jun Zang and Joseph L. Birman, Phys. Rev. B **46**, 5020 (1992).

2. *Theory of Coherent Transport Through A Strongly Disordered System: Resonant Tunneling in 1D Tight-binding Model*, Jun Zang and Joseph L. Birman, Phys. Rev. B **47**, 10654 (1993).

3. *Farey Series, Hierarchy Structure and Scaling Theory of Fractional Quantum Hall Effect*, Jun Zang and Joseph L. Birman, Phys. Rev. B **47**, 16305 (1993).

4. *Optical Fermi Edge Singularity of Double Layer Quantum Hall Systems*, Jun Zang, David Schmeltzer, and Joseph L. Birman, Phys. Rev. Lett. **71**, 773 (1993).

5. *Optical Second Order Emission from Tomanaga-Luttinger Liquid*, Jun Zang, Joseph L. Birman, Zhao-Bin Su, Sol. Sta. Comm. (1994 to appear).

6. *Anharmonic and Non-classical Effects of q-Deformed Quantum Harmonic Oscillator, M. Artoni, J. Zang, and J. L. Birman, Phys. Rev. A* **47**, 2555 (1993).

7. *Condition For Equivalence of q-Deformed And Anharmonic Oscillators*, M. Artoni, J. Zang, and J. L. Birman, (NATO series, 1993).

8. *Fractional Quantum Hall Systems in the Disk Geometry: Properties of Laughlin Droplets*, Jun Zang and Joseph. L. Birman (submitted to Phys. Rev. B).

9. *Structure of the Magneto-Exciton and Optical Properties in Fractional Quantum Hall Systems*, Jun Zang and Joseph. L. Birman (submitted to Phys. Rev. Lett.).

Autobiographical Statement

Jun Zang, born March 6, 1967 in Weifang City, Shangdong Province, People's Republic of China. He graduated from Weifang First High School in 1985, and obtained his B.Sc. in Physics from Fudan University in 1989. He married Ying Shi in 1991.